ERDC/GSL TR-06-16

Geotechnical and Structures Laboratory

US Army Corps of Engineers®
Engineer Research and Development Center

Laboratory Characterization of White Masonry Concrete

Erin M. Williams, Stephen A. Akers, and Paul A. Reed

September 2006

ERDC/GSL TR-06-16
September 2006

Laboratory Characterization of White Masonry Concrete

Erin M. Williams, Stephen A. Akers, and Paul A. Reed

Geotechnical and Structures Laboratory
U.S. Army Engineer Research and Development Center
3909 Halls Ferry Road
Vicksburg, MS 39180-6199

Final report
Approved for public release; distribution is unlimited

Prepared for Headquarters, U.S. Army Corps of Engineers
Washington, DC 20314-1000

Under AT40 Work Unit, Dynamic Behavior of Complex Geologic/Structural Materials

Abstract: Personnel of the Geotechnical and Structures Laboratory, U.S. Army Engineer Research and Development Center, conducted a laboratory investigation to characterize the strength and constitutive property behavior of a white masonry concrete (WMC). Forty-four mechanical property tests consisting of two hydrostatic compression tests, four unconfined compression (UC) tests, 17 triaxial compression (TXC) tests, two uniaxial strain tests, four uniaxial strain load/biaxial unload (UX/BX) tests, five uniaxial strain load/constant volume tests, two uniaxial strain load/constant strain ratio tests, five direct pull (DP) tests, and three reduced triaxial extension (RTE) tests were successfully completed. In addition to the mechanical property tests, nondestructive pulse-velocity measurements were performed on each specimen. The TXC tests exhibited a continuous increase in principal stress difference with increasing confining stress. A recommended compression failure surface was developed from the TXC and UC test results. Test data from the RTE and DP tests were used to develop a recommended extension failure surface for WMC. Results from the stress paths of the strain path tests and the recommended compression failure surface exhibited good agreement except for the UX/BX tests.

Contents

List of Figures

Preface

This laboratory mechanical property investigation of white masonry concrete was conducted by personnel of the U.S. Army Engineer Research and Development Center (ERDC). The study was conducted with funds provided by the Directorate of Military Programs, Headquarters, U.S. Army Corps of Engineers, under the Research, Development, Test, and Evaluation (RDT&E) Program. The investigation reported herein was accomplished under the Military RDT&E Work Package AT40, Weapons Effects and Structural Response; Dynamic Behavior of Complex Geologic/Structural Materials Work Unit.

This study was conducted from February 2003 to August 2003 by staff members of the Impact and Explosion Effects Branch (IEEB), Engineering Systems and Materials Division (ESMD), Geotechnical and Structures Laboratory (GSL), ERDC, under the general direction of Henry S. McDevitt, Jr., Chief, IEEB; Dr. Albert J. Bush III, Chief, ESMD; Dr. William P. Grogan, Deputy Director, GSL; and Dr. David W. Pittman, Director, GSL.

The Principal Investigator for this project was Dr. Stephen A. Akers, IEEB. Material property data were processed by Erin M. Williams, IEEB, the Co-Investigator for this project. Laboratory characterization tests were performed by Paul A. Reed, IEEB, under the technical direction of Dr. Akers. Instrumentation support was provided by A. Leroy Peeples, formerly of the Engineering and Informatic Systems Division, Information Technology Laboratory, ERDC. This report was written by Ms. Williams under the direction of Dr. Akers.

COL Richard B. Jenkins was Commander and Executive Director of ERDC. Dr. James R. Houston was Director.

1 Introduction

Background

Personnel of the U.S. Army Engineer Research and Development Center, Geotechnical and Structures Laboratory (ERDC-GSL), conducted a laboratory investigation to characterize the strength and constitutive property behavior of white masonry concrete (WMC) for the Dynamic Behavior of Complex Geologic/Structural Materials Work Unit of the AT40 Weapons Effects and Structural Response Work Package. ERDC-GSL personnel conducted a total of 47 mechanical property tests of which 44 were successfully completed. The 44 tests consisted of two hydrostatic compression tests, four unconfined compression tests, 17 triaxial compression tests, two uniaxial strain tests, four uniaxial strain load/biaxial unload tests, five uniaxial strain load/constant volume tests, two uniaxial strain load/ constant strain ratio tests, five direct pull tests, and three reduced triaxial extension tests. In addition to the mechanical property tests, nondestructive pulse-velocity measurements were performed on each specimen.

Purpose and Scope

The purpose of this report is to document the results from the laboratory mechanical property tests conducted on the WMC specimens. In addition, results from the nondestructive pulse-velocity measurements are documented. The physical and composition properties, test procedures, and test results are documented in Chapter 2. Comparative plots and analyses of the experimental results are presented in Chapter 3. A summary is provided in Chapter 4.

2 Laboratory Tests

Material Description

The test specimens used in this investigation were prepared from samples cored from solid concrete masonry units of WMC. The company that produced the 0.30-scale concrete masonry units also produced the solid standard-size concrete masonry units. The 0.30-scale concrete masonry units were used for penetration tests. The WMC mechanical property tests were performed in correlation to the penetration tests. Typically, each solid concrete masonry unit produced six to eight cored test specimens. Additional details are documented in the "Specimen preparation" section of this chapter.

Composition Property Tests

Prior to performing the mechanical property tests, the height, diameter, and mass for each test specimen were determined. These measurements were used to compute the specimen's wet, bulk, or "as-tested" density. Results from these determinations are provided in Table 1. Measurements of posttest water content[1] were conducted in accordance with procedures given in American Society for Testing and Materials (ASTM) D 2216 (ASTM 2002e). Based on the appropriate values of posttest water content, wet density, and an assumed grain density of 2.77 Mg/m^3, values of dry density, porosity, degree of saturation, and volumes of air, water, and solids were calculated (Table 1). Also listed in the table are maximum, minimum, and mean values and the standard deviation about the mean for each quantity. The WMC specimens had a mean wet density of 2.055 Mg/m^3 (based on data from 44 specimens), a mean water content of 1.42 percent, and a mean dry density of 2.025 Mg/m^3 (based on data from 43 specimens).

Ultrasonic Pulse-Velocity Determinations

Prior to performing a mechanical property test, ultrasonic pulse-velocity measurements were collected on each test specimen. This involved measuring the

[1] Water content is defined as the mass of water (removed during drying in a standard oven) divided by the mass of dry solids.

transit distance and time for each P (compressional) or S (shear) pulse to propagate through a given specimen. The velocity was then computed by dividing the transit distance by the transit time. A matching pair of 1-MHz piezoelectric transducers was used to transmit and receive the ultrasonic P waves. A pair of 2.25-MHz piezoelectric transducers was used to transmit and receive the ultrasonic S waves. The transit time was measured with a 100-MHz digital oscilloscope and the transit distance with a digital micrometer. All of these wave-velocity determinations were made under atmospheric conditions. That is, no prestress of any kind was applied to the specimens. The tests were conducted in accordance with procedures given in ASTM C 597 (ASTM 2002c).

One compressional-wave (P-wave) and one shear-wave (S-wave) velocity were determined axially through each specimen. Radial P- and S-wave velocities were determined for each specimen in the following manner. Six radial P-wave velocities were determined; i.e., two transverse to each other at elevations of one-quarter, one-half, and three-quarters of the specimen height. Two radial S-wave velocities were measured; both of these determinations were made at the mid-height of the specimen transverse to each other. The various P- and S-wave velocities determined for the test specimens are provided in Table 1; the radial-wave velocities listed in Table 1 are the average values.

Mechanical Property Tests

Forty-four mechanical property tests were successfully performed on the WMC specimens to characterize the strength and constitutive properties of the material. All of the mechanical property tests were conducted quasi-statically with axial strain rates on the order of 10^{-4} to 10^{-5} per second and times to peak load on the order of 5 to 30 min. Mechanical property data were obtained under several different stress and strain paths. Undrained compressibility data were obtained during the hydrostatic loading phase of the triaxial compression (TXC) tests and from two hydrostatic compression (HC) tests. Shear and failure data were obtained from unconfined compression (UC) tests, consolidated-undrained TXC tests, the direct pull (DP) tests, and from consolidated-undrained reduced triaxial extension (RTE) tests. One-dimensional compressibility data were obtained from undrained uniaxial strain (UX) tests with lateral stress measurements or K_0 tests. Three types of undrained strain-path tests were conducted during the test program. All of the strain-path tests were initially loaded under uniaxial strain boundary conditions to a prescribed level of stress or strain. At the end of the UX loading, constant axial to radial strain ratios (ARSR) of 0, -1.33, and -2.0 were applied. The ARSR = 0 path is a constant axial strain unloading path and produces a forced state of volumetric expansion; these tests will be referred to as UX/BX tests. The UX/SR tests have an ARSR = -1.33, which produces a path that has a constant strain ratio when loaded. The ARSR = -2.0 path is a constant volume strain loading path, and these paths will be referred to as UX/CV tests. The terms undrained and unconsolidated signify that no pore fluid (liquid or gas) was allowed to escape or drain from the membrane-enclosed specimens. The completed test matrix is presented in Table 2, which lists the types of tests conducted, the number of tests, the test numbers for each group, the

test numbers of the specimens that had cyclic loading, and the nominal peak radial stress applied to specimens prior to shear loading or during the HC, UX, or strain-path loading.

Specimen preparation

The mechanical property test specimens were cut from sections of WMC using a diamond-bit core barrel by following the procedures provided in ASTM C 42 (ASTM 2002b). The test specimens were cut to the correct length, and the ends were ground flat and parallel to each other and perpendicular to the sides of the core in accordance with procedures in ASTM D 4543 (ASTM 2002f). Prior to testing, the prepared specimens were measured for height, diameter, and mass and were ultrasonically pulsed. This information was used to calculate the composition properties and wave velocities of the specimens. The prepared test specimens had a nominal height of 110 mm and a diameter of 50 mm.

Prior to testing, each specimen was placed between hardened steel top and base caps. With the exception of the UC and the DP test specimens, two 0.6-mm-thick synthetic latex membranes, and an Aquaseal® membrane were placed around the specimen, and the exterior of the outside membrane was coated with a liquid synthetic rubber to inhibit deterioration caused by the confining-pressure fluid (Figure 1). The fluid was a mixture of kerosene and hydraulic oil. Finally, the specimen, along with its top cap and base cap assembly, was placed on the instrumentation stand of the test apparatus, and the instrumentation setup was initiated.

Test devices

Four sets of test devices were used in this test program. The axial load for all of the UC tests was provided by a 3.3-MN (750,000-lb) loader. The application of load was manually controlled with this test device. No pressure vessel was required for the UC tests; only a base, load cell, and vertical and radial deformeters were necessary.

Direct pull tests were performed by using the direct pull apparatus, in which end caps were attached to the specimens with a high-modulus high-strength epoxy. A manual hydraulic pump was used to pressurize the direct pull chamber. When the direct pull chamber was pressurized, a piston retracted and produced tensile loading on the test specimen. Measurements for the tensile loading of the specimen were recorded with an 89-kN load cell.

To perform the RTE test, a static high-pressure triaxial test device (HPTX) was used (Figure 2). This device was manually controlled and can be pressurized up to 100 MPa. The pumping equipment that was used during the operation of this device limited the peak pressure that was achieved to 70 MPa. When the triaxial extension top cap was used with the HPTX device, independent control of the vertical and lateral stresses was permitted. The specimen top cap was bolted to the extension loading piston, and the surface on top of the piston was

pressurized. During the RTE test, the confining pressure (or radial stress) was kept constant while the vertical stress was reduced (Akers et al. 1986).

All of the remaining tests were conducted in a 600-MPa-capacity pressure vessel, and the axial load was provided by an 8.9-MN (2-million-lb) loader. With the 8.9-MN loader, the application of load, pressure, and axial displacement were regulated by a servo-controlled data acquisition system. This servo-controlled system allowed the user to program rates of load, pressure, and axial displacement to achieve the desired stress or strain path. Confining pressure was measured external to the pressure vessel by a pressure transducer mounted in the confining fluid line. A load cell mounted in the base of the specimen pedestal was used to measure the applied axial loads inside the pressure vessel (Figure 1).

Outputs from the various instrumentation sensors were electronically amplified and filtered, and the conditioned signals recorded by computer-controlled 16-bit analog-to-digital converters. The data acquisition systems were programmed to sample the data channels every 1 to 5 sec, convert the measured voltages to engineering units, and store the data for further posttest processing.

Test instrumentation

The vertical deflection measurement system in all the test areas except the DP test area consisted of two linear variable differential transformers (LVDTs) mounted vertically on the instrumentation stands and positioned 180 deg apart. They were oriented to measure the displacement between the top and base caps, thus providing a measure of the axial deformations of the specimen. For the confined tests, a linear potentiometer was mounted external to the pressure vessel so as to measure the displacement of the piston through which axial loads were applied. This provided a backup to the vertical LVDTs in case they exceeded their calibrated range.

Two types of radial deflection measurement systems (lateral deformeters) were used in this test program. The output of each deformeter was calibrated to the radial displacement of the two footings that were glued to the sides of the test specimen (Figure 1). These two small steel footings were mounted 180 deg apart at the specimen's mid-height. The footing faces were machined to match the curvature of the test specimen. A threaded post extended from the outside of each footing and protruded through the membrane. The footings must be mounted to the specimen prior to placement of the membrane. Once the membranes were in place, steel caps were screwed onto the threaded posts to seal the membrane to the footing. The lateral deformeter ring was attached to these steel caps with set-screws. The completed specimen lateral deformeter setup is shown in Figure 3.

One type of lateral deformeter consisted of an LVDT mounted on a hinged ring; the LVDT measured the expansion or contraction of the ring. This lateral deformeter was used over smaller ranges of radial deformation when the greatest measurement accuracy was required. This lateral deformeter was used for all of the HC, UC, UX, and strain-path tests and for the TXC tests at confining pressures less than 50 MPa. This design is similar to the radial-deformeter design

provided by Bishop and Henkel (1962). When the specimen expanded (or contracted), the hinged-deformeter ring opened up (or closed) causing a change in the electrical output of the horizontally mounted LVDT.

The second type of lateral deformeter, which was used for all of the TXC tests at confining pressures of 50 MPa and greater, consisted of two strain-gauged spring-steel arms mounted on a double-hinged ring. The strain-gauged arms deflected as the ring expanded or contracted. This lateral deformeter was used when the greatest radial deformation range was required and, therefore, was less accurate than the LVDT deformeter. With this deformeter, when the specimen expanded or contracted, the rigid deformeter ring flexed about its hinge causing a change in the electrical output of the strain-gauged spring-arm. The output of the spring-arms was calibrated to the specimen's deformation. Radial measurements were not performed during the DP tests.

Test descriptions

The UC and TXC tests were performed in accordance with ASTM C 39 (ASTM 2002a) and ASTM C 801 (ASTM 2002d), respectively. A TXC test was conducted in two phases. During the first phase, the hydrostatic compression phase, the cylindrical test specimen was subjected to an increase in hydrostatic pressure while measurements of the specimen's height and diameter changes were made. The data are typically plotted as pressure versus volumetric strain, the slope of which, assuming elastic theory, is the bulk modulus, K. The second phase of the TXC test, the shear phase, was conducted after the desired confining pressure was applied during the HC phase. While holding the desired confining pressure constant, axial load was increased, and measurements of the changes in the specimen's height and diameter were made. The axial (compressive) load was increased until the specimen failed. The shear data are generally plotted as principal stress difference versus axial strain, the slope of which represents Young's modulus, E. The maximum principal stress difference that a given specimen can support or the principal stress difference at 15 percent axial strain during the shear loading, whichever occurs first, is defined as the peak strength.

Note that the UC test is a TXC test in which no confining pressure is applied. The maximum principal stress difference observed during a UC test is defined as the unconfined compressive strength of the material.

Extension data were obtained for WMC by performing direct pull tests and reduced triaxial extension tests. The DP tests have no confining pressure during the tests. To conduct the DP tests, end caps were attached with epoxy to the specimen. The end caps were screwed into the direct pull apparatus, and the specimen was pulled apart vertically when pressure was applied to the piston. The RTE tests were conducted with the HPTX device and the TXE top cap (Figure 2). To begin the RTE test, the specimen was loaded hydrostatically to a desired confining pressure. After the hydrostatic loading was applied and while the radial stress was held constant, the vertical stress was reduced until the specimen failed. Throughout the RTE test, the specimen's height and diameter

changes were recorded (Akers et al. 1986). Extension shear data for the material are generally plotted as principal stress difference versus axial strain.

A uniaxial strain (UX) test was conducted by applying an axial load and confining pressure simultaneously so that, as the cylindrical specimen shortened, its diameter remained unchanged. That is, zero radial strain boundary conditions were maintained. The data are generally plotted as axial stress versus axial strain, the slope of which is the constrained modulus, *M*. The data are also plotted as principal stress difference versus mean normal stress, the slope of which is twice the shear modulus *G* divided by the bulk modulus *K*, i.e., *2G/K*, or, in terms of Poisson's ratio ν, $3(1-2\nu)/(1+\nu)$.

The strain-path tests in this test program were conducted in two phases. Initially, the specimen was subjected to a uniaxial-strain loading up to a desired level of mean normal, radial, or axial stress. At the end of the UX loading, constant axial-to-radial-strain ratios of 0, -1.33, or -2.0 were applied; these tests were identified earlier as UX/BX, UX/SR, and UX/CV tests, respectively. To conduct these tests, the software controlling the servo-controls had to correct the measured inputs for system compressibility and for the nonlinear calibrations of specific transducers.

Definition of stresses and strains

During the mechanical property tests, measurements were typically made of the axial and radial deformations of the specimen as confining pressure and/or axial load was applied or removed. These measurements along with the pretest measurements of the initial height and diameter of the specimen were used to convert the measured test data to true stresses and engineering strains.[2]

Axial strain, ε_a, was computed by dividing the measured axial deformation, Δh (change in height), by the original height h_o ; i.e., $\varepsilon_a = \Delta h/h_o$. Similarly, radial strain, ε_r , was computed by dividing the measured radial deformation, Δd (change in diameter), by the original diameter d_o ; i.e., $\varepsilon_r = \Delta d/d_o$. For this report, volumetric strain was assumed to be the sum of the axial strain and twice the radial strain, $\varepsilon_v = \varepsilon_a + 2\varepsilon_r$.

The principal stress difference, *q*, was calculated by dividing the axial load by the cross-sectional area of the specimen *A*, which is equal to the original cross-sectional area, A_o, multiplied by $(1 - \varepsilon_r)^2$. In equation form,

$$q = (\sigma_a - \sigma_r) = \frac{\text{Axial Load}}{A_o (1-\varepsilon_r)^2} \tag{1}$$

where σ_a is the axial stress and σ_r is the radial stress. The axial stress is related to the confining pressure and the principal stress difference by

[2] Compressive stresses and strains are positive in this report.

$$\sigma_a = q + \sigma_r \tag{2}$$

The mean normal stress, *p*, is the average of the applied principal stresses. In cylindrical geometry,

$$p = \frac{(\sigma_a + 2\sigma_r)}{3} \tag{3}$$

Results

Results from all of the mechanical property tests except from the direct pull tests are presented in Plates 1-39. One data plate is presented for each test with reliable results. Results from the HC tests are presented on the plates in four plots: (a) mean normal stress versus volumetric strain, (b) mean normal stress versus axial strain, (c) radial versus axial strain, and (d) mean normal stress versus radial strain. Each plate for the UC, TXC, UX, strain-path, and RTE tests displays four plots: (a) principal stress difference versus mean normal stress, (b) principal stress difference versus axial strain, (c) volumetric strain versus mean normal stress, and (d) volumetric strain versus axial strain.

Table 1
Physical and Composition Properties of White Masonry Concrete

Test Number	Type of Test	Plate Number	Wet Density Mg/m^3	Posttest Water Content %	Dry Density Mg/m^3	Porosity %	Degree of Saturation %	Volume of Air %	Volume of Water %	Volume of Solids %	Axial P-Wave Velocity km/s	Radial P-Wave Velocity km/s	Axial S-Wave Velocity km/s	Radial S-Wave Velocity km/s
01	UC	1	2.075	1.61	2.042	26.3	12.5	23.0	3.3	73.7	3.986	3.854	2.253	2.299
02	UC	2	1.987	1.51	1.958	29.3	10.1	26.4	3.0	70.7	3.654	3.568	2.096	2.105
03	UC	3	2.083	1.58	2.051	26.0	12.5	22.7	3.2	74.0	3.982	3.885	2.339	2.350
04	UC	4	2.079	1.12	2.056	25.8	8.9	23.5	2.3	74.2	3.840	3.757	2.230	2.255
06	HC	5	2.092	1.57	2.060	25.6	12.6	22.4	3.2	74.4	3.870	3.870	2.274	2.337
07	HC	6	2.028	1.65	1.995	28.0	11.8	24.7	3.3	72.0	3.625	3.625	2.154	2.207
08	TXC/5	7	2.013	1.41	1.985	28.3	9.9	25.5	2.8	71.7	3.577	3.577	2.150	2.193
09	TXC/5	8	2.068	1.23	2.043	26.2	9.6	23.7	2.5	73.8	3.667	3.667	2.205	2.204
10	TXC/10	10	2.064	1.28	2.038	26.4	9.9	23.8	2.6	73.6	3.844	3.844	2.290	2.319
11	TXC/10	11	2.082	1.28	2.055	25.8	10.2	23.2	2.6	74.2	3.663	3.663	2.187	2.230
12	TXC/20	12	2.024	1.39	1.996	27.9	9.9	25.2	2.8	72.1	3.520	3.520	2.111	2.148
13	TXC/20	13	2.057	1.60	2.025	26.9	12.0	23.7	3.2	73.1	3.693	3.693	2.266	2.268
14	TXC/50	14	2.084	1.58	2.051	25.9	12.5	22.7	3.2	74.1	3.770	3.770	2.186	2.266
15	TXC/50	15	2.042	1.78	2.007	27.6	13.0	24.0	3.6	72.4	3.625	3.625	2.164	2.199
17	TXC/100	16	2.024	1.72	1.990	28.2	12.2	24.7	3.4	71.8	3.613	3.613	2.198	2.172
18	TXC/100	17	2.056	1.76	2.021	27.0	13.2	23.5	3.6	73.0	3.699	3.699	2.276	2.242
19	TXC/200	18	2.056	1.89	2.018	27.1	14.1	23.3	3.8	72.9	3.630	3.630	2.238	2.167
20	TXC/200	19	2.049	1.89	2.011	27.4	13.9	23.6	3.8	72.6	3.614	3.614	2.209	2.207
21	TXC/300	20	2.096	1.92	2.056	25.8	15.3	21.8	3.9	74.2	3.767	3.863	2.279	2.298
22	TXC/300	21	2.050	1.78	2.014	27.3	13.1	23.7	3.6	72.7	3.757	3.598	2.160	2.221
23	TXC/400	22	2.021	1.87	1.984	28.4	13.1	24.7	3.7	71.6	3.680	3.574	2.102	2.229
24	TXC/400	23	2.062	1.87	2.024	26.9	14.0	23.2	3.8	73.1	3.647	3.733	2.170	2.195
25	UX	24	2.036	1.67	2.002	27.7	12.1	24.4	3.3	72.3	3.545	3.418	2.103	2.092
26	UX	25	2.049	1.65	2.015	27.2	12.2	23.9	3.3	72.8	3.859	3.645	2.241	2.240
27	UX/BX	26	2.072	1.46	2.042	26.3	11.3	23.3	3.0	73.7	3.712	3.836	2.234	2.269

(Continued)

Table 1 (Concluded)

Test Number	Type of Test	Plate Number	Wet Density Mg/m^3	Posttest Water Content %	Dry Density Mg/m^3	Porosity %	Degree of Saturation %	Volume of Air %	Volume of Water %	Volume of Solids %	Axial P-Wave Velocity km/s	Radial P-Wave Velocity km/s	Axial S-Wave Velocity km/s	Radial S-Wave Velocity km/s
28	UX/BX	27	2.021	1.48	1.991	28.1	10.5	25.2	2.9	71.9	3.792	3.657	2.218	2.192
29	UX/BX	28	2.040	1.27	2.015	27.3	9.4	24.7	2.6	72.7	3.695	3.647	2.153	2.230
30	UX/BX	29	2.017	1.33	1.991	28.1	9.4	25.5	2.6	71.9	3.666	3.549	2.088	2.112
31	UX/CV	30	2.110	1.40	2.081	24.9	11.7	22.0	2.9	75.1	3.736	3.894	2.277	2.335
32	UX/CV	31	2.089	1.46	2.059	25.7	11.7	22.7	3.0	74.3	3.810	3.712	2.281	2.202
33	UX/CV	32	2.019	1.35	1.992	28.1	9.6	25.4	2.7	71.9	3.703	3.624	2.189	2.151
34	UX/SR	35	2.036	1.34	2.009	27.5	9.8	24.8	2.7	72.5	3.669	3.566	2.190	2.177
35	UX/SR	36	2.066	1.26	2.040	26.3	9.8	23.8	2.6	73.7	3.720	3.662	2.205	2.216
36	TXC/5	9	2.022	1.12	1.999	27.8	8.0	25.6	2.2	72.2	3.694	3.585	2.194	2.148
37	UX/CV	33	2.125	1.60	2.092	24.5	13.7	21.1	3.3	75.5	3.908	3.733	2.309	2.284
38	UX/CV	34	2.046	1.42	2.017	27.2	10.5	24.3	2.9	72.8	3.688	3.570	2.176	2.199
39	RTE/63	37	2.004	1.08	1.983	28.4	7.5	26.3	2.1	71.6	3.762	3.667	2.217	2.186
40	RTE/42	38	2.094								3.729	3.612	2.212	2.218
42	RTE/63	39	2.044	1.20	2.020	27.1	9.0	24.6	2.4	72.9	3.695	3.565	2.175	2.175
43	DP	--	2.089	0.71	2.074	25.1	5.9	23.6	1.5	74.9	3.690	3.683	2.183	2.258
44	DP	--	2.111	0.79	2.095	24.4	6.8	22.7	1.7	75.6	3.918	3.804	2.292	2.307
45	DP	--	2.024	0.74	2.009	27.5	5.4	26.0	1.5	72.5	3.676	3.604	2.145	2.116
46	DP	--	2.033	0.72	2.018	27.1	5.4	25.7	1.5	72.9	3.749	3.603	2.203	2.156
47	DP	--	2.071	0.75	2.055	25.8	6.0	24.3	1.5	74.2	3.677	3.573	2.204	2.176
N			44	43	43	43	43	43	43	43	44	44	44	44
Mean			2.055	1.42	2.025	26.9	10.7	24.0	2.9	73.1	3.723	3.669	2.205	2.217
Stdv			0.032	0.33	0.032	1.1	2.5	1.2	0.7	1.1	0.106	0.110	0.060	0.064
Max			2.125	1.92	2.095	29.3	15.3	26.4	3.9	75.6	3.986	3.894	2.339	2.350
Min			1.987	0.71	1.958	24.4	5.4	21.1	1.5	70.7	3.520	3.418	2.088	2.092

Table 2
Completed WMC Test Matrix

Type of Test	No. of Tests	Test Nos.	Cycles in Test Nos.	Nominal Peak Radial Stress, MPA
Hydrostatic Compression	1	6	6	330
	1	7	--	522
Triaxial Compression	4	1,2,3,4	--	0
	3	8,9,36	--	5
	2	10,11	11	10
	2	12,13	13	20
	2	14,15	15	50
	2	17,18	18	100
	2	19,20	19	200
	2	21,22	--	300
	2	23,24	23	400
UX Strain	2	25,26	25	500
UX/BX	2	27,28	--	200
	2	29,30	--	100
UX/CV	3	31,32,38	--	100-120
	1	33	--	50
	1	37	--	190
UX/SR	2	34,35	--	50
DP	5	43,44,45,46,47	--	0
RTE	2	39,42	--	63
	1	40	--	42
Total # Tests	44			

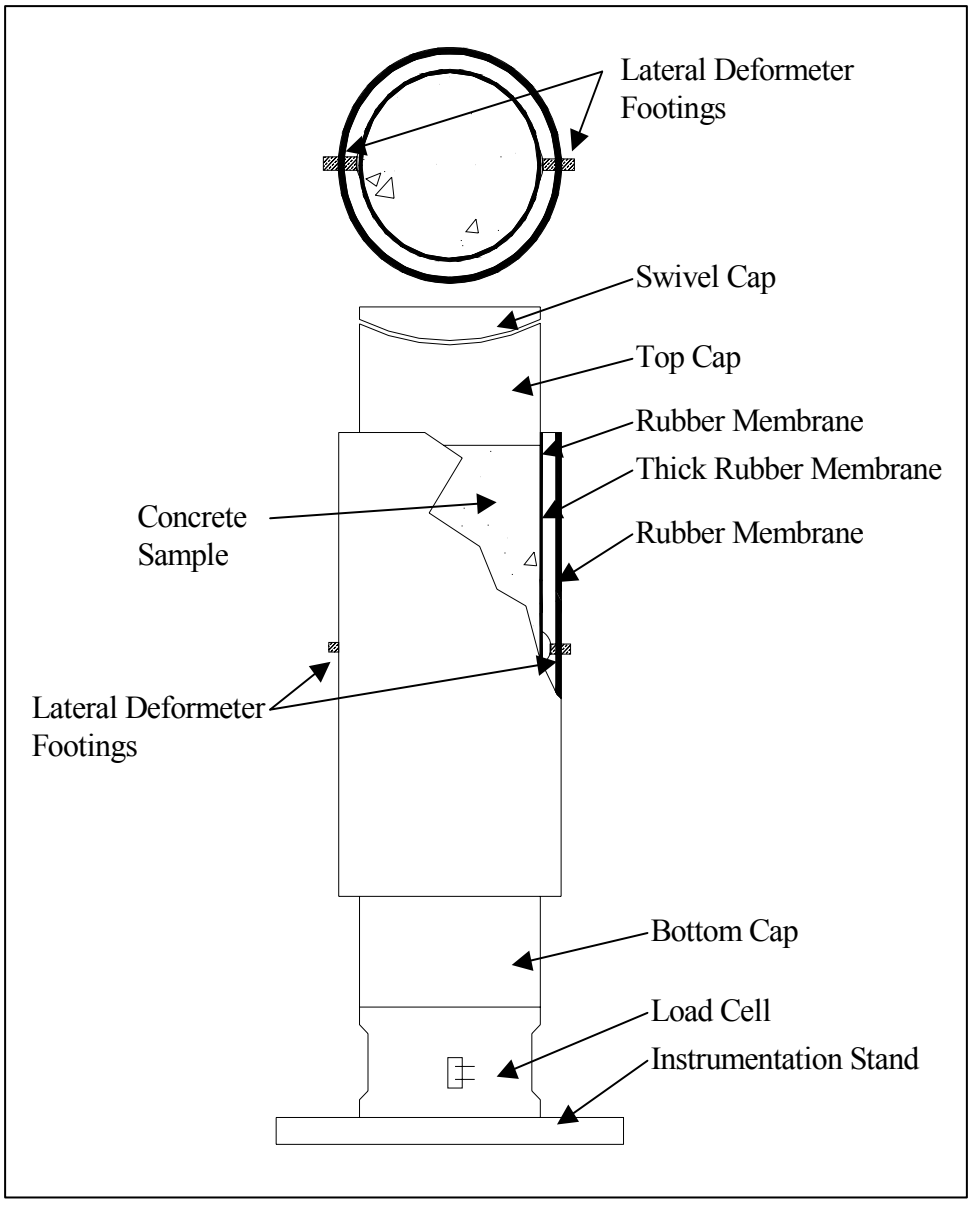

Figure 1. Typical test specimen setup

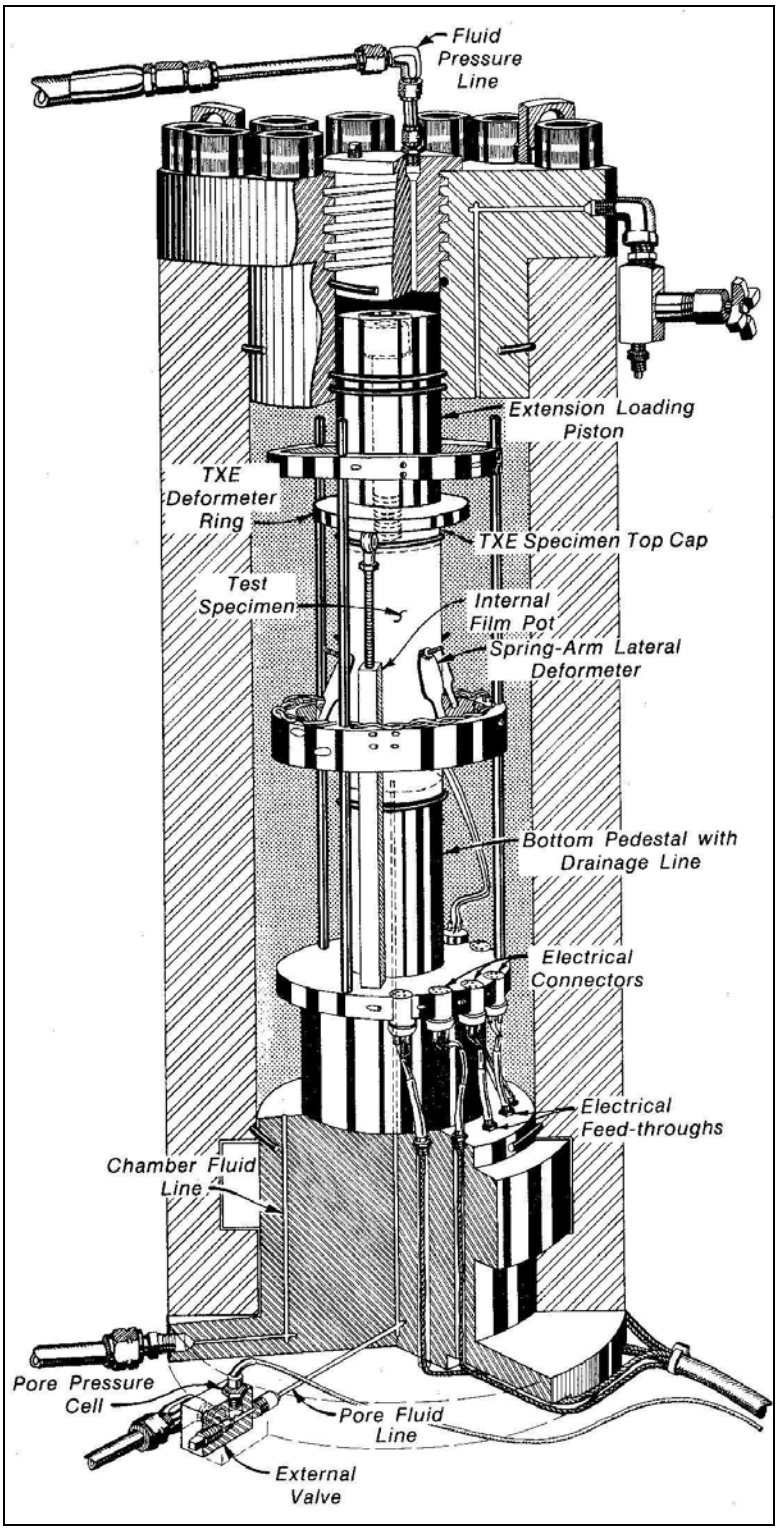

Figure 2. HPTX test device with TXE top cap

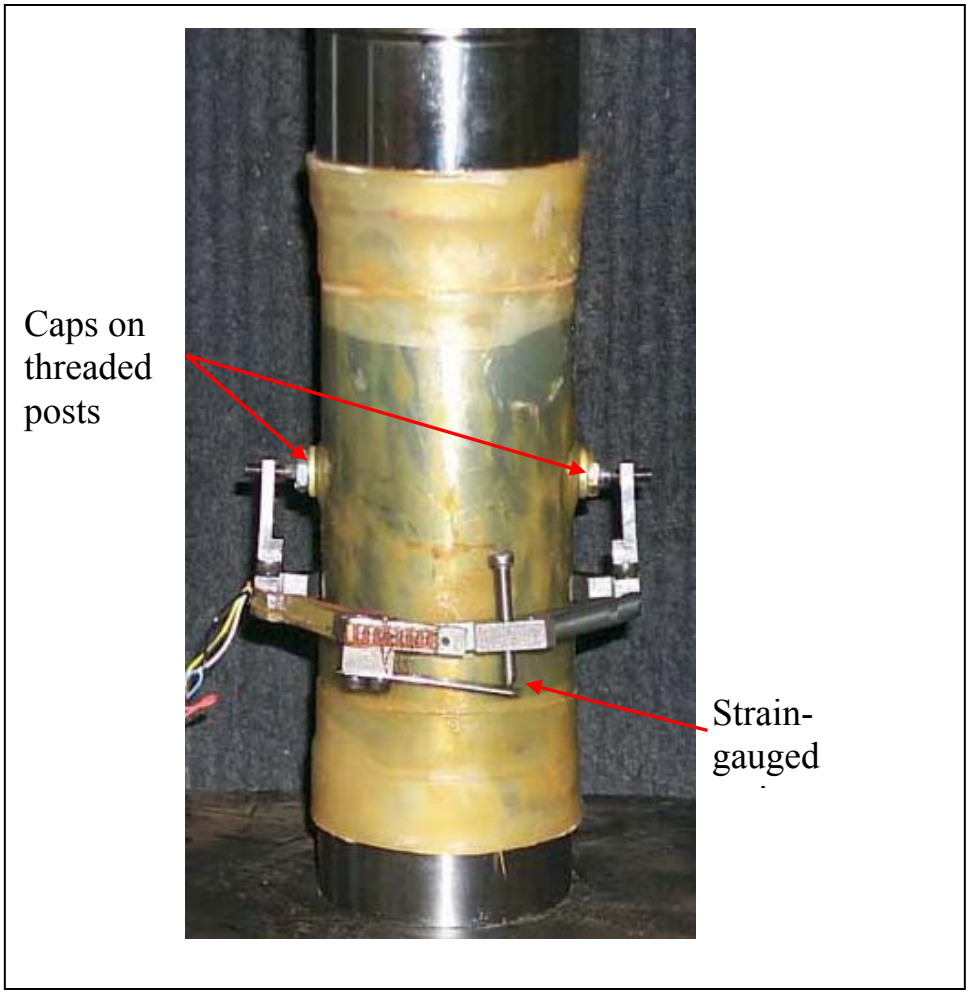

Figure 3. Spring-arm lateral deformeter mounted on test specimen

3 Analysis of Test Results

Introduction

An analysis is presented in this chapter of the results from laboratory tests conducted on the white masonry concrete. The purpose of this investigation was to characterize the strength and constitutive properties of the material. As described in Chapter 2, a total of 47 mechanical property tests were conducted in this investigation and, of the 47 tests, 44 tests were successfully completed. The analysis in this chapter is based on the results from the following numbers and types of tests: two HC tests, four UC tests, 17 TXC tests, two UX tests, four UX/BX tests, five UX/CV tests, two UX/SR tests, five DP tests, and three RTE tests.

Hydrostatic Compression Test Results

Undrained compressibility data were obtained from two HC tests and during the hydrostatic loading phases of the 17 TXC tests. The pressure-volume data from the two HC tests are plotted in Figure 4. Unload-reload cycles were applied to HC test specimen 06 in order to obtain unload-reload data at intermediate levels of confining stress. The initial dry densities of the specimens for HC tests 06 and 07 were 1.995 and 2.060 Mg/m^3, respectively. The HC compressibility is affected by initial dry density, i.e., increased compressibility with decreased dry density. Figure 5 presents the pressure time-histories for the HC tests. During HC test 06, the pressure was intentionally held constant for a period of time prior to the unloading cycles. During each hold in pressure, the volumetric strains continue to increase, which indicates that WMC is susceptible to creep at high pressures (Figure 4). At the peak of the first cycle, the pressure was held at 99 MPa for 230 sec, during which time a volumetric strain of 0.75 percent occurred. During the second cycle, the pressure was held at 199 MPa for 675 sec, and a volumetric strain of 0.69 percent occurred.

Pressure-volume data were also obtained during the hydrostatic loading phases of the TXC tests (Figures 6 and 7). There is no significant scatter in the pressure-volume data for the TXC tests. The results plotted in Figure 6 indicate that WMC begins to exhibit inelastic strains at a pressure level of approximately 14 MPa and at a volumetric strain of approximately 0.25 percent. These are the pressure and strain levels at which the pressure-volume response and the initial

bulk modulus begin to soften appreciably. Based on the data from HC test 07 and the TXC tests in Figure 8, the initial elastic bulk modulus for WMC is approximately 5.6 GPa. HC test specimen 06 was not used to determine the elastic bulk modulus because the test data were noisy during the test.

Triaxial Compression Test Results

Shear and failure data were successfully obtained from four unconfined compression tests and 17 unconsolidated-undrained TXC tests. Recall from Chapter 2 that the second phase of the TXC test, the shear phase, is conducted after the desired confining pressure was applied during the HC phase. The UC tests are a special type of TXC test without the application of confining pressure. Results from the UC tests are plotted in Figures 9 and 10, and results from the TXC tests are plotted in Figures 11-26. In all the figures, the axial and volumetric strains at the beginning of the shear phase were set to zero; i.e., only the strains during shear are plotted.

Stress-strain data from the four UC tests in Figures 9 and 10 are plotted as principal stress difference versus axial strain during shear and as principal stress difference versus volumetric strain during shear. Deformeters instead of strain gauges were used to measure the axial and radial strains of the UC test specimens. During the UC tests, no attempt was made to capture the post-peak (or softening) stress-strain behavior of this material. The mean unconfined strength of white masonry concrete determined from specimens 01, 03, and 04 was 17.3 MPa. Specimen 02 was not included in the determination of the unconfined strength, since the dry density of specimen 02 was 1.958 Mg/m^3, which is below the average dry density of all the test specimens (2.025 Mg/m^3), resulting in an outlying result for specimen 02. For WMC the dry density of the specimen affects the specimen's strength. That is, specimens with higher dry densities should have higher strengths for a given level of confining pressure.

Figures 11-26 present the results from the TXC tests conducted at nominal confining pressures of 5, 10, 20, 50, 100, 200, 300, and 400 MPa. The TXC results are plotted as principal stress difference versus axial strain during shear and as principal stress difference versus volumetric strain during shear. The results are very good considering the inherent variability of the initial wet and dry densities and water contents of the specimens. The wet densities of the TXC specimens ranged from 2.013 to 2.096 Mg/m^3, the dry densities ranged from 1.984 to 2.056 Mg/m^3, and the water contents ranged from 1.23 to 1.92 percent.

A few comments should also be made concerning the unloading results in general. The final unloading stress-strain responses at axial strains approaching 15 percent are less reliable than the unloadings at axial strains less than 11 percent. The vertical deformeters go out of range at axial strains of approximately 11 percent. After that, an external deformeter with less resolution is used to measure axial displacement. During the initial unloadings, the creep strains are greater in magnitude than the recovered elastic strains. This behavior results in a

net increase in axial strain (for example) during the initial unloading, rather than an expected decrease in axial strain.

Results of TXC tests conducted at a constant confining pressure of 5 MPa are shown in Figures 11 and 12. The tests at 5 MPa exhibit increasing peak principal stress difference with increasing initial dry density. The dry densities for specimens 08, 09, and 36 were 1.985, 2.043, and 1.999 Mg/m^3, relatively. The volumetric responses in Figure 12 indicate that the materials initially compacted until just below the peak principal stress difference, and then began to dilate. At 5 MPa confining pressure, the material is still in the elastic region of the pressure-volume response.

Figures 13 and 14 display the results of TXC tests conducted at 10 MPa confining pressure. Both test specimens had higher than average values of initial dry density (2.025 Mg/m^3) and exhibited little differences in peak principal stress difference (Figure 13). Minimal post-peak data were obtained for test specimen 10 because equipment problems occurred after reaching the peak principal stress difference. No post-peak data were obtained for test specimen 11 because the specimen failed above the center. To prevent damage to the test equipment, tests are stopped early when there is a failure above the center of the specimen. The volumetric response data in Figure 14 indicate that at 10 MPa confining pressure, the specimens compacted during shear loading throughout the test.

Test results for TXC tests conducted at a confining pressure of 20 MPa are shown in Figures 15 and 16. Results in Figure 15 display a ductile shear response; i.e., the stress-strain curves exhibit strain hardening. Since the tests at 10 MPa displayed brittle behavior (the material strain softens and little valid post-peak stress or strain data are acquired), the brittle-to-ductile transition is between 10 and 20 MPa. The brittle-to-ductile transition occurs when the material flows at a near constant value of principal stress difference.

Results of TXC tests conducted at a confining pressure of 50 MPa are shown in Figures 17 and 18. The shear data in Figure 17 exhibited a stiff initial response followed by a ductile response. A mechanical malfunction prevented test specimen 15 from being loaded to an axial strain of 15 percent. From Figure 17, it appears that test specimen 15 would have produced a peak principal stress difference similar to the peak principal stress difference of test specimen 14 (115 MPa). The volumetric response data in Figure 18 indicate that the specimens compacted during shear loading.

Results of TXC tests conducted at confining pressures of 100, 200, 300, and 400 MPa are shown in Figures 19-20, 21-22, 23-24, and 25-26, respectively. The qualitative responses at these four levels of confining pressure are essentially the same. The shear responses were predominantly ductile, peak strength increased with increased level of confining pressure, and volumetric dilation just prior to peak strength was between 0.5 and 1.5 percent for each set of data. After completing the TXC tests, it was determined that none of the specimens reached full saturation during the shear loading. The stress-strain curves continued to

exhibit increases in principal stress difference over the entire range of imposed confining stresses.

For comparison purposes, stress-strain curves from selected TXC tests at confining pressures equal to or less than 50 MPa are plotted in Figure 27, and selected tests at confining pressures greater than 50 MPa are plotted in Figure 28. Stress-strain data from the TXC tests in Figures 27 and 28 are plotted in Figures 29 and 30, respectively, as principal stress difference versus volumetric strain during shear. One should note that the initial loading of the TXC stress-strain curves (Figures 27-28) is a function of the material's initial volume changes during shear, which in turn are a function of the specimens' position on the material's pressure-volume curve at the start of shear. As confining pressure increases, the initial loading of the material softens as the stress state moves into the crush regime of the pressure-volume curve, and then stiffens again as the material approaches void closure, i.e., the point at which all of the specimen's air-porosity is crushed out. At confining pressures of 5 and 10 MPa, the specimens' initial volume changes are basically within the elastic regime of the pressure-volume curve, which results in the stiff initial loading of the stress-strain curves. The TXC tests conducted at a confining pressure of 20 and 50 MPa had a softer response (lower moduli) during the initial shear loading than the tests at 5 and 10 MPa (Figure 27). The tests conducted at a confining pressure of 100 MPa had the softest initial loading results in stress difference-axial strain space (Figure 31 and 32). The test specimens at 100 MPa also had the softest response in stress difference-volumetric strain space (see Figure 33). The TXC tests conducted at 200, 300, and 400 MPa exhibited increasingly stiffer initial loading, and the results were all stiffer than the tests at 100 MPa. The subsequent increase in initial loading with increasing confining pressure during shear is directly related to the increasing stiffness in the pressure-volume response of the concrete.

Results from TXC tests at confining pressures from 5 to 400 MPa are plotted in Figure 34 as radial strain during shear versus axial strain during shear. A contour of zero volumetric strain during shear is also plotted on this figure. When the instantaneous slope of a curve is shallower than the contour of zero volumetric strain, the specimen is in a state of volume compression; when steeper, the specimen is in a state of dilation or volume expansion. Data points plotting below the contour signify that a test specimen has dilated, and the current volume of the specimen is greater than the volume at the start of shear. The plotted results show that the specimens tested at 5 MPa dilated during shear. All the other tests exhibited volumetric compression during shear.

The failure data from all of the UC and TXC tests are plotted in Figure 35 as principal stress difference versus mean normal stress; one stress path at each confining stress is also plotted. In Figure 35, a recommended failure surface is plotted with the failure points. The quality of the failure data is very good; it exhibits very little scatter. It is important to note that the failure points exhibit a continuous increase in principal stress difference with increasing values of mean normal stress. The response data from the 400 MPa TXC tests indicate that, at a mean normal stress of approximately 640 MPa, the concrete still has not reached void closure and is far from full saturation. Concrete materials can continue to

gain strength with increasing pressure until all of the air porosity in the concrete has been crushed out, i.e., when void closure is reached. It is important to recognize that void closure can be attained during the shear loading phase of the TXC tests as well as under hydrostatic loading conditions. At levels of mean normal stress above void closure, the failure surface will have a minimal slope.

Reduced Triaxial Extension Test Results

Extension stress-strain and failure data were successfully obtained from five direct pull tests and three unconsolidated-undrained RTE tests. The DP tests are a special type of RTE test without the application of confining pressure. Results from the DP tests are plotted in Figure 36, results from the RTE tests are plotted in Figures 37 and 38, and the recommended failure surfaces from the triaxial test results are plotted in Figures 39 and 40. Data from the DP tests exhibit some scatter. The stress-strain data in Figure 37 display the RTE test results conducted at confining pressures of approximately 40 and 60 MPa. All of the RTE specimens fractured. Tests 39 and 42 exhibit slight variations during the loading that were caused by the confining pressure and the manual operation of the equipment used for RTE tests. Only the DP, RTE, and UC tests included in this test program used manual operation rather then a servo-controlled data acquisition system to control the load and confining pressure. Figure 39 displays failure data from the UC, TXC, DP, and RTE tests, and the recommended compression and extension failure surfaces for WMC. The compression and extension failure surfaces are also exhibited in Figure 40. Figure 40 includes the failure points from the tests used to develop the recommended failure surfaces. The resulting compression and extension failure surfaces were well defined and nonsymmetric about the mean normal stress axis. White masonry concrete can withstand more deviatoric stress in compression than extension before failure occurs, which is typical behavior for concrete materials.

Uniaxial Strain Test Results

One-dimensional compressibility data were obtained from two undrained uniaxial strain (UX) tests with lateral stress measurements. Data from the tests are plotted in Figures 41-43. The stress-strain data from the UX tests are plotted in Figure 41, the pressure-volume data in Figure 42, and the stress paths with the failure surface data in Figure 43. The UX responses in Figures 41 and 42 are initially very stiff because of the cementitious bonds in WMC. When the cement was crushed, the compressibility responses softened, and the material compacted significantly. As the material became denser, compressibility stiffened.

From the UX stress-strain loading data (Figure 41), an initial constrained modulus of 12.5 GPa was calculated. UX data may also be plotted as principal stress difference versus mean normal stress; the slope of an elastic material in this space is 2G/K. A shear modulus of 5.2 GPa was calculated from the constrained modulus and the elastic bulk modulus (5.6 GPa) determined from the HC and

TXC tests. These two values may be used to calculate any of the other elastic constants. For example, the Young's modulus is 11.9 GPa and Poisson's ratio is 0.15.

The UX stress paths in Figure 43 have a steep initial stress path until almost reaching the TXC recommended failure surface. The stress paths soften after the material is crushed, causing the data to lie well below the failure surface. The pressure-volume responses from HC and UX tests are compared in Figure 44. Up to a volumetric strain of about 12 percent, the HC data are somewhat stiffer than the UX data. This implies that the UX state of stress is providing additional shear-induced compaction to the specimen. The differences in these responses at volumetric strains greater than 12 percent are caused by the differences in the dry densities of the specimens.

Strain Path Test Results

Three types of strain-path tests were conducted in this test program. UX/BX refers to tests with uniaxial strain loading followed by constant axial strain unloading. UX/CV refers to tests with uniaxial strain loading followed by constant volumetric strain loading. UX/SR refers to tests with uniaxial strain loading then continued loading along a constant ratio of axial strain to radial strain of -1.33.

Two UX/BX tests were conducted to a peak axial stress of approximately 200 MPa, and the other two tests were conducted to a peak axial stress of approximately 400 MPa. Data from the tests are plotted in Figures 45-48. The stress-strain data from the UX/BX tests are plotted in Figure 45, the pressure-volume data in Figure 46, the stress paths with the failure surface data in Figure 47, and the strain paths in Figure 48. The stress-strain response of the material (Figure 45) displays variations during the UX loading that are a function of the test specimens' initial dry densities. That is, stiffer loading responses resulted from specimens with higher dry densities. In addition, the stress-strain curves illustrate that the specimens were allowed to creep under zero-radial-strain boundary conditions prior to initiating the BX unloading. The pressure-volume data presented in Figure 46 illustrate the large amount of volume recovery that occurs during the BX unloading. Most of the specimens recover about one-third to one-half of their peak compressive volumetric strain. The stress paths plotted in Figure 47 are typical of most concretes. At the end of the UX loading and prior to the BX unloading, some stress relaxation occurred in the system, hence the slight unload just after peak stress (Figure 47). During the unloading, the stress paths show a small increase in principal stress difference followed by a significant decrease in stress difference with decreasing mean normal stress. This unloading appears to follow a limiting surface, which is normally the material's failure relation (the TXC recommend failure surface in most cases). In this case, the BX unloading exceeds the failure surface by an unusually large amount. The BX unloading exceeds the failure surface because the density of the specimen is increased during the UX loading prior to the BX unloading. The increased density of the specimens results in a higher limiting surface since the increased

density increases the strength of the material. Figure 48 shows the strain paths that were followed during the four tests.

Results from five UX/CV tests conducted to three different peak axial stresses during the initial UX phase are shown in Figures 49-52. The stress-strain data from the UX/CV tests are plotted in Figure 49, the pressure-volume data in Figure 50, the stress paths with the failure surface data in Figure 51, and the strain paths in Figure 52. The CV portions of the stress path data in Figure 51 initially exhibit an increase in stress difference with a slight decrease in mean normal stress and then follow the failure relation. For this series of tests, the CV portions of the data provide an excellent confirmation of the failure relation by following along the recommended TXC failure surface.

Data were obtained from two UX/SR tests that were loaded to approximately the same nominal peak axial stresses during the initial UX phase. Data from the tests are plotted in Figures 53-56. The stress-strain data from the UX/SR tests are plotted in Figure 53, the pressure-volume data in Figure 54, the stress paths with the failure surface in Figure 55, and the strain paths in Figure 56. The compressibility data from the UX/SR tests have small differences, a result of the slight difference of the dry densities for the test specimens. The plotted stress paths (Figure 55) demonstrate increasing values of principal stress difference and decreasing values of mean normal stress after the SR loading initiates. After reaching the material's limiting surface, both stress difference and mean normal stress decrease. The stress paths in Figure 55 confirm that the limiting surface for the UX/SR tests is similar to the material's recommended TXC failure surface.

Comparison plots of the results of selected UX, UX/BX, UX/CV, and UX/SR tests are plotted in Figures 57-60. The stress-strain data are plotted in Figure 57, the pressure-volume data are plotted in Figure 58, the stress paths with the failure surface are plotted in Figure 59, and the strain-paths are plotted in Figure 60. As seen in other test results, Figure 57 displays the effect of the material's dry density on the initial stiffness of the curves during the UX loading, i.e., increased stiffness with increased dry density. The following statements provide an interpretation of the measured pressure-volume data during the strain paths. When loading along the constant volume strain path, the specimens want to increase in volume because of the material's inherent shear-induced dilation characteristics. Increasing levels of pressure are required to maintain constant volume boundary conditions (Figure 58). The material's behavior while loading along a constant strain ratio path displays decreasing pressure and decreasing volumetric strain. The specimen does not want to expand faster than the boundary conditions permit, unlike the specimens loaded along the constant-volume strain path. To maintain the boundary conditions during the UX/SR tests, the pressure is reduced. The boundary conditions applied during the BX unloading require significant amounts of volume expansion. To maintain the boundary conditions, pressure must be reduced. In Figure 59, one stress path for each of the different strain path tests and the TXC failure surface are overlaid to illustrate the merger of the data in the vicinity of a failure surface. The convergence of the data from the UX/CV tests and the UX/SR tests validates both the TXC failure data and the strain-path data.

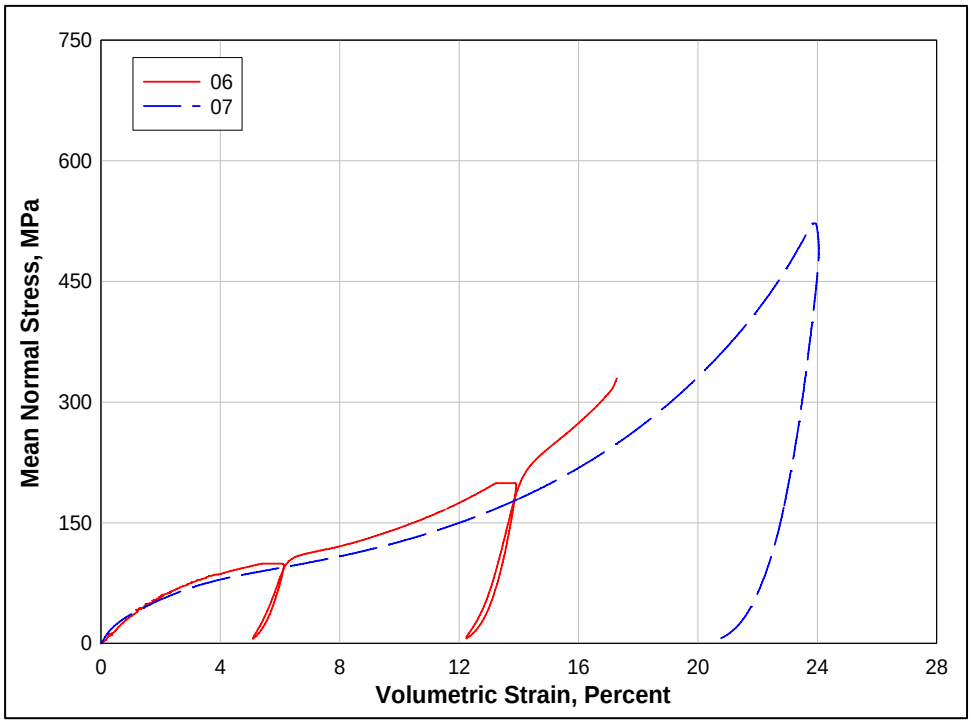

Figure 4. Pressure-volume responses from the HC tests

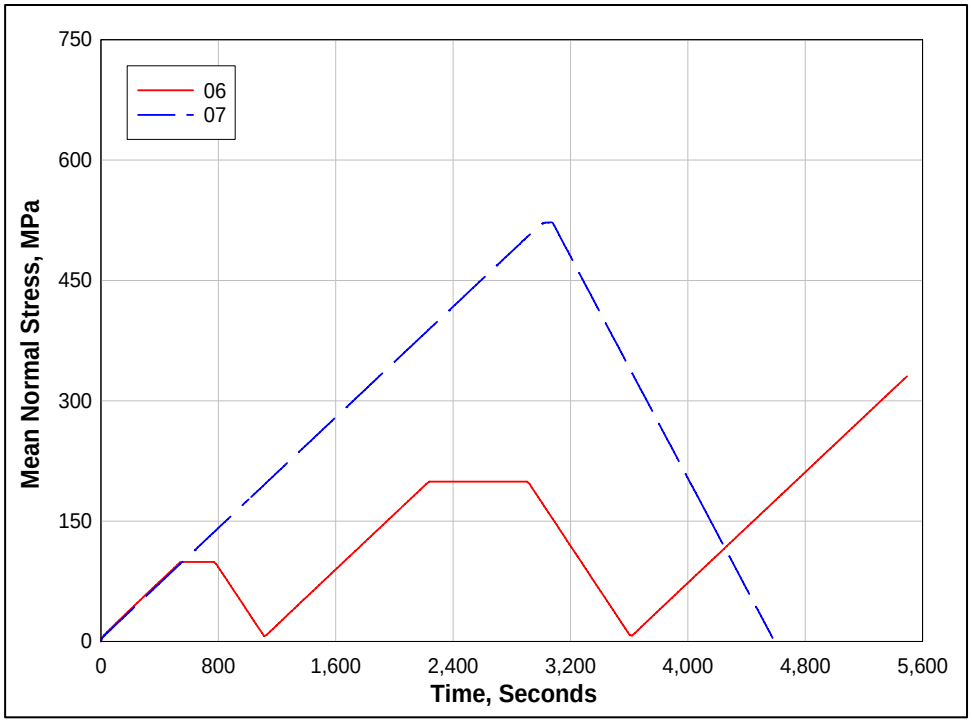

Figure 5. Pressure time-histories from the HC tests

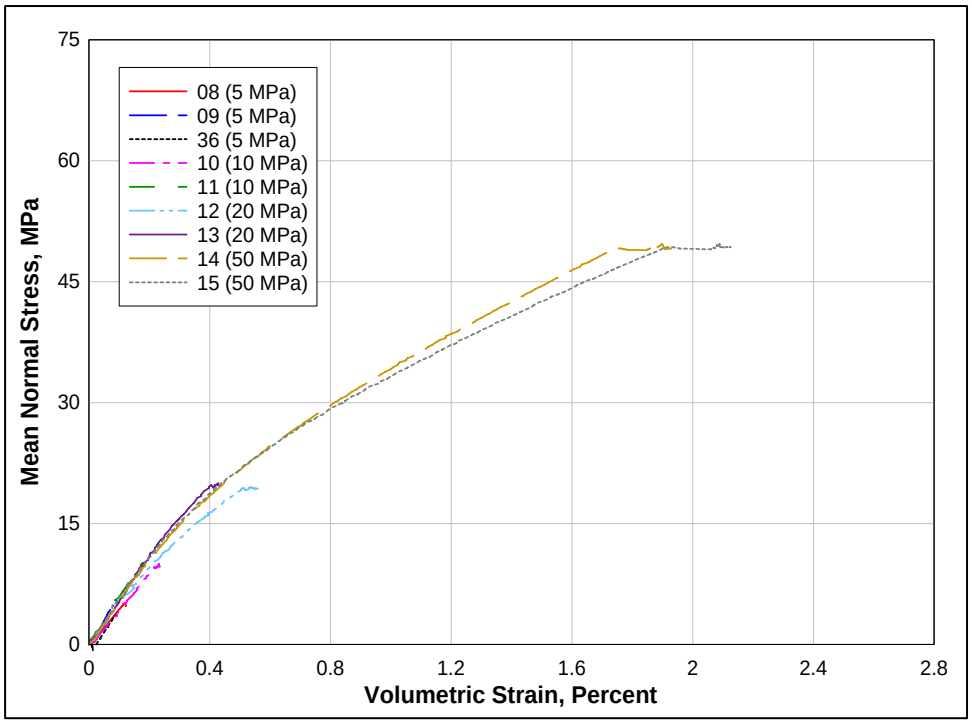

Figure 6. Pressure-volume responses from selected TXC tests

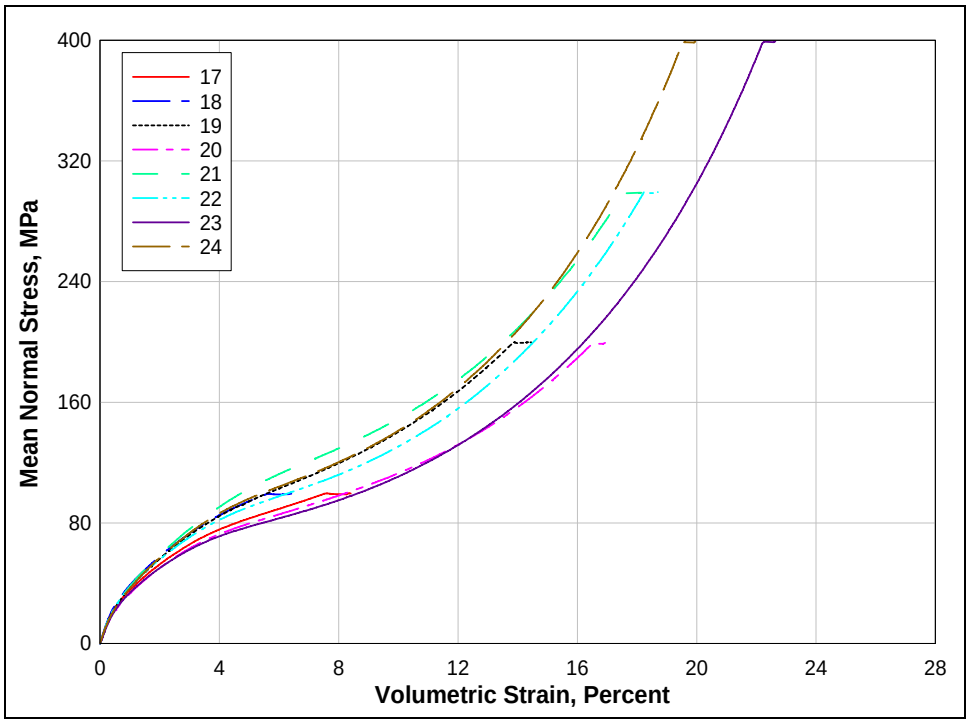

Figure 7. Pressure-volume responses from selected TXC tests

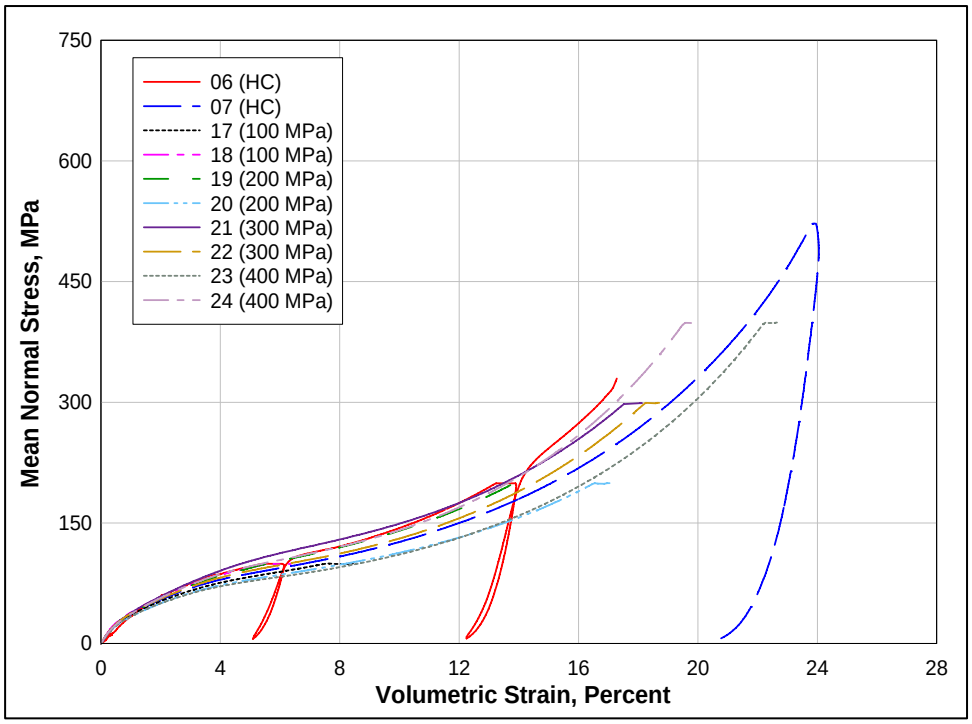

Figure 8. Pressure-volume responses from HC and TXC tests

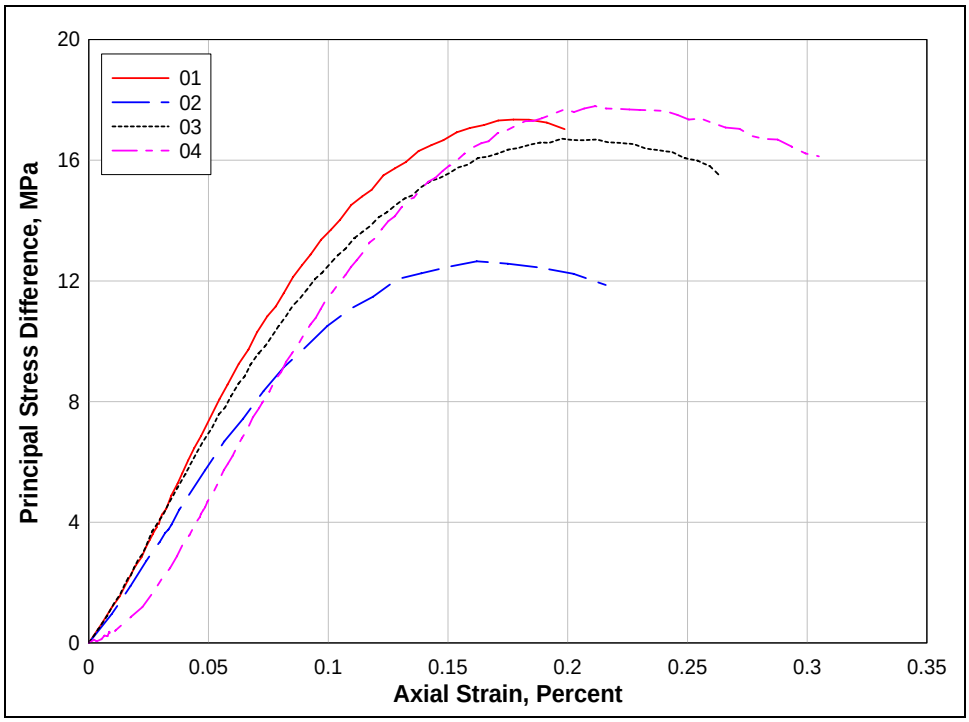

Figure 9. Stress-strain curves from UC tests

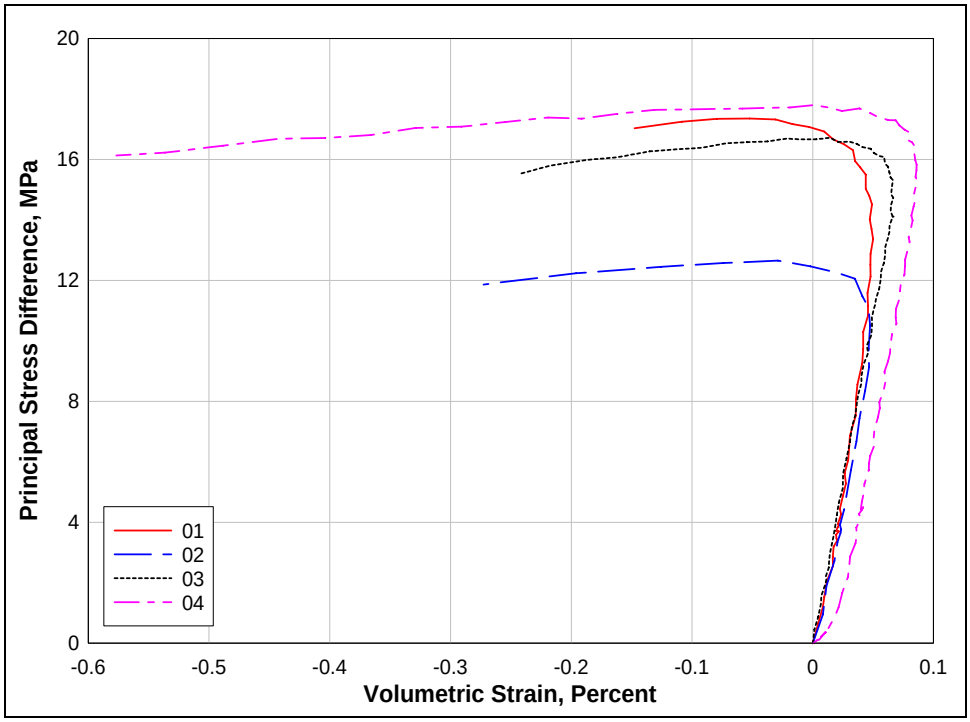

Figure 10. Stress difference-volumetric strain during shear from UC tests

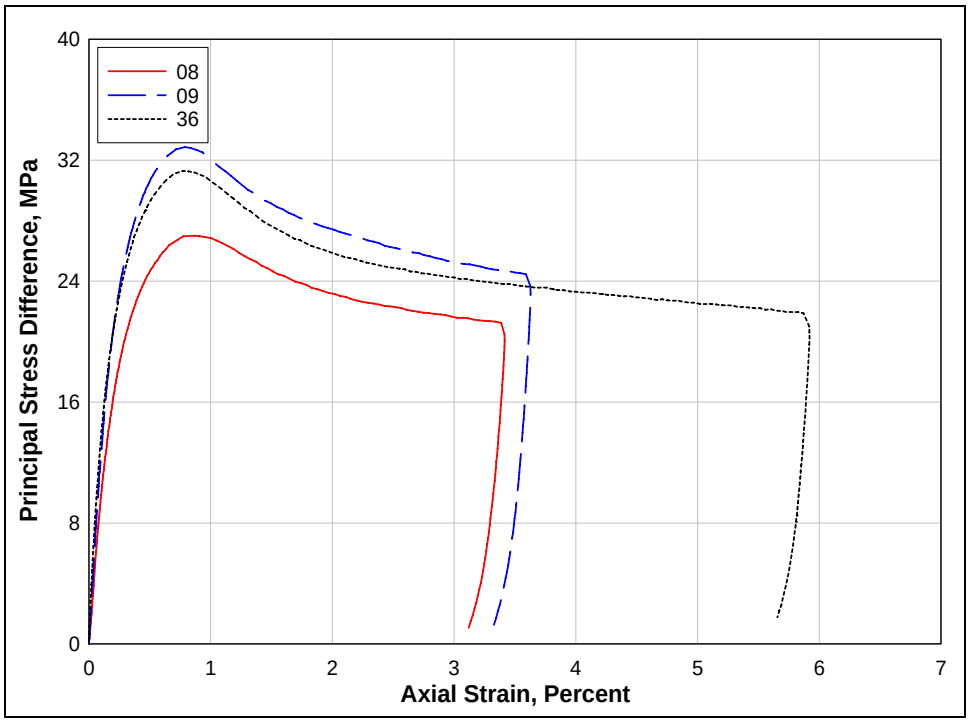

Figure 11. Stress-strain curves from TXC tests at a confining pressure of 5 MPa

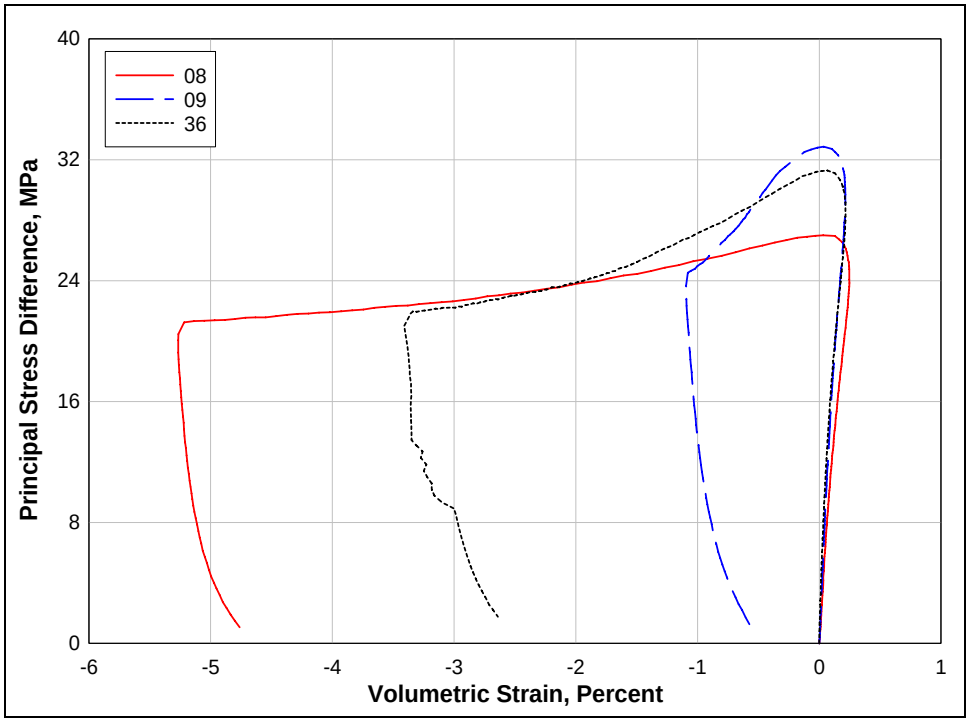

Figure 12. Stress difference-volumetric strain during shear from TXC tests at a confining pressure of 5 MPa

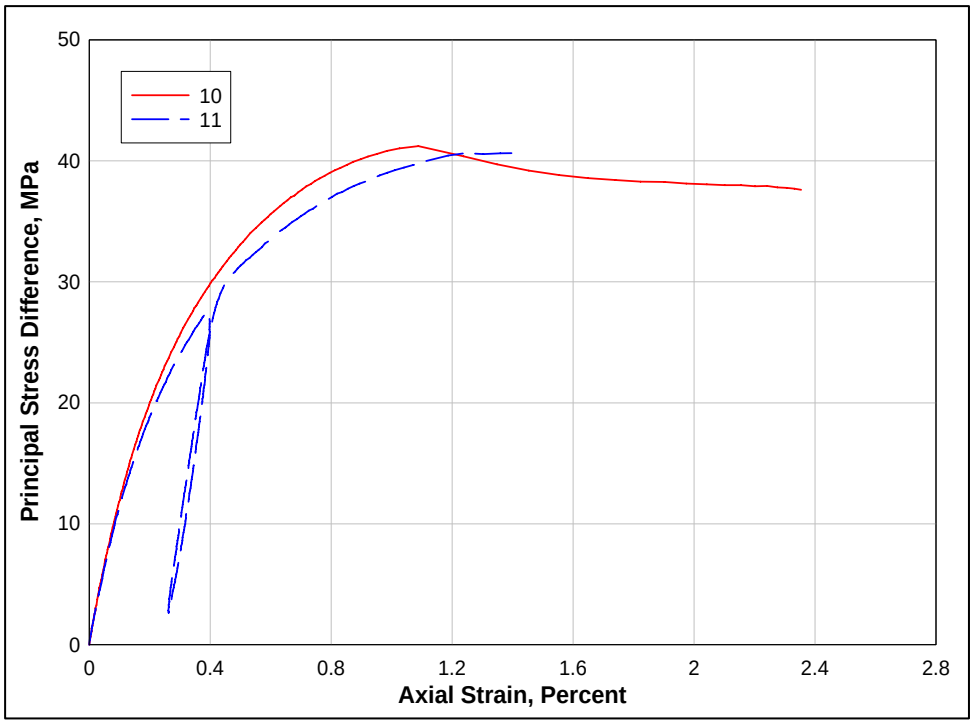

Figure 13. Stress-strain curves from TXC tests at a confining pressure of 10 MPa

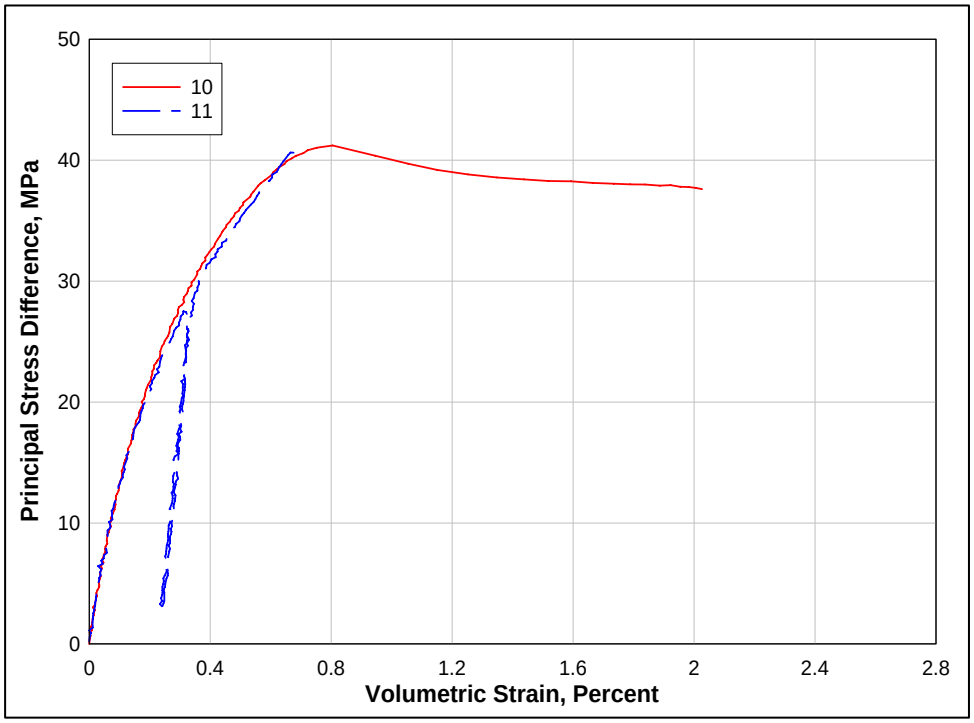

Figure 14. Stress difference-volumetric strain during shear from TXC tests at a confining pressure of 10 MPa

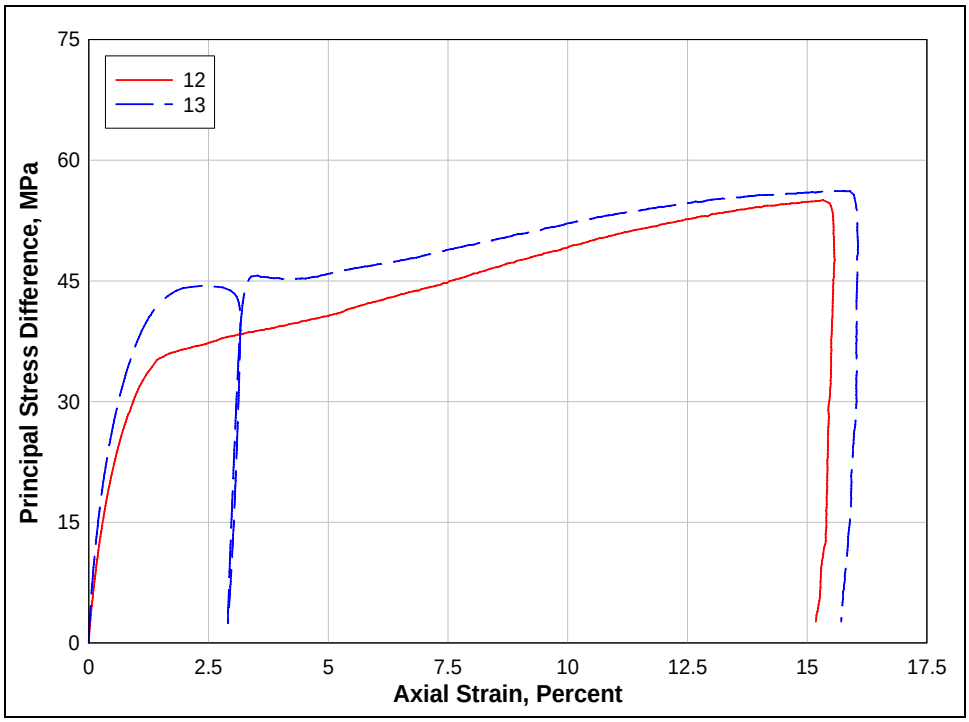

Figure 15. Stress-strain curves from TXC tests at a confining pressure of 20 MPa

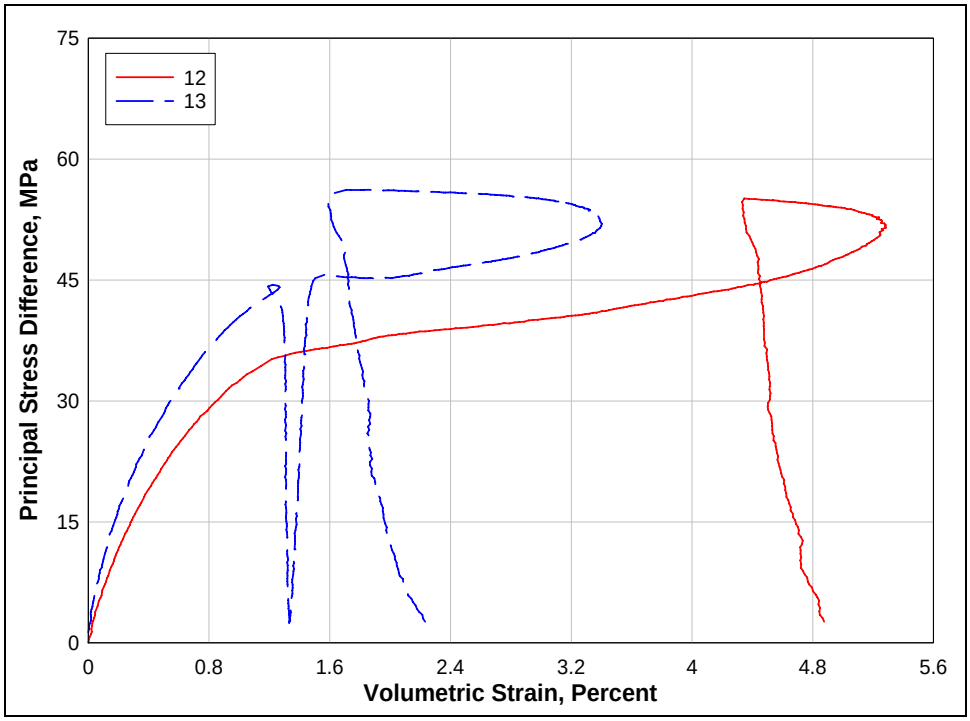

Figure 16. Stress difference-volumetric strain during shear from TXC tests at a confining pressure of 20 MPa

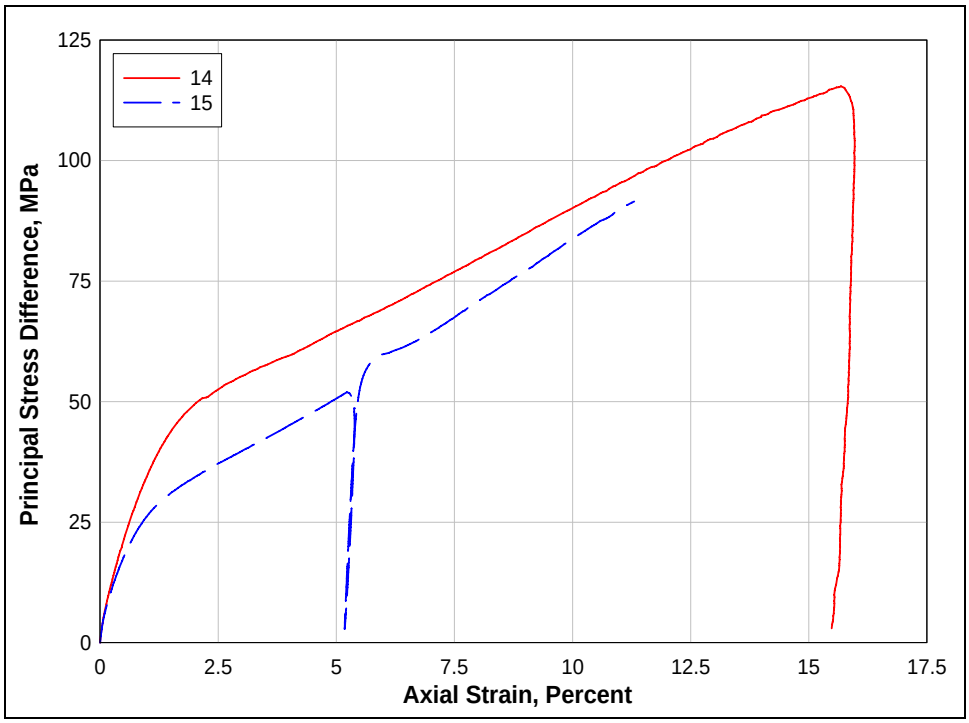

Figure 17. Stress-strain curves from TXC tests at a confining pressure of 50 MPa

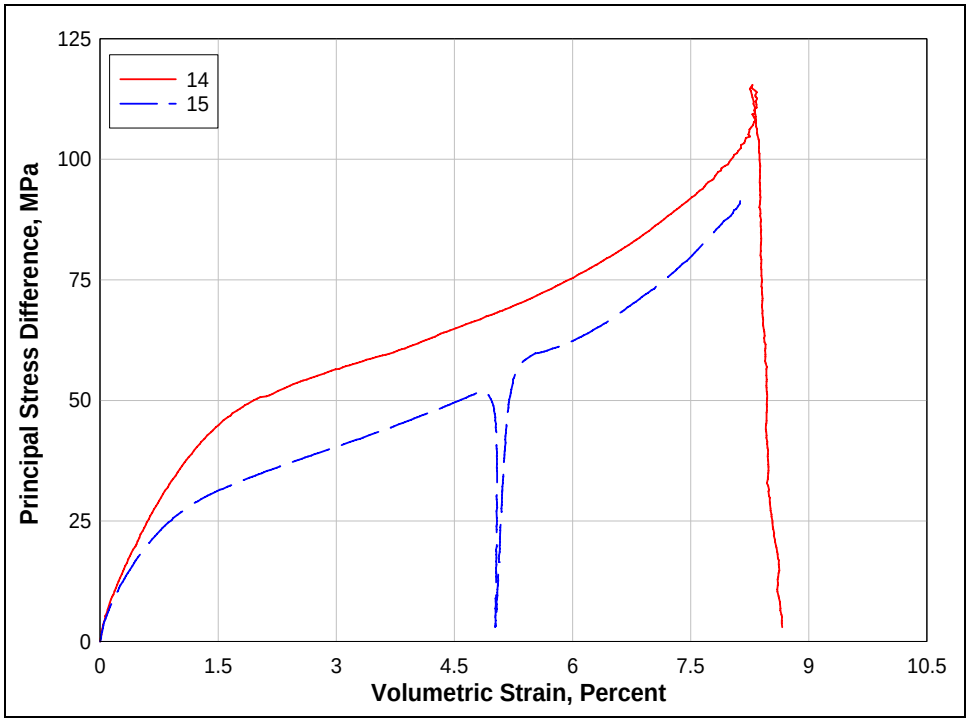

Figure 18. Stress difference-volumetric strain during shear from TXC tests at a confining pressure of 50 MPa

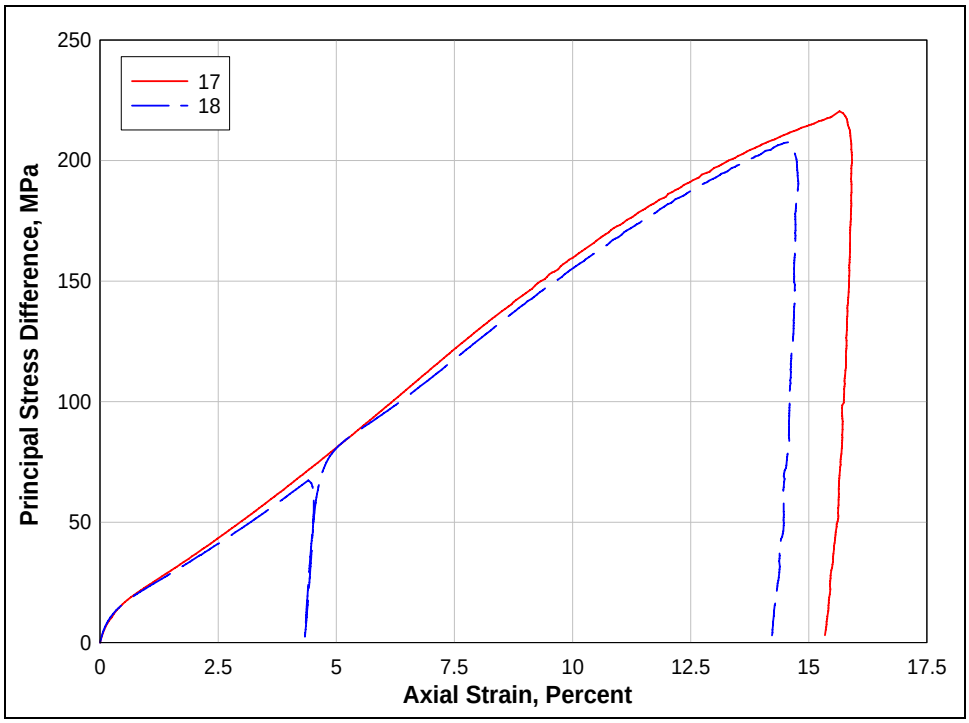

Figure 19. Stress-strain curves from TXC tests at a confining pressure of 100 MPa

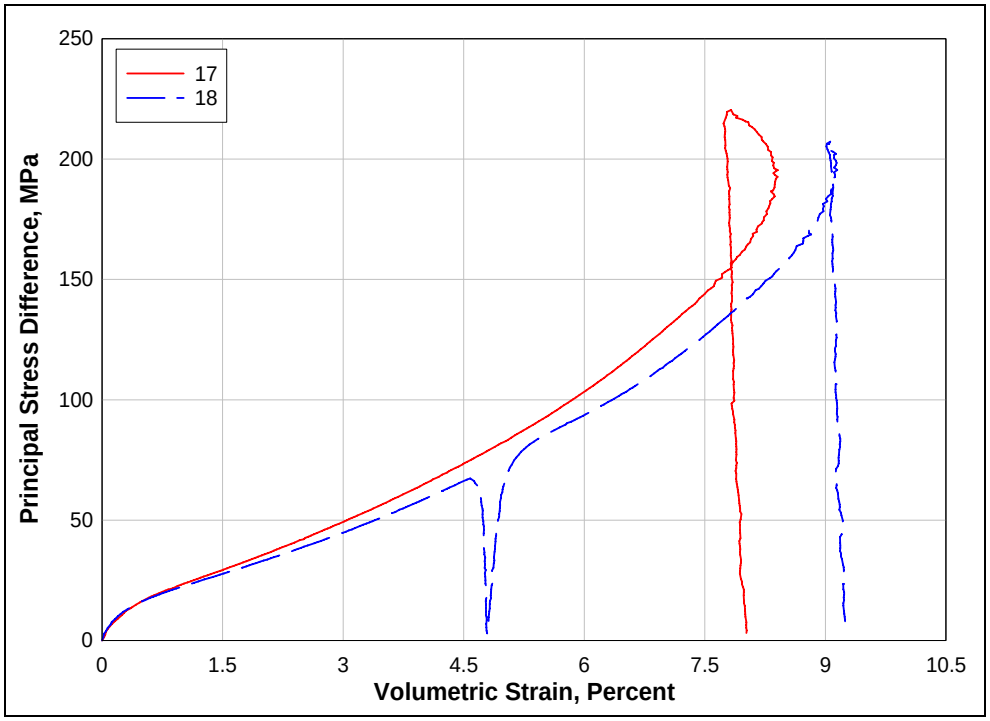

Figure 20. Stress difference-volumetric strain during shear from TXC tests at a confining pressure of 100 MPa

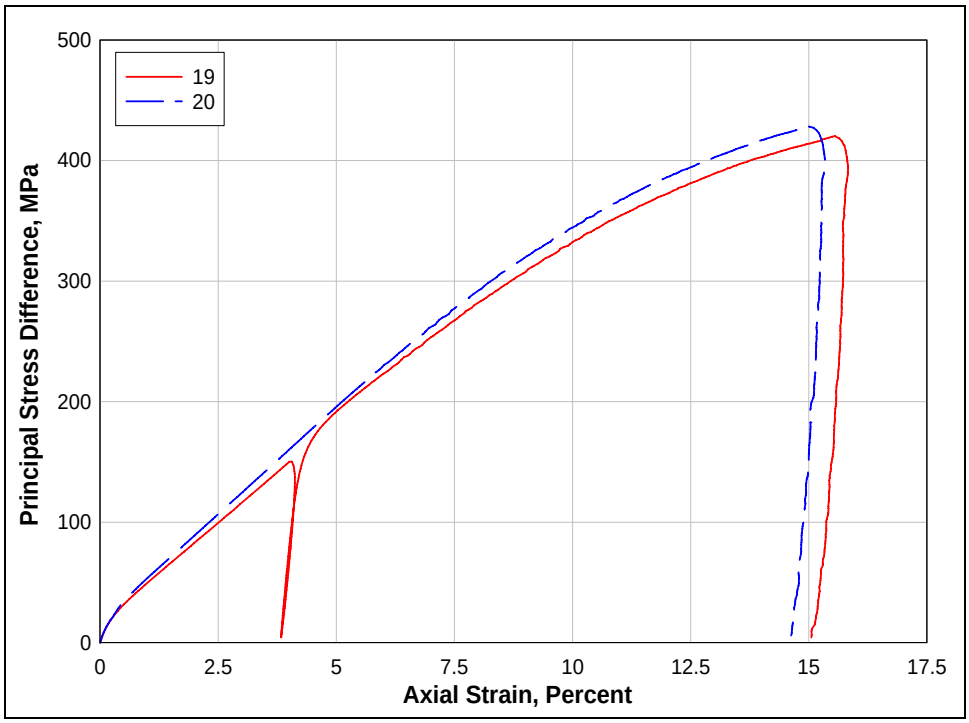

Figure 21. Stress-strain curves from TXC tests at a confining pressure of 200 MPa

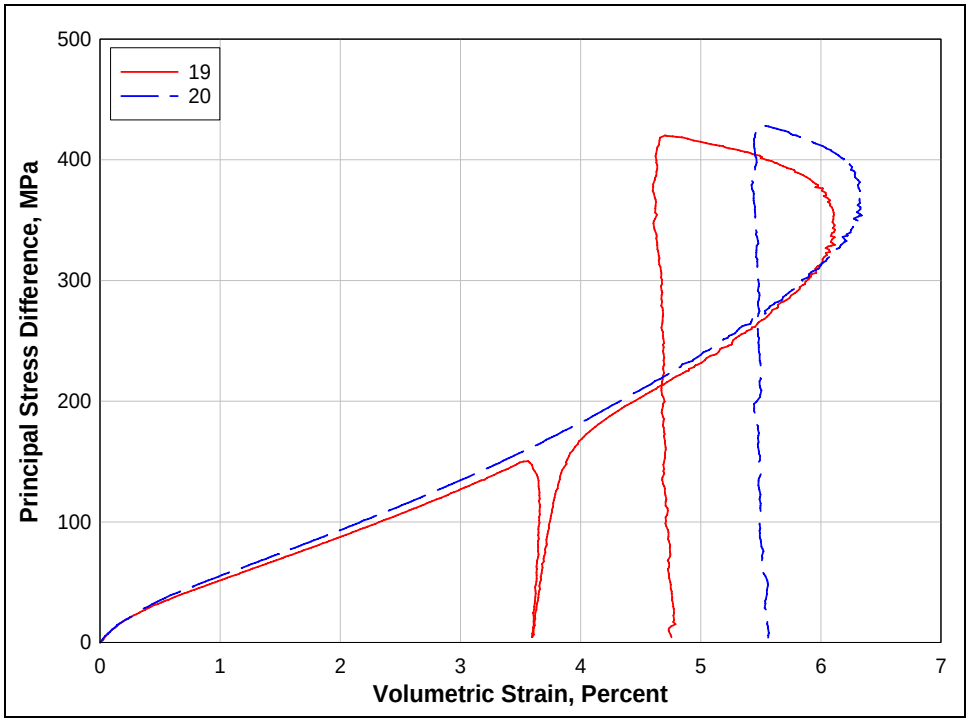

Figure 22. Stress difference-volumetric strain during shear from TXC tests at a confining pressure of 200 MPa

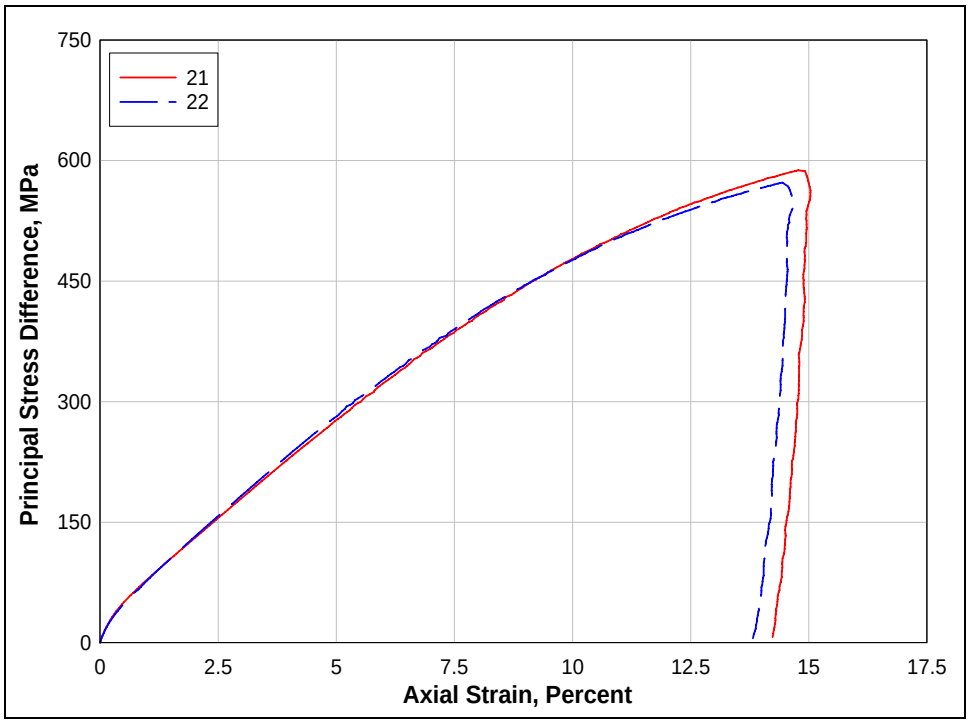

Figure 23. Stress-strain curves from TXC tests at a confining pressure of 300 MPa

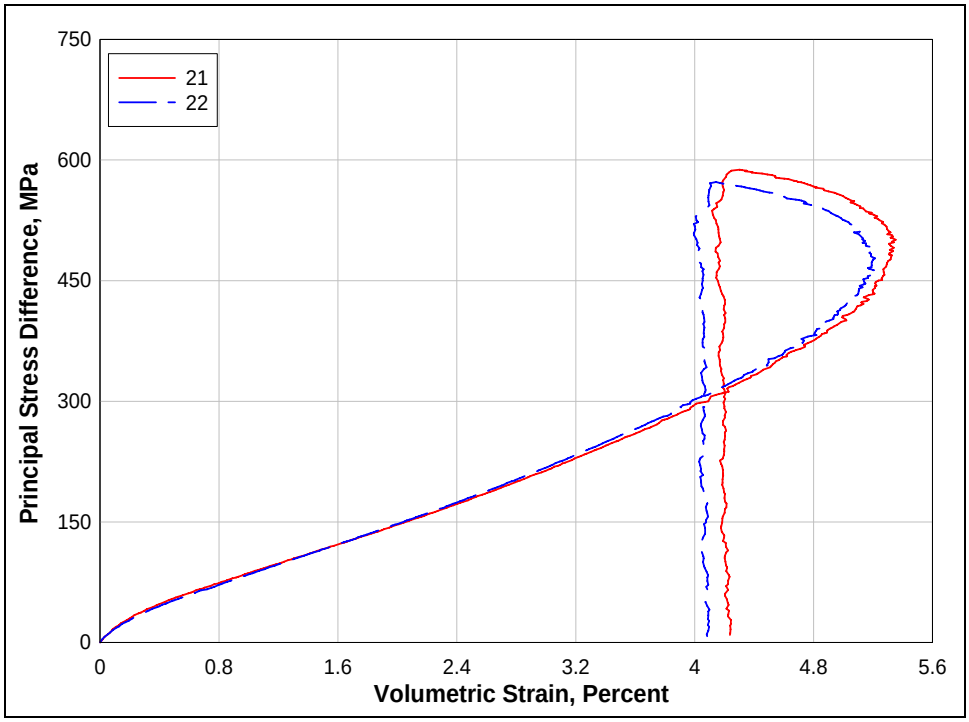

Figure 24. Stress difference-volumetric strain during shear from TXC tests at a confining pressure of 300 MPa

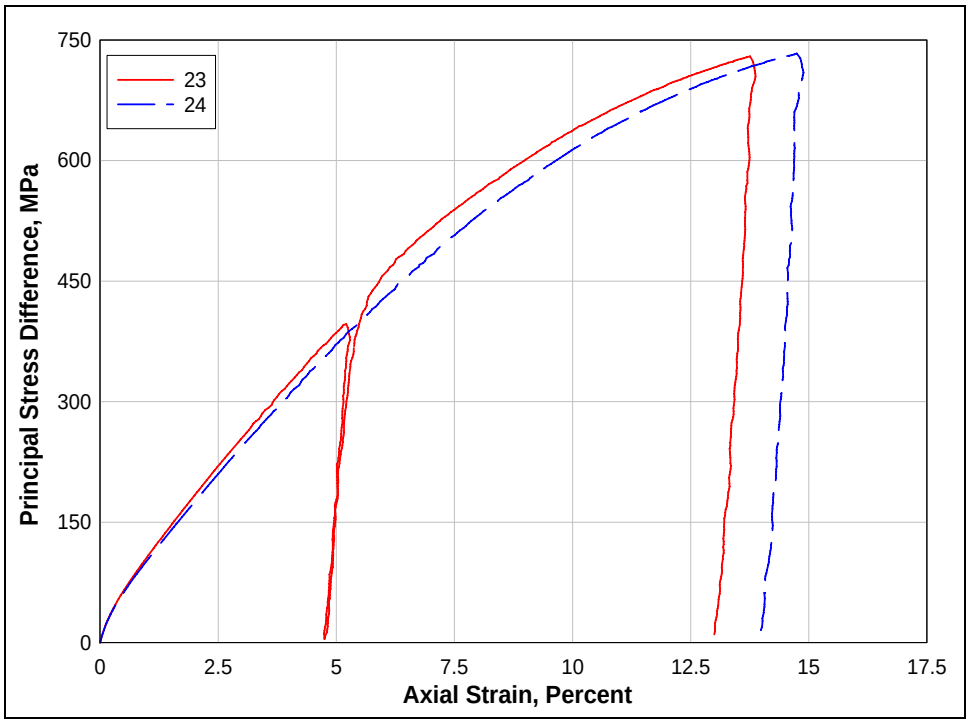

Figure 25. Stress-strain curves from TXC tests at a confining pressure of 400 MPa

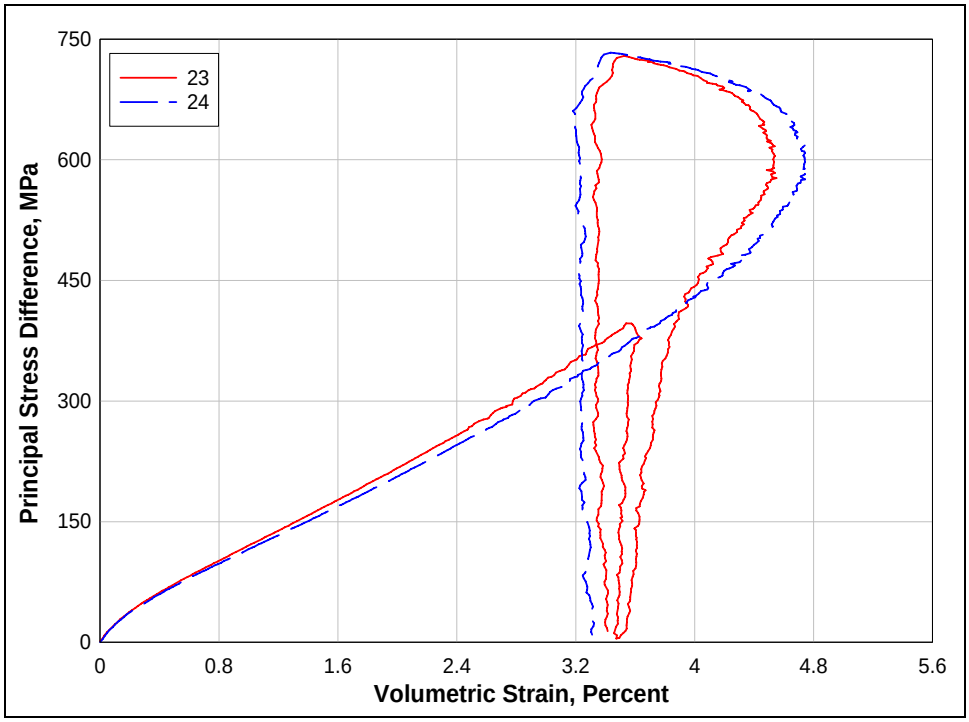

Figure 26. Stress difference-volumetric strain during shear from TXC tests at a confining pressure of 400 MPa

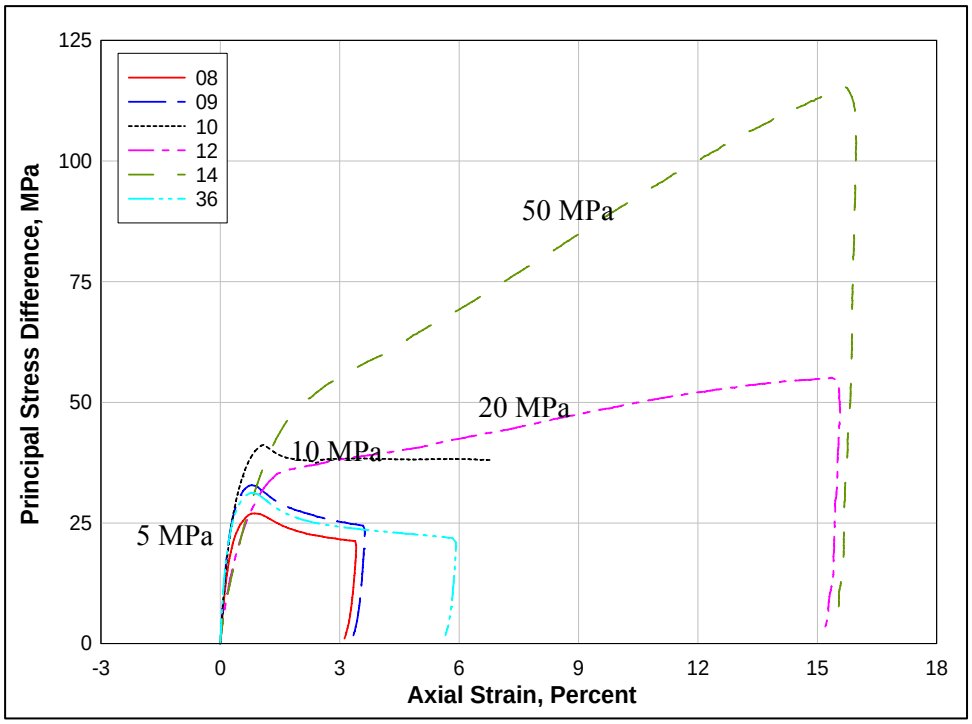

Figure 27. Stress-strain data from TXC non-cyclic tests at confining pressures between 5 and 50 MPa

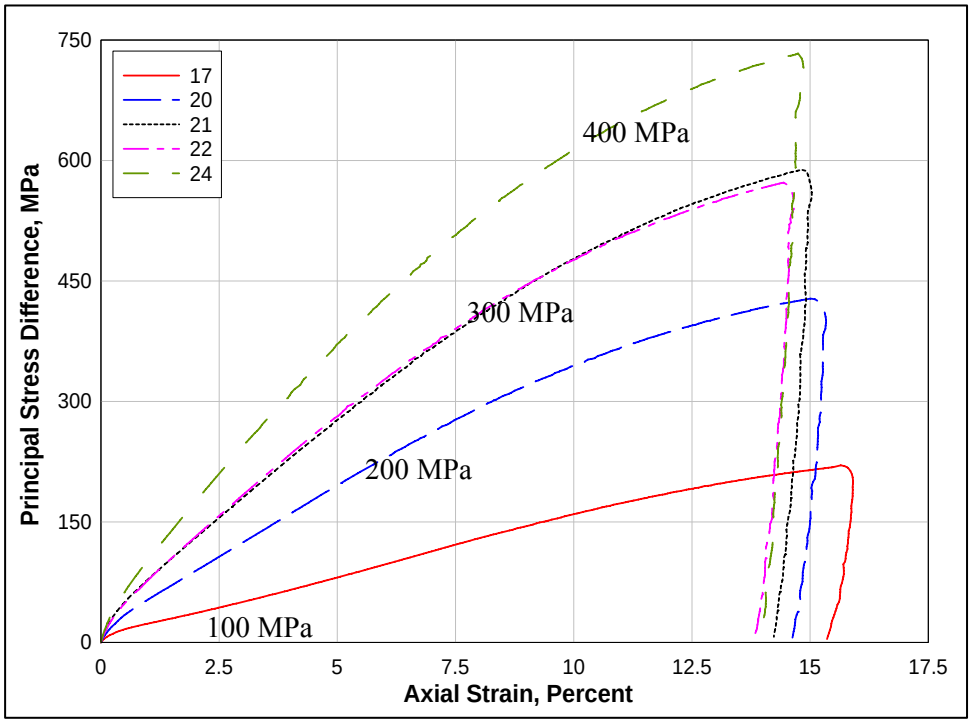

Figure 28. Stress-strain data from TXC non-cyclic tests at confining pressures between 100 and 400 MPa

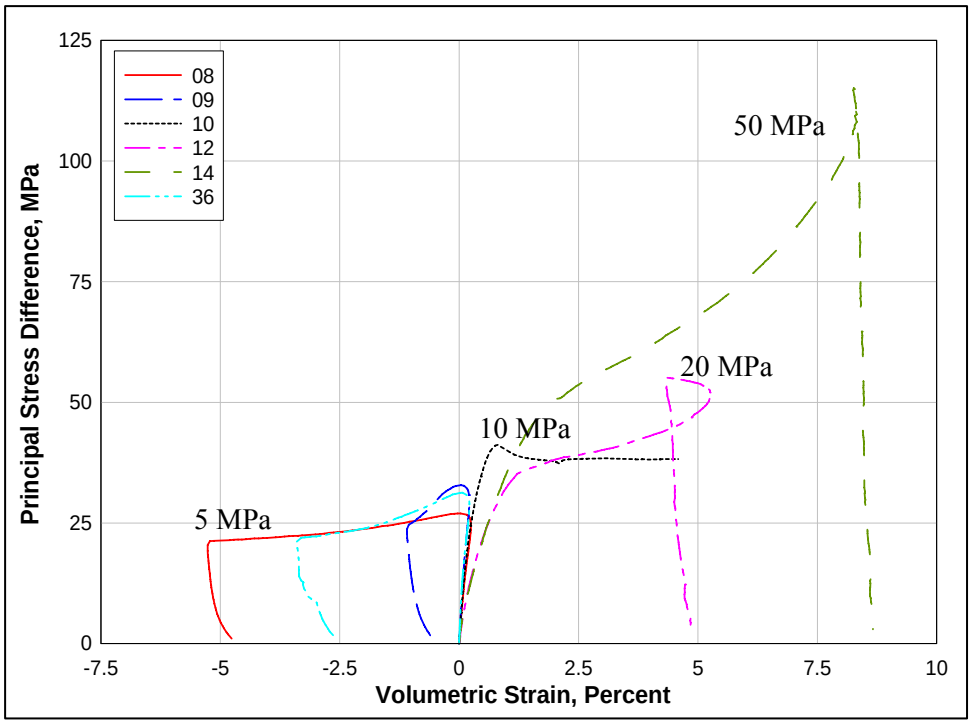

Figure 29. Stress difference-volumetric strain during shear from TXC non-cyclic tests at confining pressures between 5 and 50 MPa

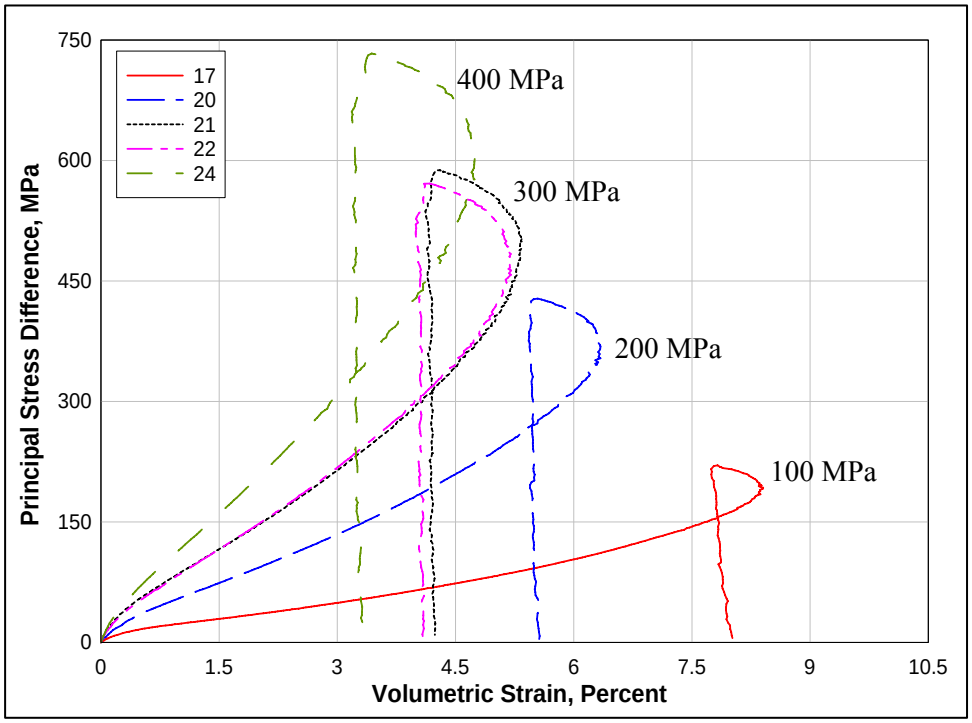

Figure 30. Stress difference-volumetric strain during shear from TXC non-cyclic tests at confining pressures between 100 and 400 MPa

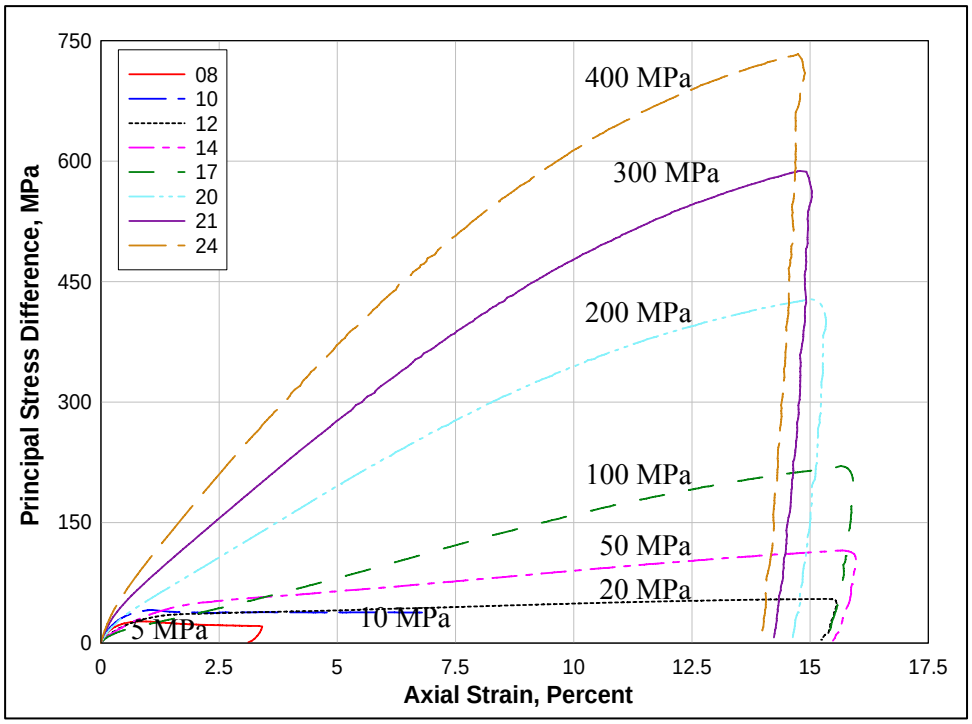

Figure 31. Stress-strain data from TXC non-cyclic tests at confining pressures between 5 and 400 MPa

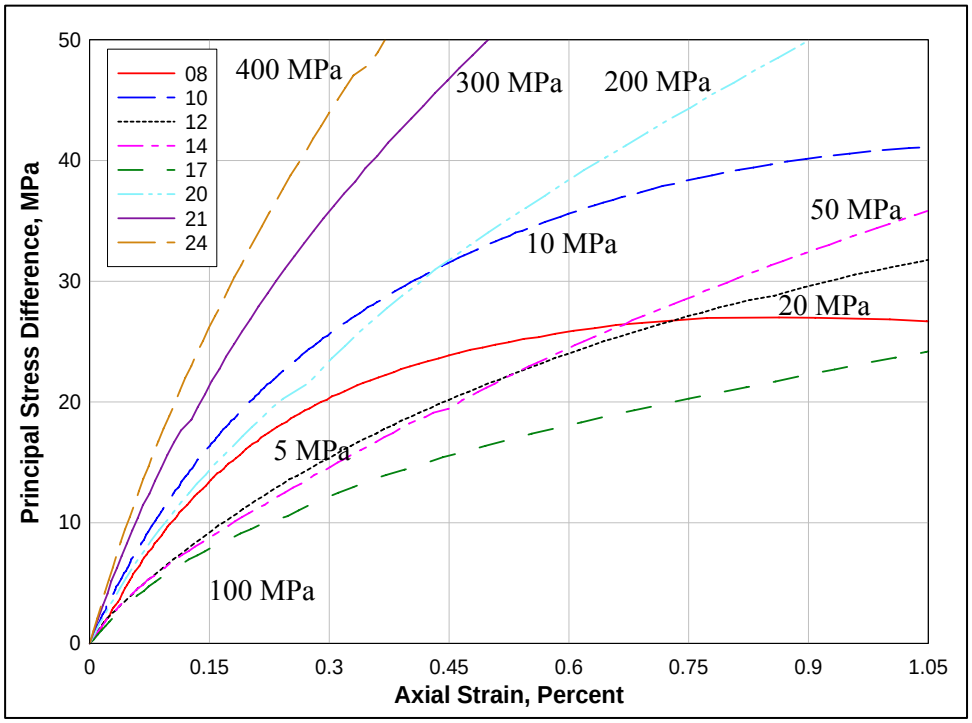

Figure 32. Initial loading stress-strain data from TXC non-cyclic tests at confining pressures between 5 and 400 MPa

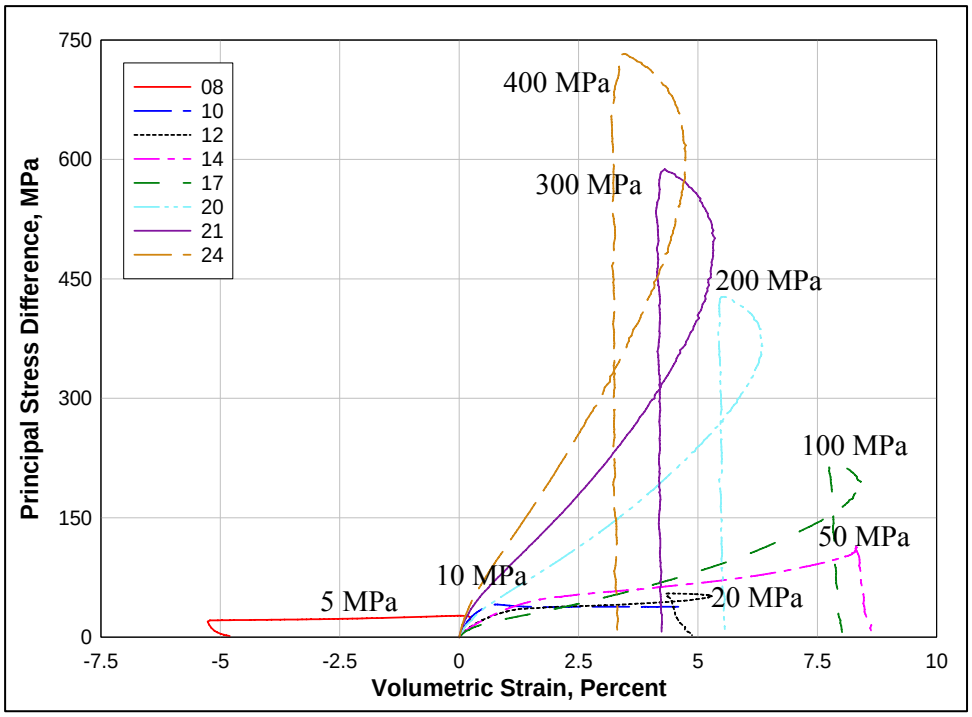

Figure 33. Stress difference-volumetric strain during shear from TXC non-cyclic tests at confining pressures between 5 and 400 MPa

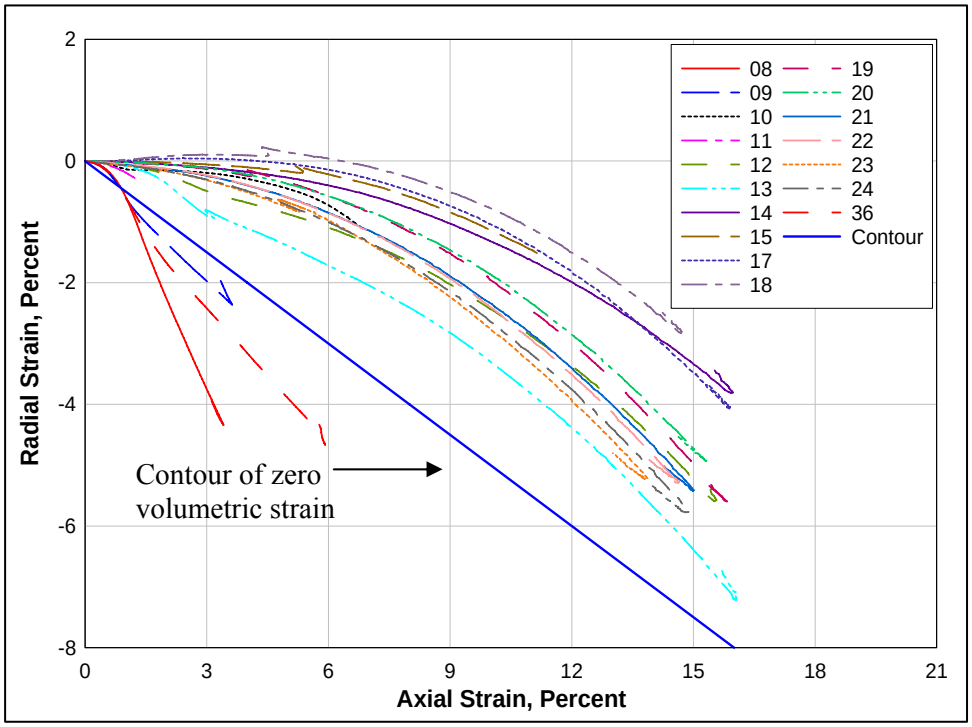

Figure 34. Radial strain-axial strain data during shear from TXC tests at confining pressures between 5 and 400 MPa

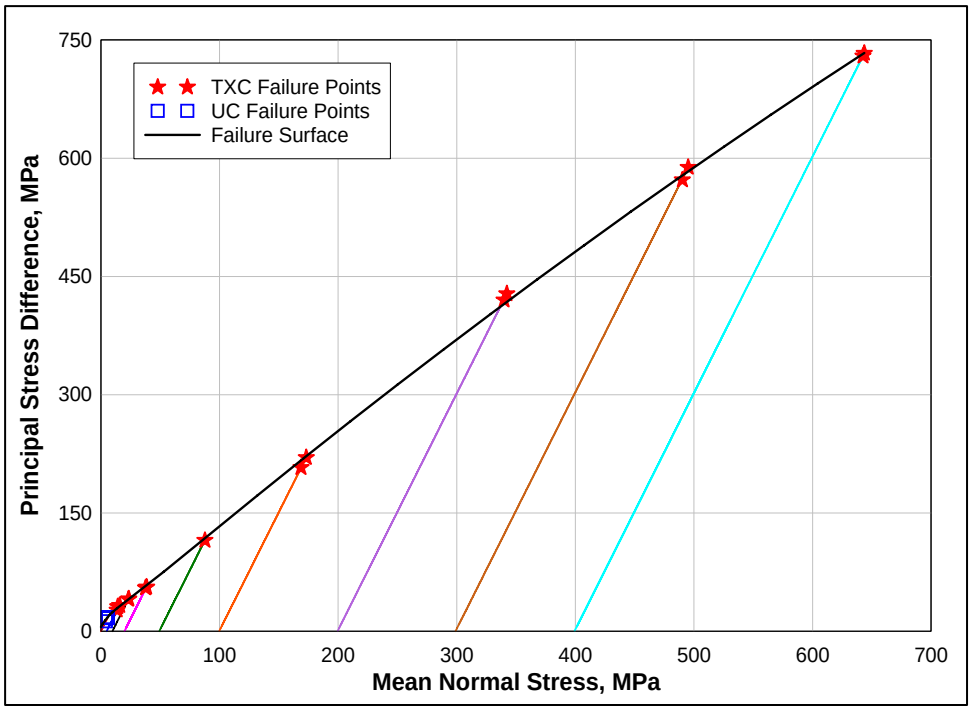

Figure 35. Failure points from UC and TXC tests and recommended failure surface

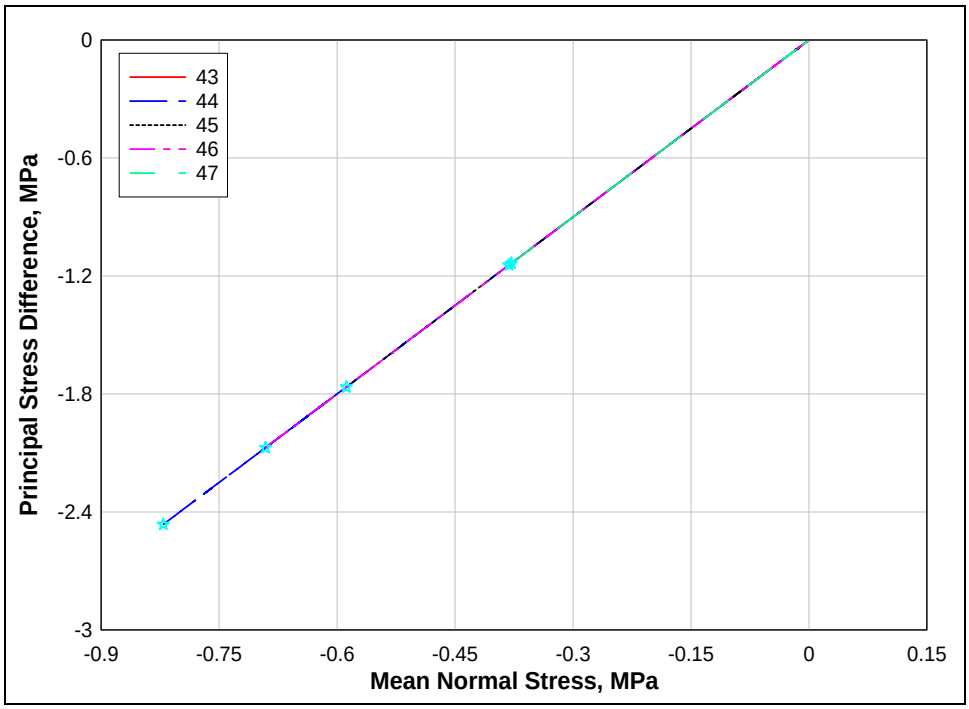

Figure 36. Stress paths from DP tests

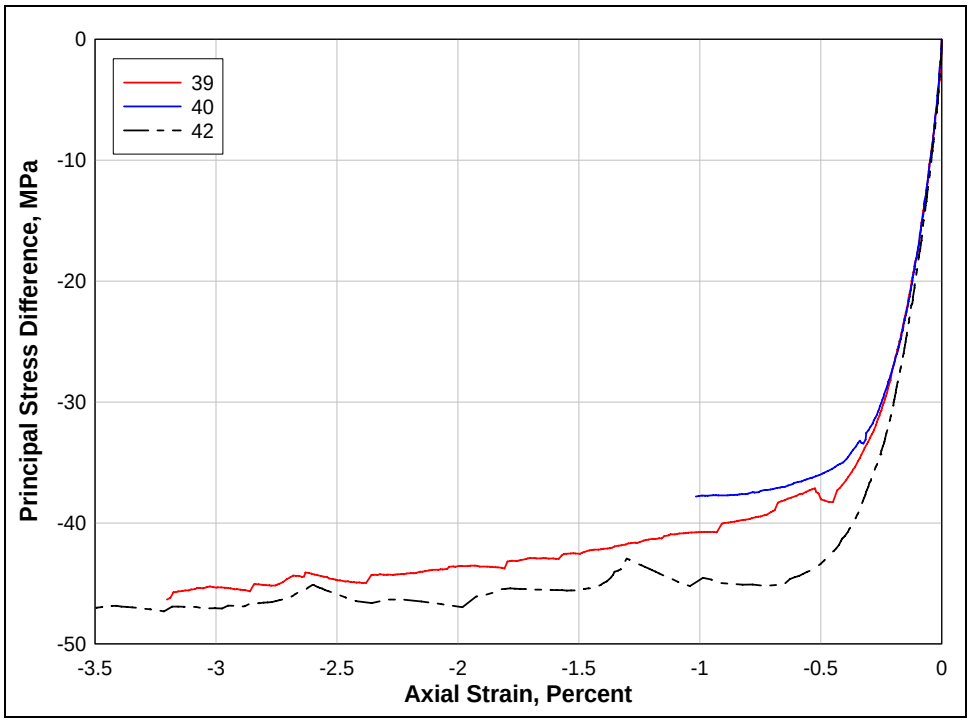

Figure 37. Stress-strain curves from RTE tests

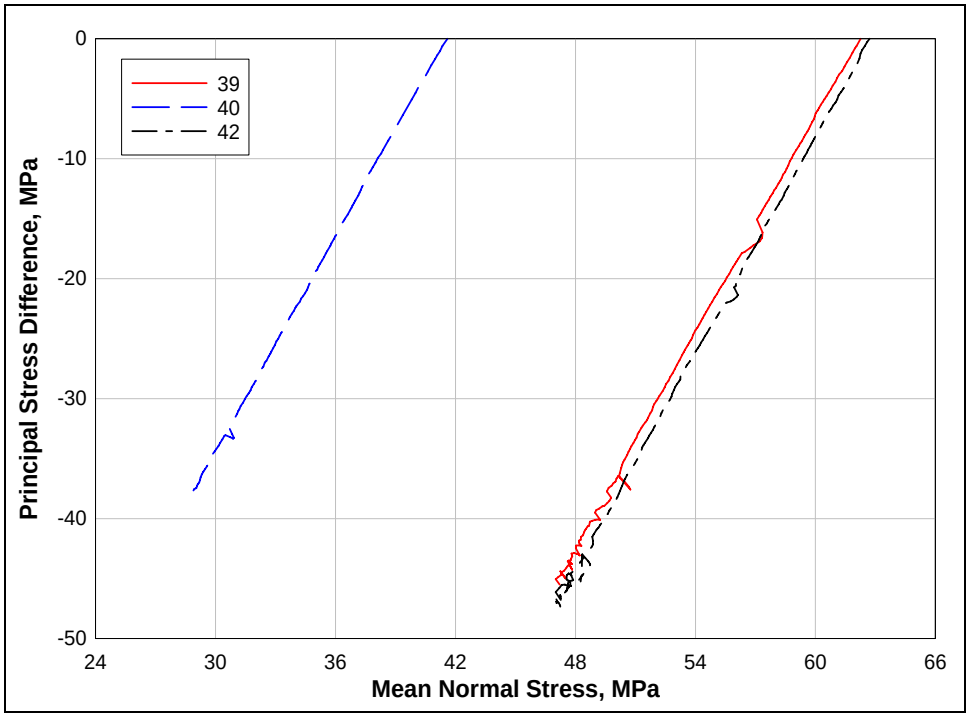

Figure 38. Stress paths from RTE tests

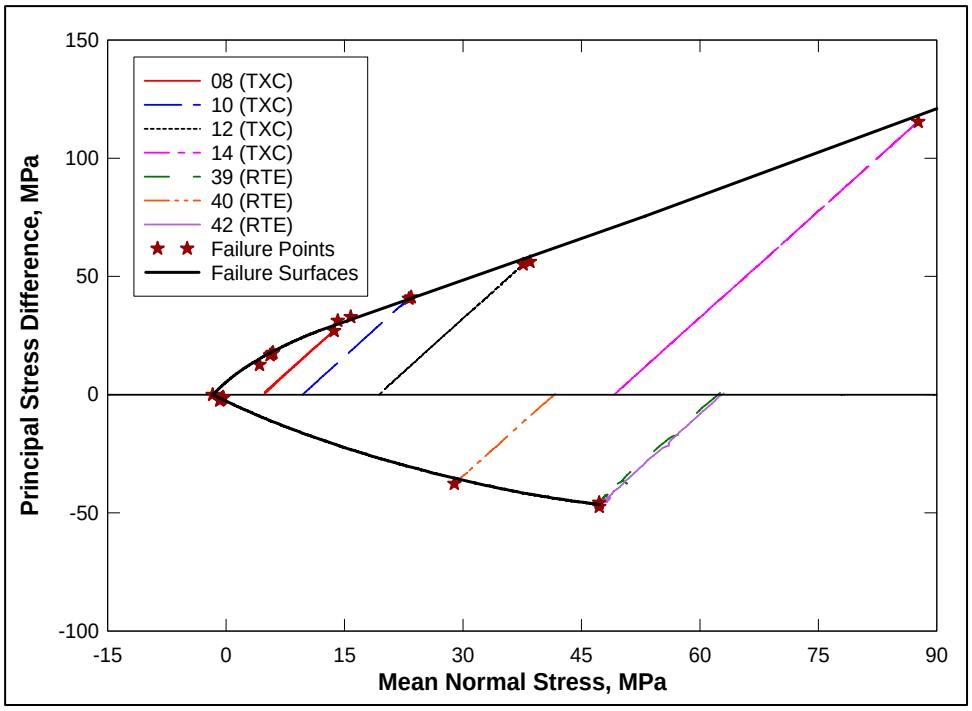

Figure 39. Failure surfaces and stress paths from RTE tests, UC tests and the TXC tests between 5 to 50 MPa

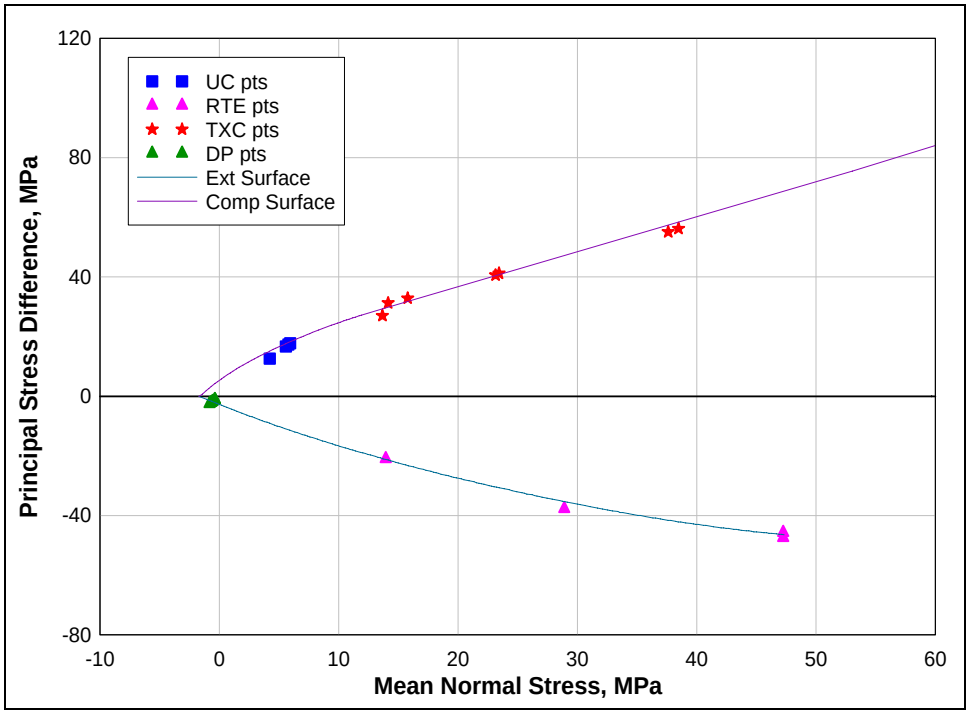

Figure 40. Compression and extension failure surfaces and failure data points from UC, TXC test 5 – 20 MPa, RTE, and DP tests

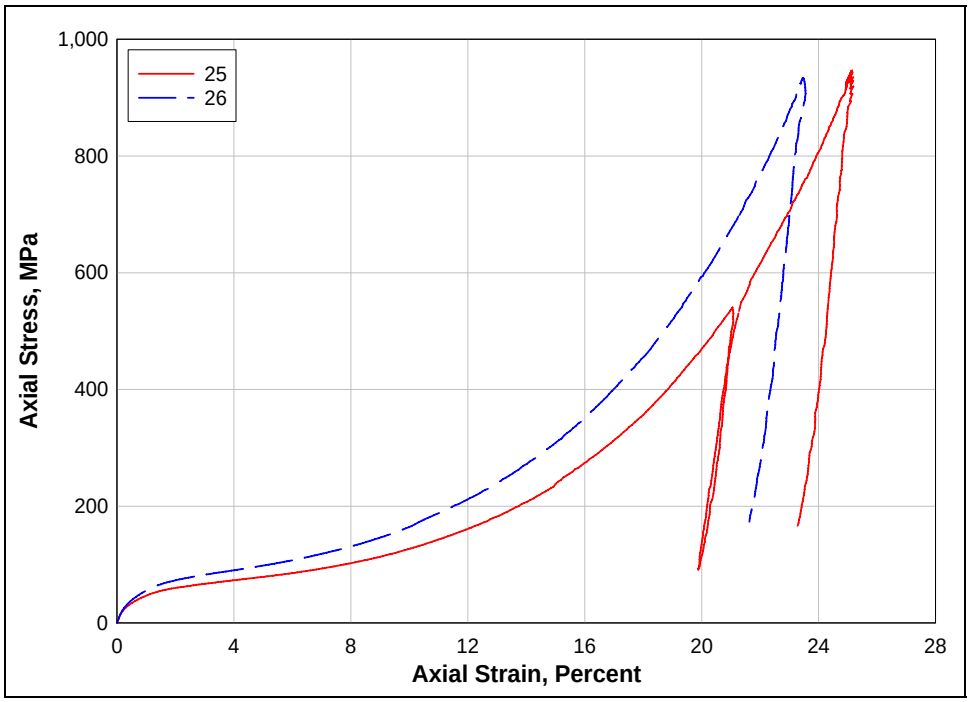

Figure 41. Stress-strain curves from UX tests

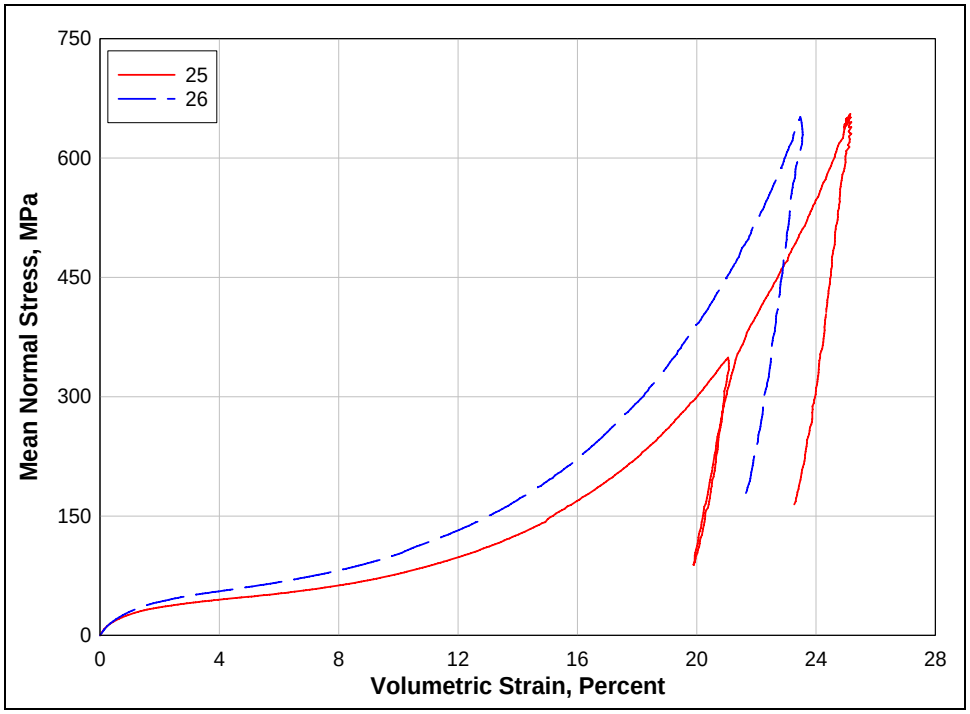

Figure 42. Pressure-volume data from UX tests

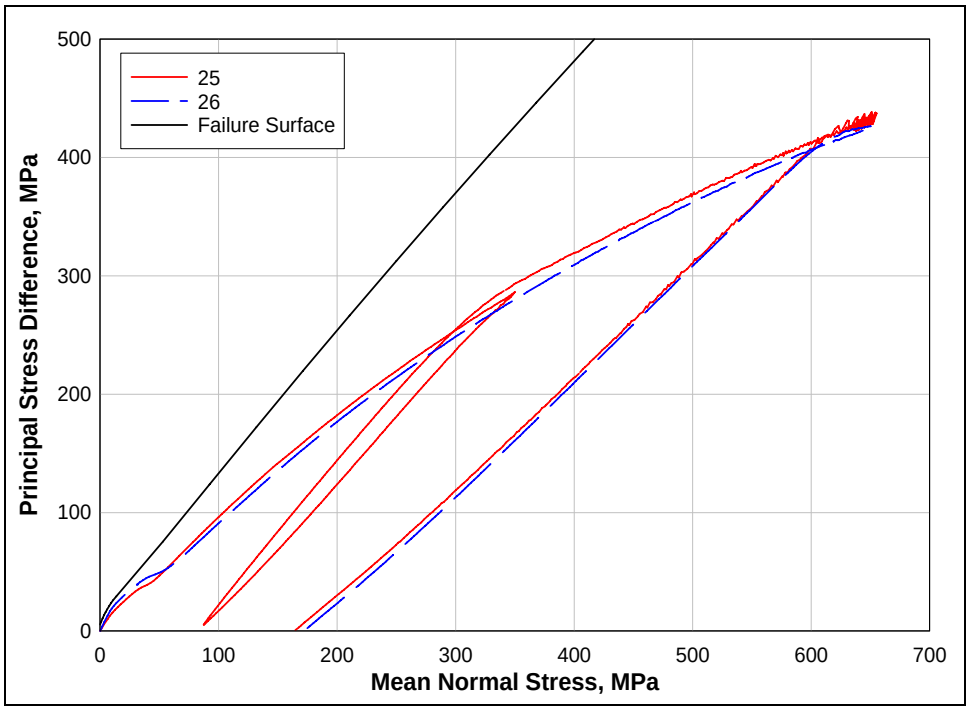

Figure 43. Stress paths from UX tests and failure surface from TXC tests

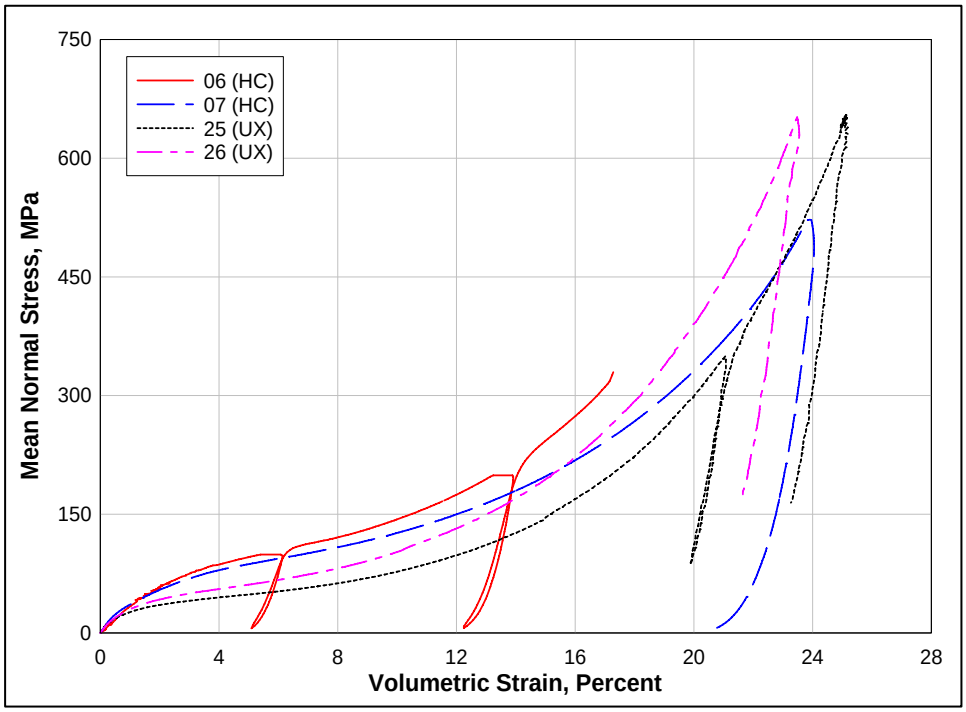

Figure 44. Comparison of pressure-volume data from HC and UX tests

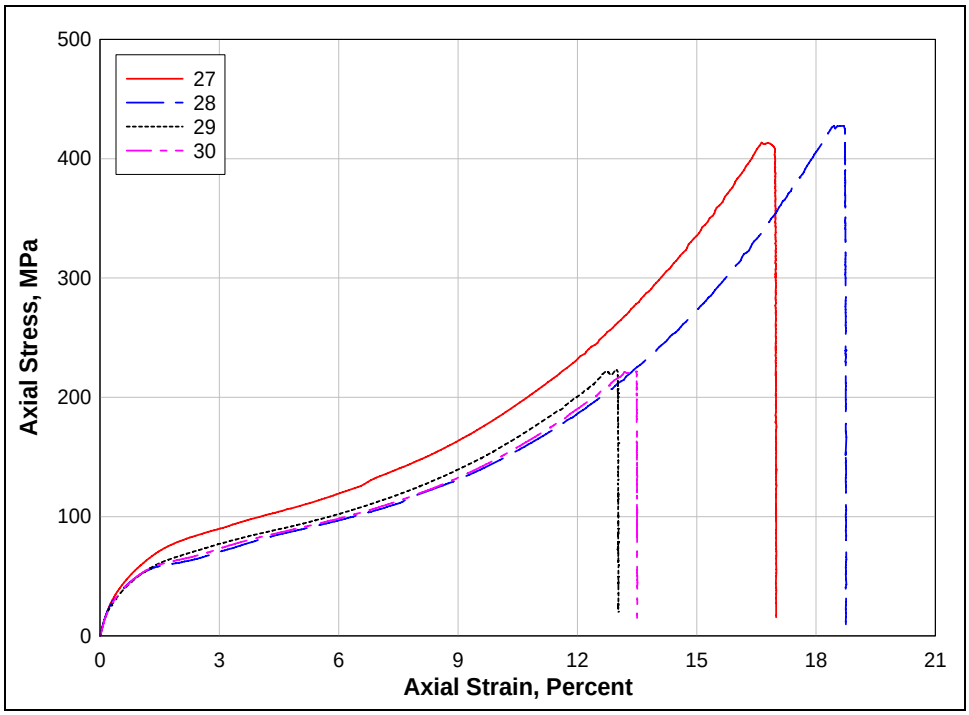

Figure 45. Stress-strain curves from UX/BX tests

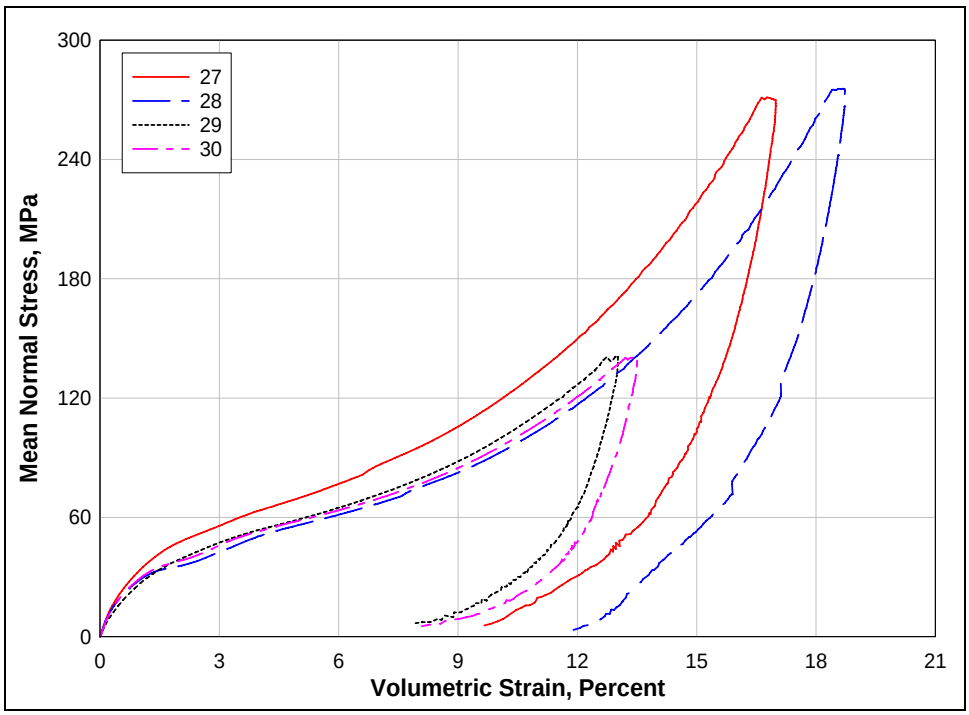

Figure 46. Pressure-volume data from UX/BX tests

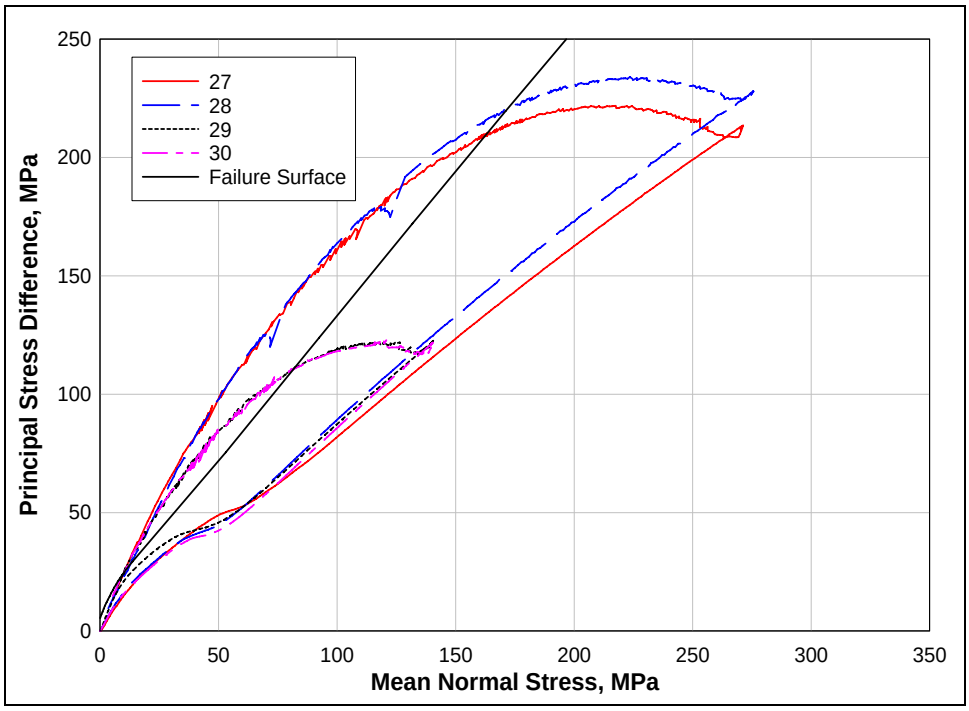

Figure 47. Stress paths from UX/BX tests and failure surface from TXC tests

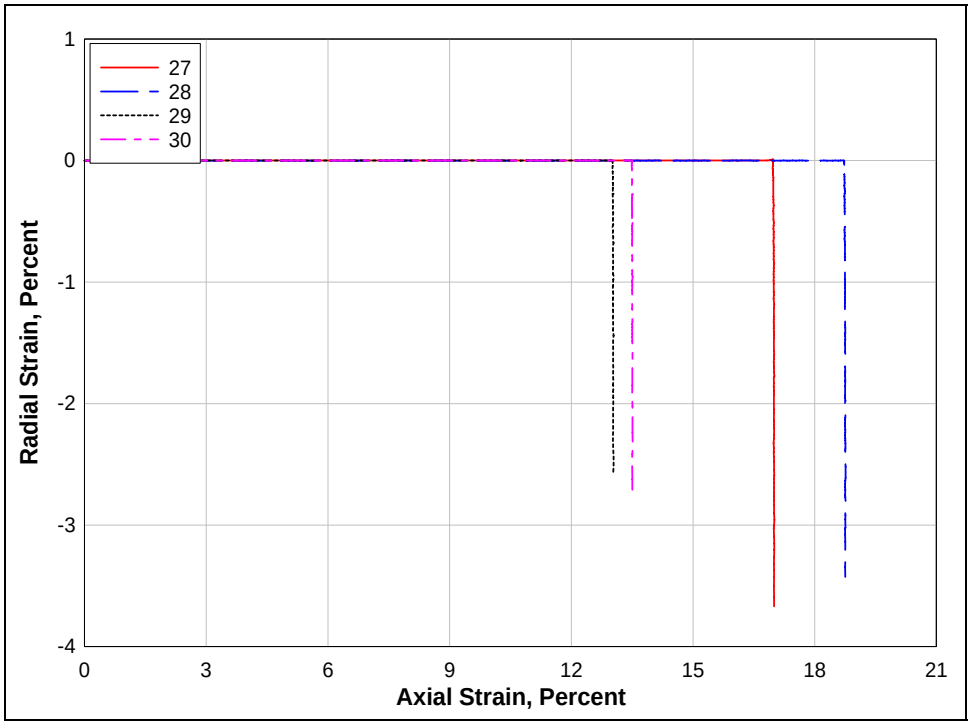

Figure 48. Strain paths from UX/BX tests

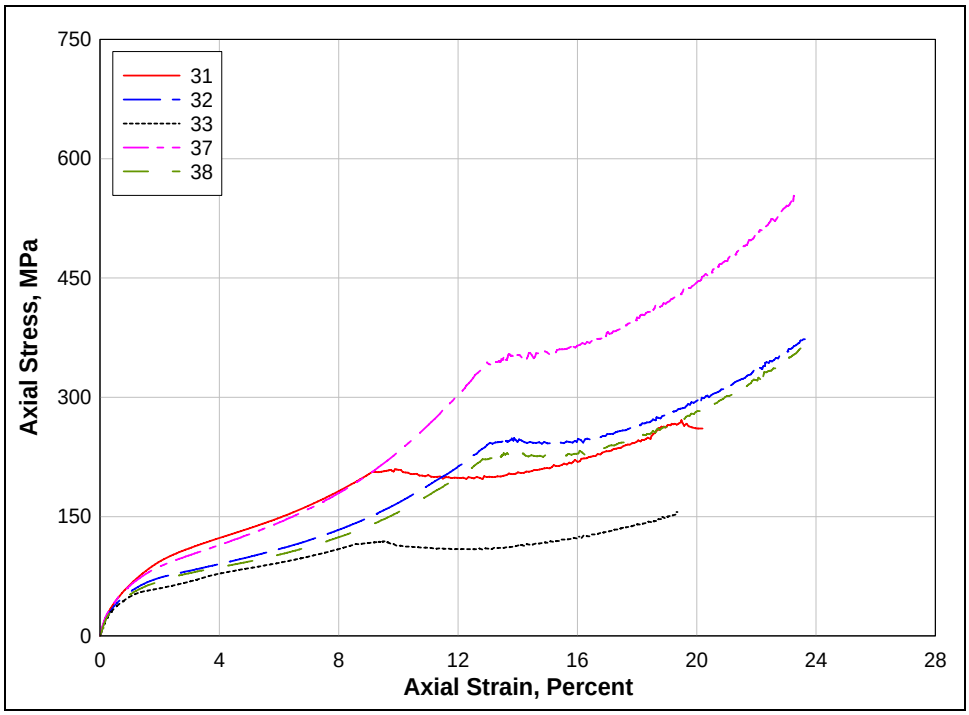

Figure 49. Stress-strain curves from UX/CV tests

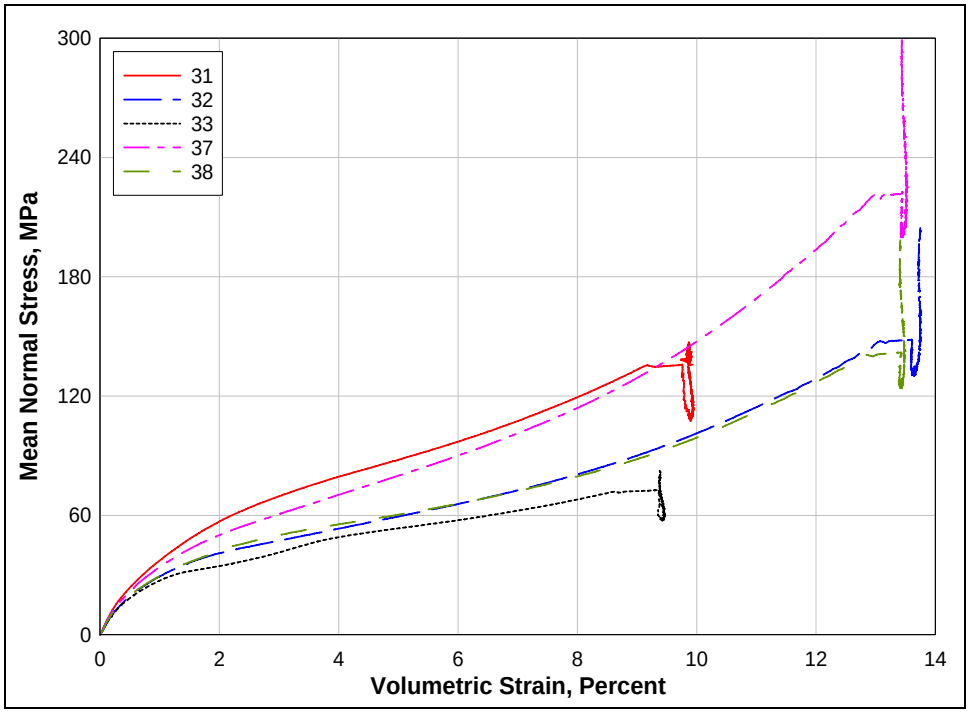

Figure 50. Pressure-volume data from UX/CV tests

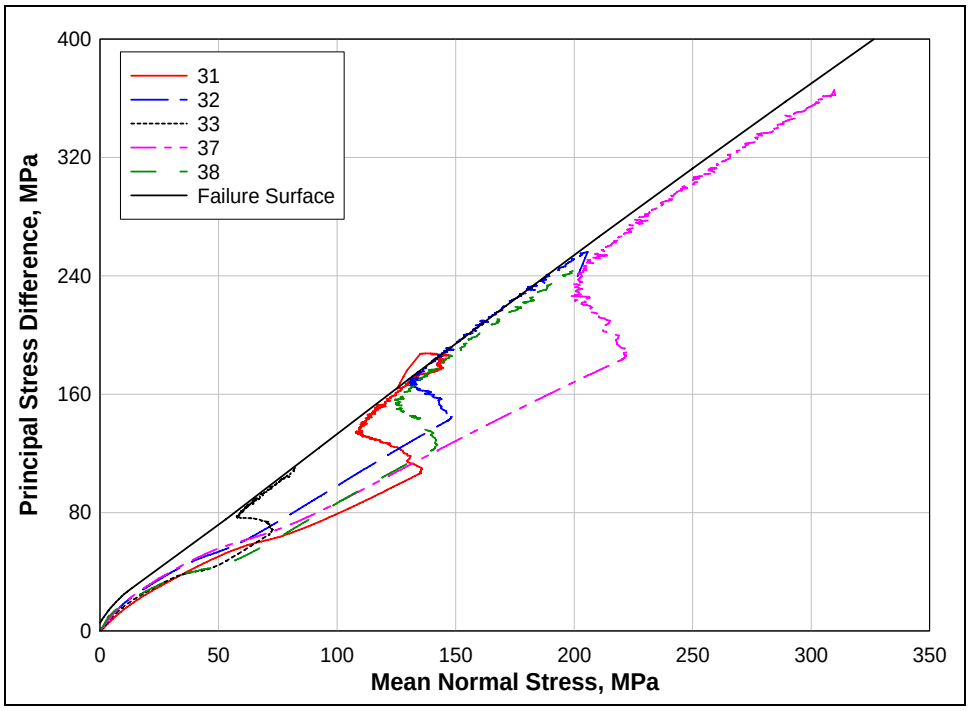

Figure 51. Stress paths from UX/CV tests and failure surface from TXC tests

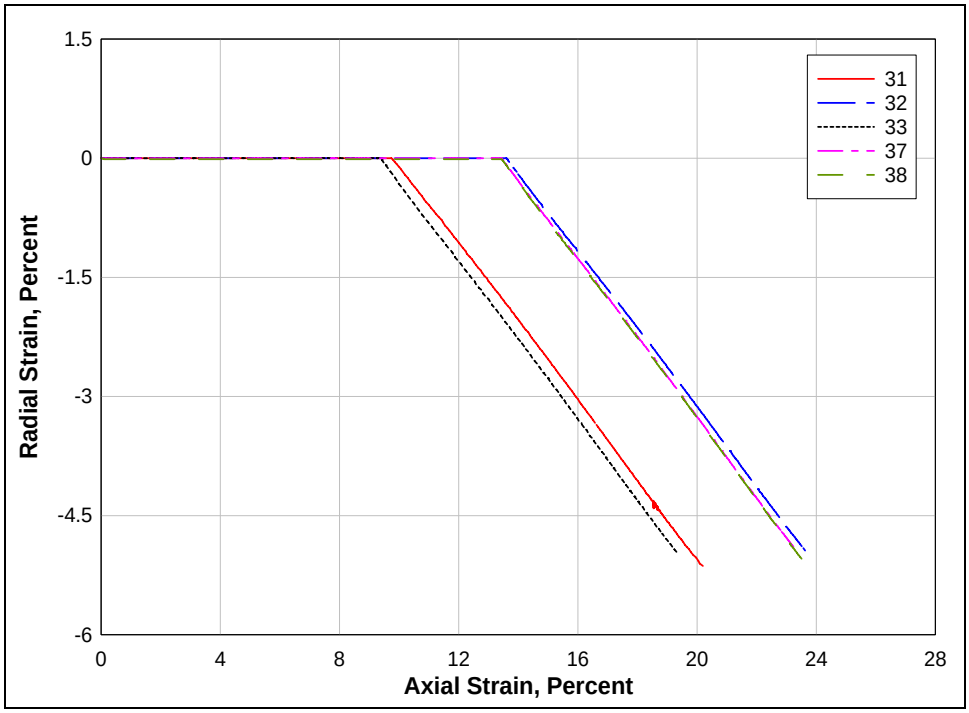

Figure 52. Strain paths from UX/CV tests

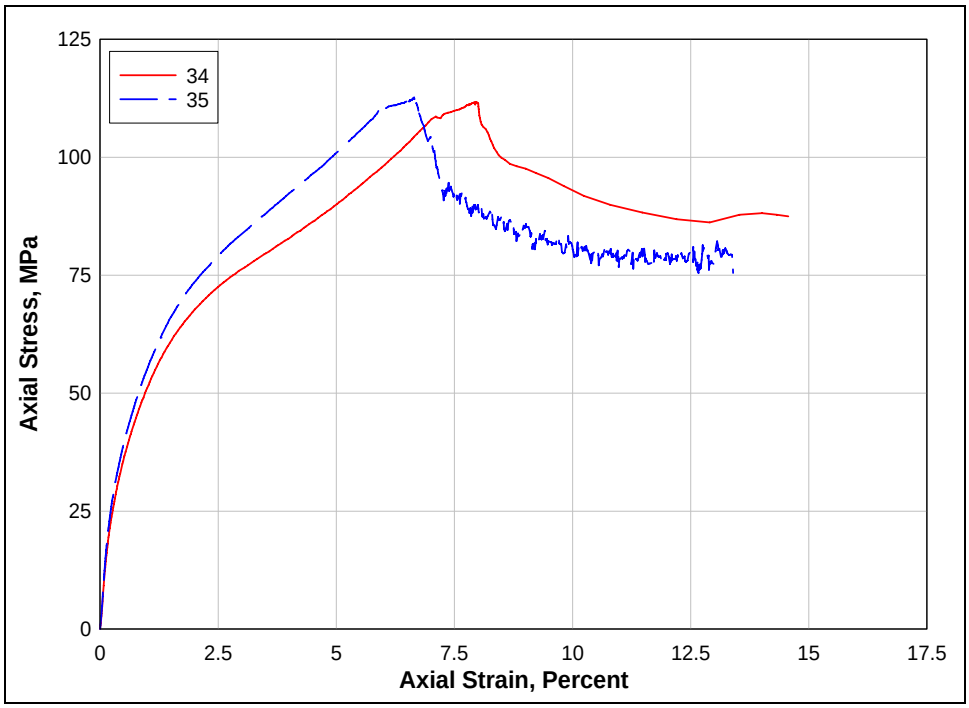

Figure 53. Stress-strain curves from UX/SR tests

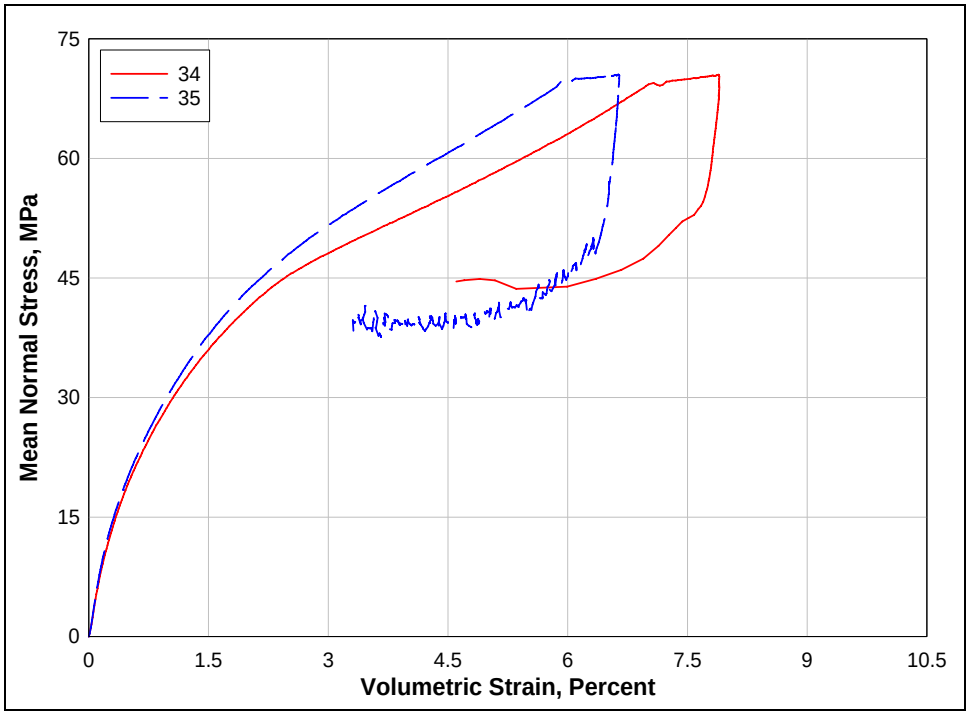

Figure 54. Pressure-volume data from UX/SR tests

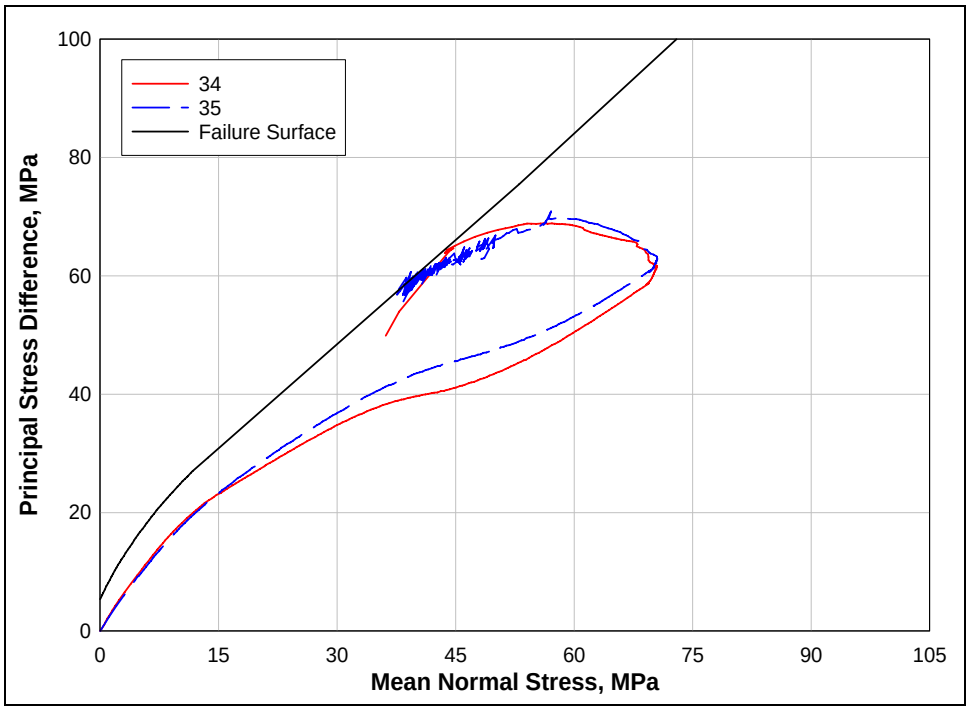

Figure 55. Stress paths from UX/SR tests and failure surface from TXC tests

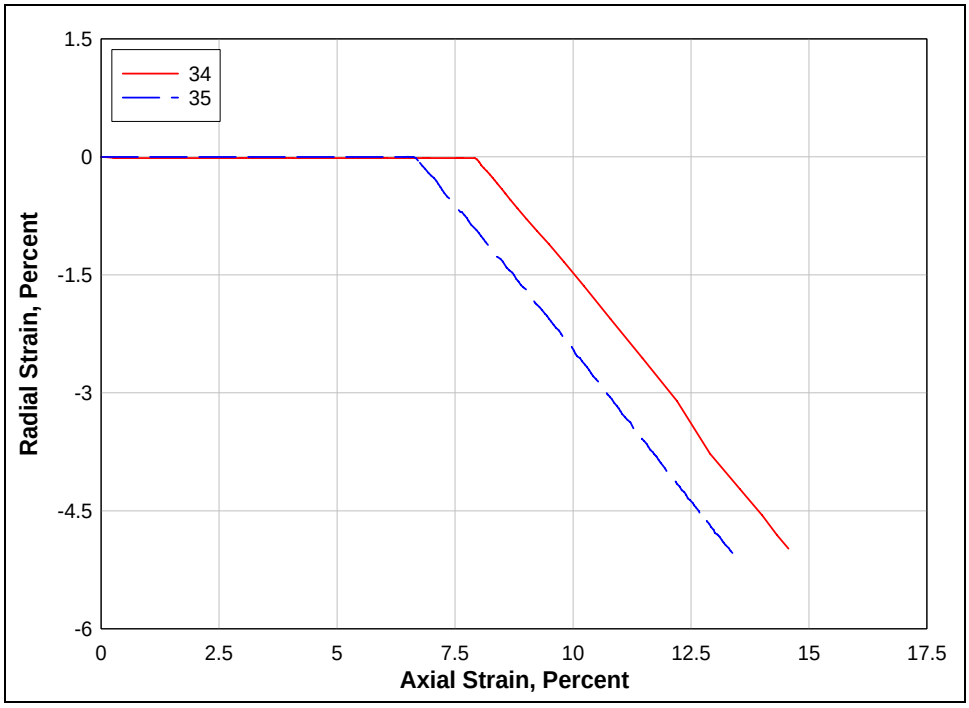

Figure 56. Strain paths from UX/SR tests

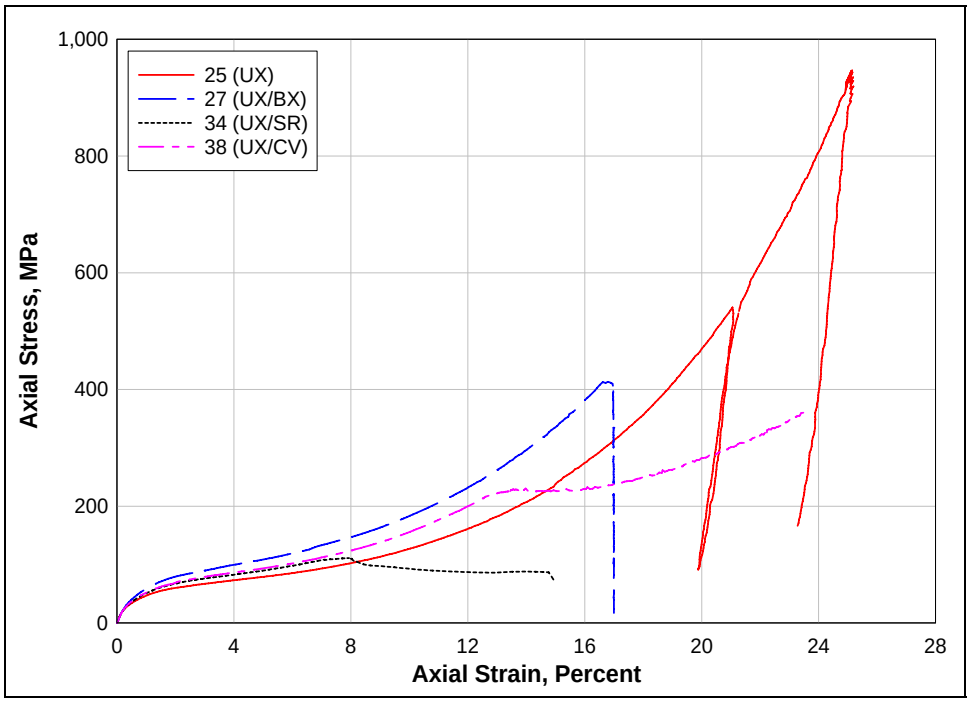

Figure 57. Stress-strain curves from selected UX, UX/BX, UX/SR, and UX/CV tests

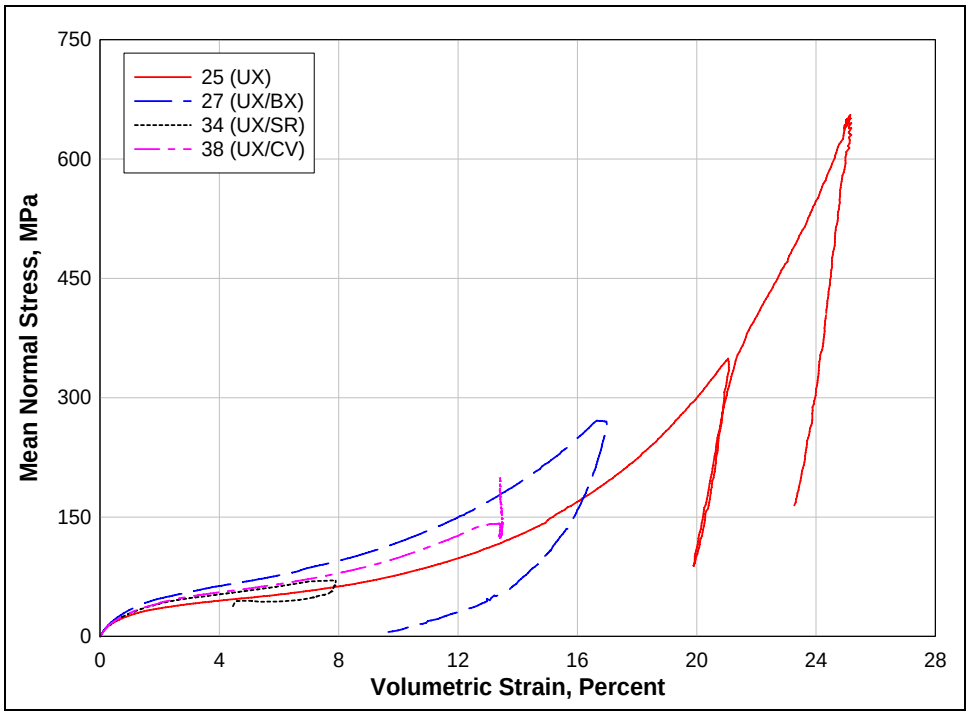

Figure 58. Pressure-volume data from selected UX, UX/BX, UX/SR, and UX/CV tests

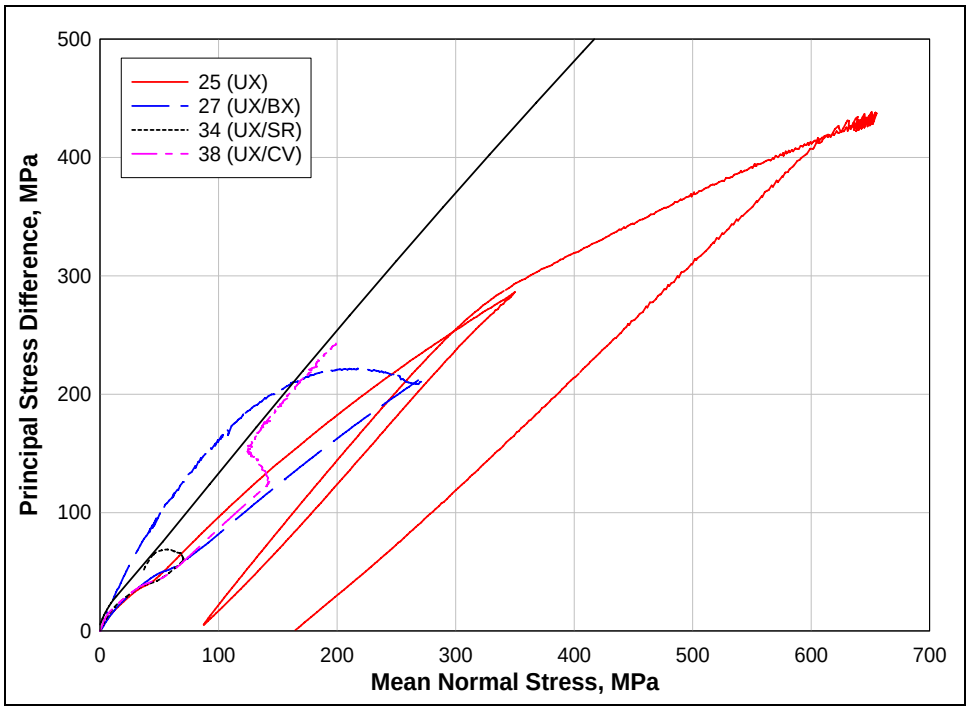

Figure 59. Stress paths from selected UX, UX/BX, UX/SR, and UX/CV tests, and failure surface from TXC tests

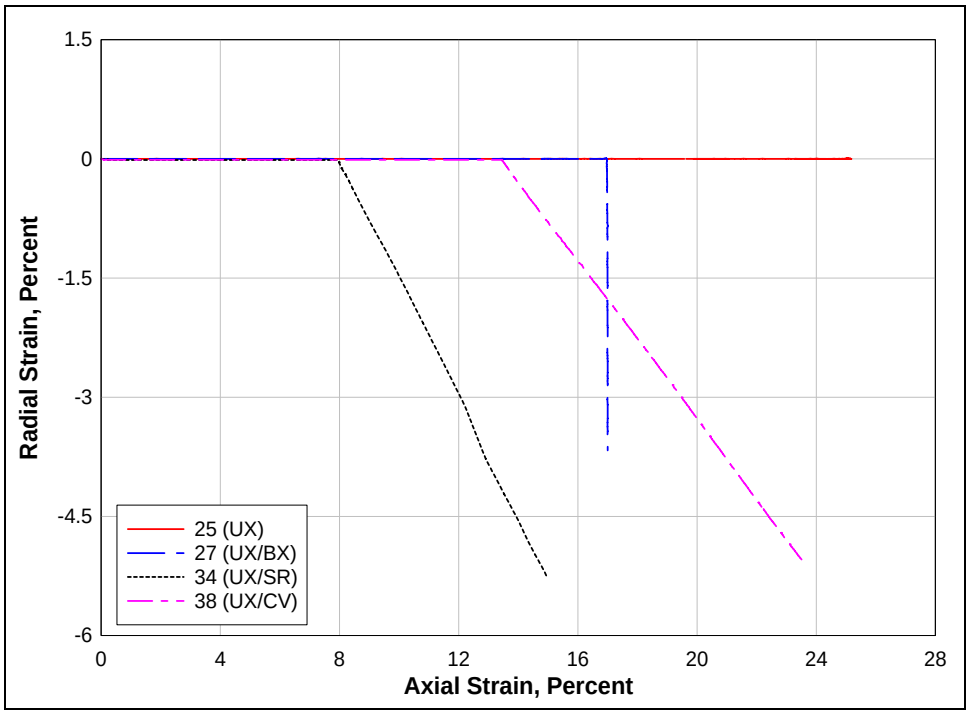

Figure 60. Strain paths from selected UX, UX/BX, UX/SR, and UX/CV tests

4 Summary

Personnel of the ERDC-GSL conducted a laboratory investigation to characterize the strength and constitutive property behavior of white masonry concrete. Forty-four successful mechanical property tests were conducted. These tests included two hydrostatic compression tests, four unconfined compression tests, 17 triaxial compression tests, five direct pull tests, three reduced triaxial extension tests, two uniaxial strain tests, four uniaxial strain load/biaxial strain unload tests, five uniaxial strain load/constant volume strain tests, and two uniaxial strain load/strain ratio strain tests. Composition properties were obtained for each test specimen along with nondestructive pulse-velocity data.

The overall quality of the test data was very good; limited scatter was observed in the data over repeated loading paths. The initial loading HC and UX compressibility responses were very stiff because of the cemented nature of the WMC material. Comparisons of the volumetric responses from the HC and UX tests showed that the WMC material exhibited increased compaction under shear-induced loading from the UX tests when compared with results from HC tests in which no shear-induced loading occurred. Creep was observed during the HC and UX tests. Results from the TXC tests exhibited a continuous increase in principal stress difference with increasing confining stress. The TXC data exhibited primarily compressive volume strains during shear. Only the UC and TXC test specimens at 5 MPa dilated during shear. A compression failure surface was developed from the TXC results at eight levels of confining stress and from the results of the UC tests. The DP and RTE tests exhibited lower absolute values of principal stress difference than comparable TXC tests. The results for the DP and RTE tests were used to develop the extension failure surface. The resulting compression and extension failure surfaces were well defined and nonsymmetric about the mean normal stress axis. During UX/BX tests, stress relaxation was evident during the change from uniaxial strain loading to biaxial strain unloading. Good correlations were observed between the stress paths obtained from the UX/CV and UX/SR strain path tests and the failure surface from the TXC tests.

References

Akers, S. A., Reed, P. A., and Ehrgott, J. Q. (1986). "*WES high-pressure uniaxial strain and triaxial shear test equipment*," Miscellaneous Paper SL-86-11, U.S. Army Engineer Waterways Experiment Station, Vicksburg, MS.

American Society for Testing and Materials. (2002). *2002 Annual book of ASTM standards*, Philadelphia, PA.

a. Designation C 39-01. "Standard test method for compressive strength of concrete specimens."

b. Designation C 42-99. "Standard test method for obtaining and testing drilled cores and sawed beams of concrete."

c. Designation C 597-97. "Standard test method for pulse velocity through concrete."

d. Designation C 801-98. "Standard test method for determining the mechanical properties of hardened concrete under triaxial loads."

e. Designation D 2216-98. "Standard test method for laboratory determination of water (moisture) content of soil and rock by mass."

f. Designation D 4543-01. "Standard test method for preparing rock core specimens and determining dimensional and shape tolerances."

Bishop, A. W., and Henkel, D. J. (1962). *The measurement of soil properties in the triaxial test*, Edward Arnold, Ltd., London, pp 72-74.

White Masonry Concrete
Test No. 01

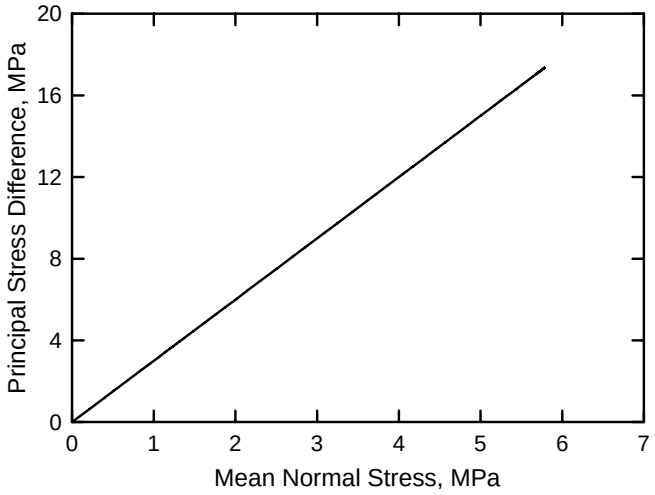

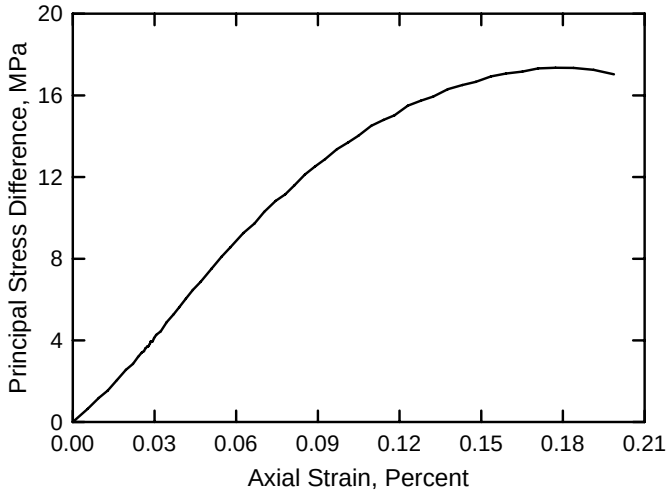

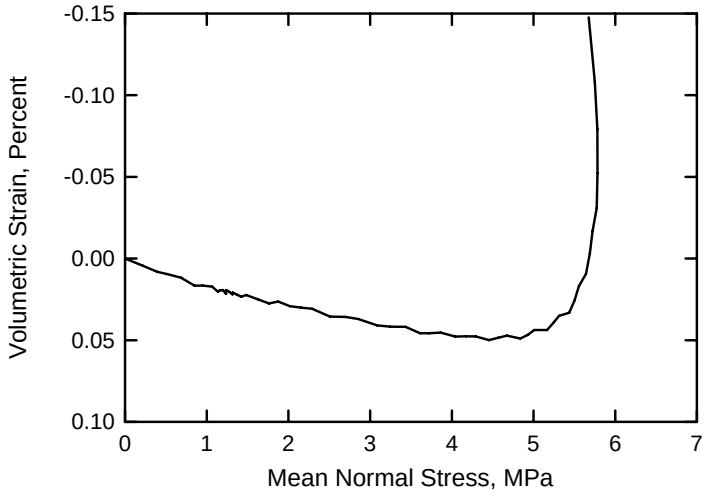

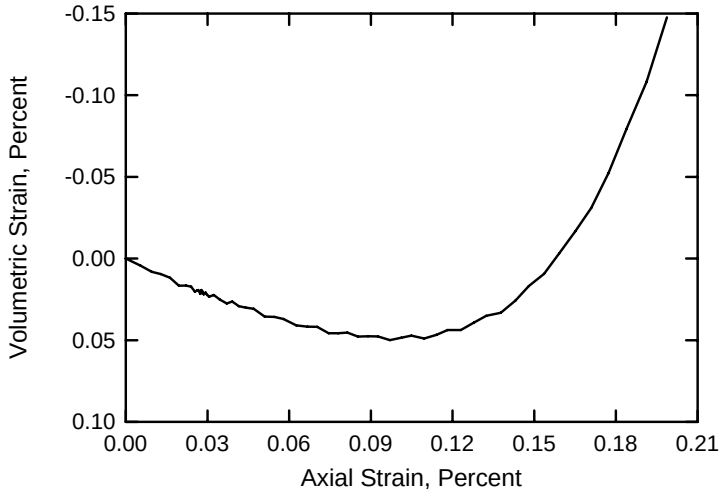

Plate 1

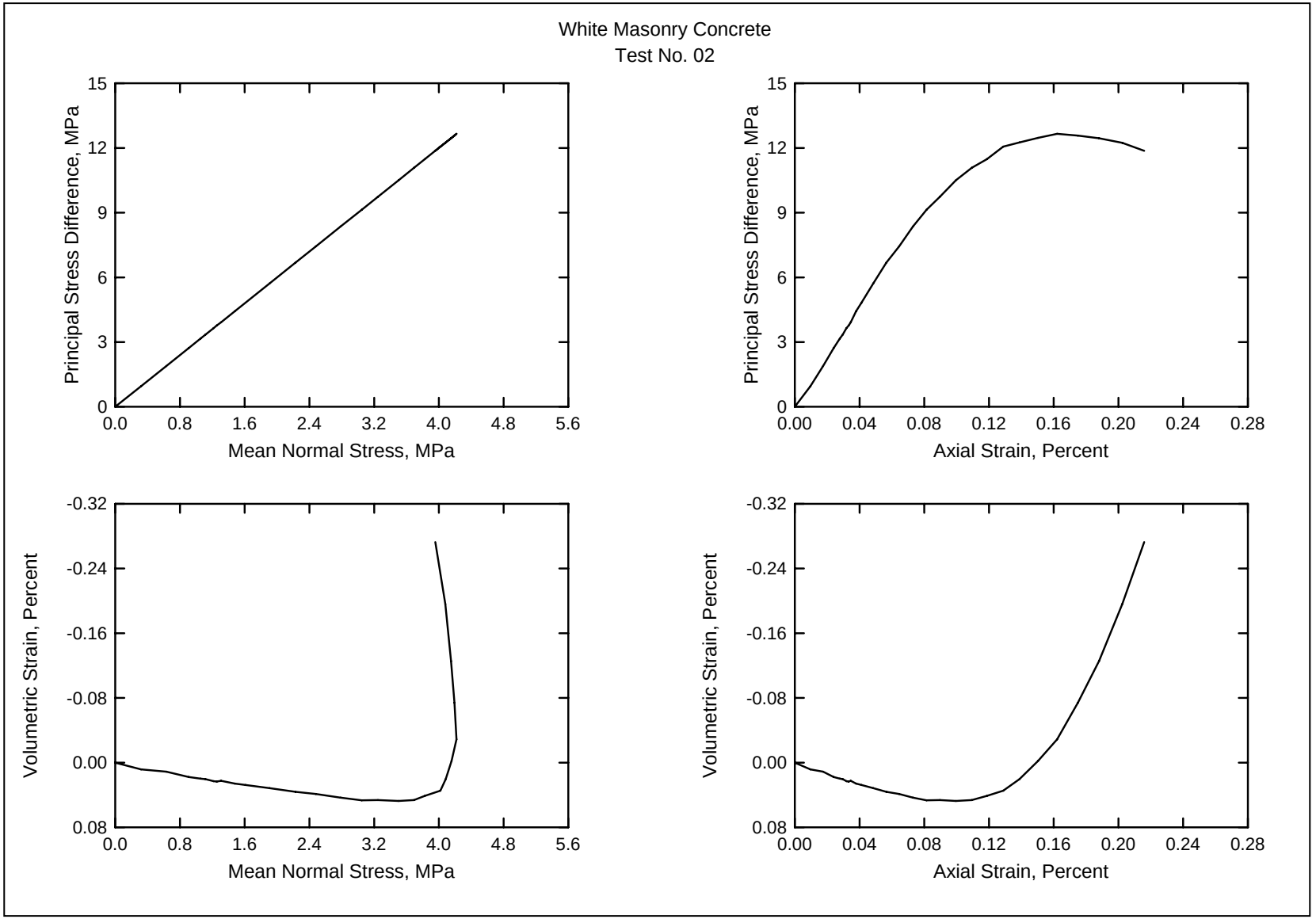
White Masonry Concrete
Test No. 02
Principal Stress Difference, MPa
Mean Normal Stress, MPa
Principal Stress Difference, MPa
Axial Strain, Percent
Volumetric Strain, Percent
Mean Normal Stress, MPa
Volumetric Strain, Percent
Axial Strain, Percent

Plate 2

White Masonry Concrete
Test No. 03

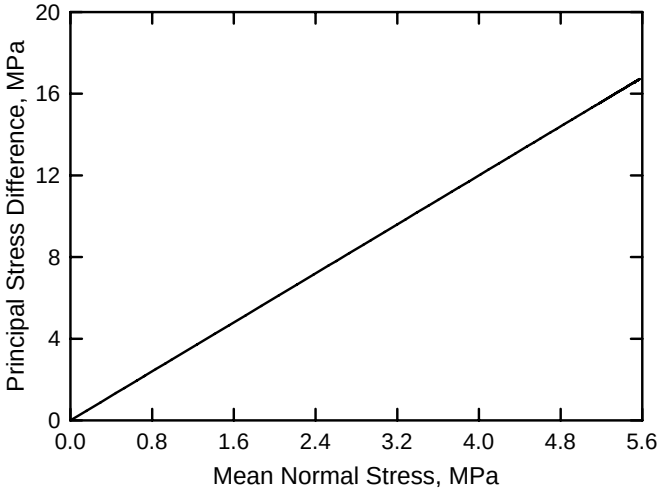

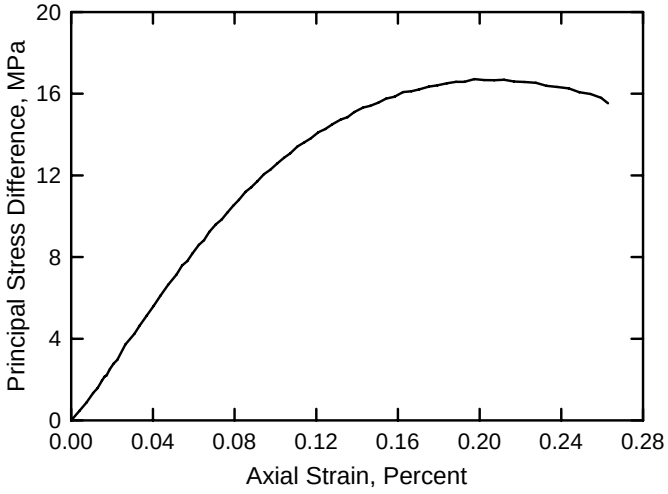

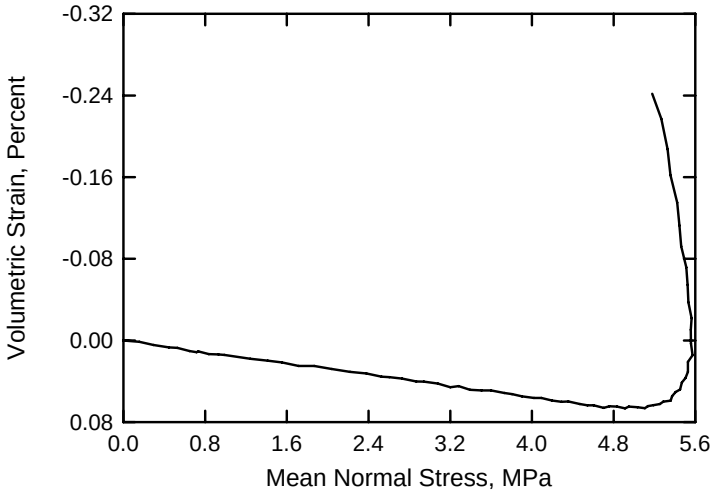

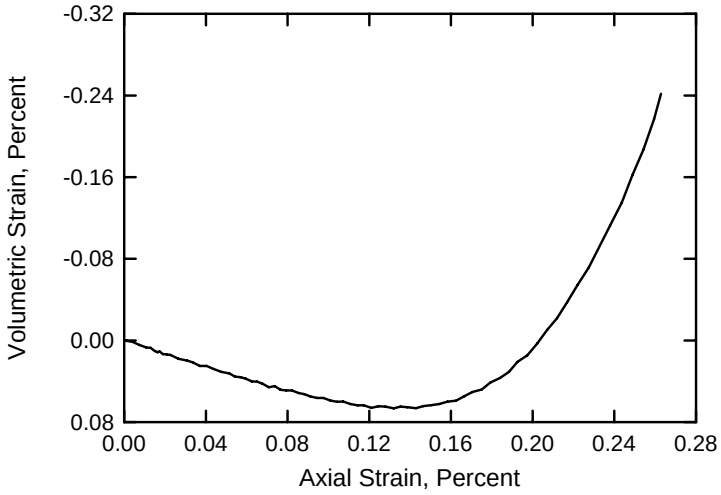

Plate 3

White Masonry Concrete
Test No. 04

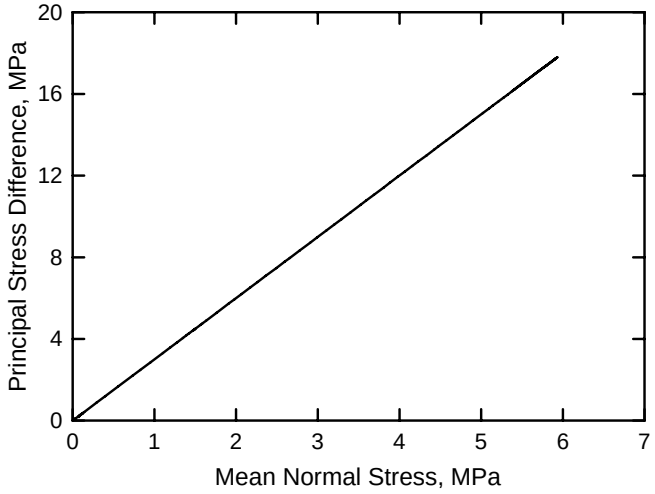

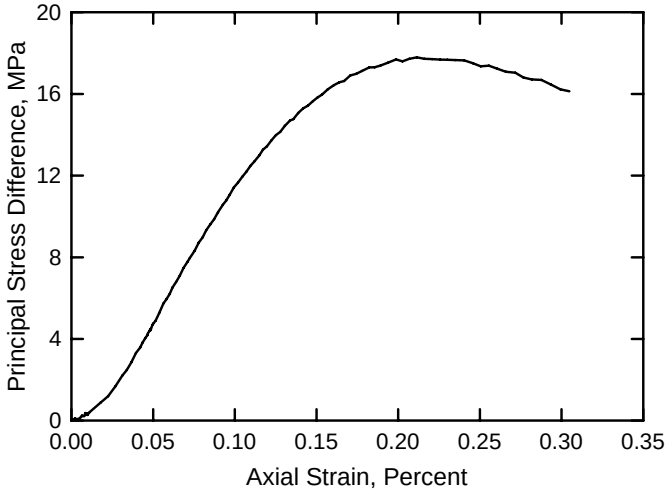

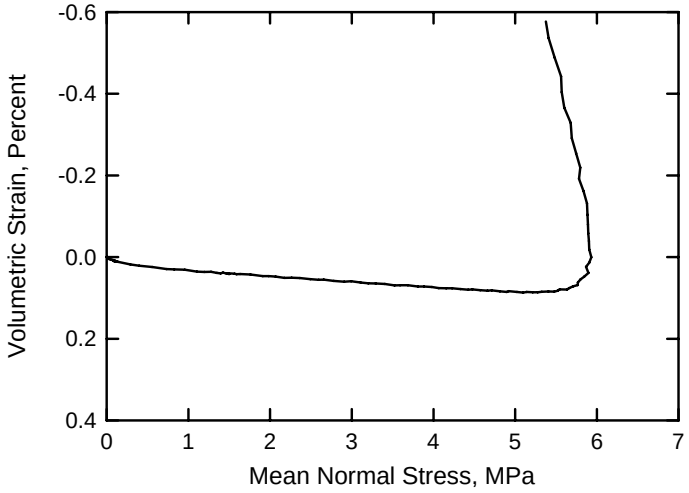

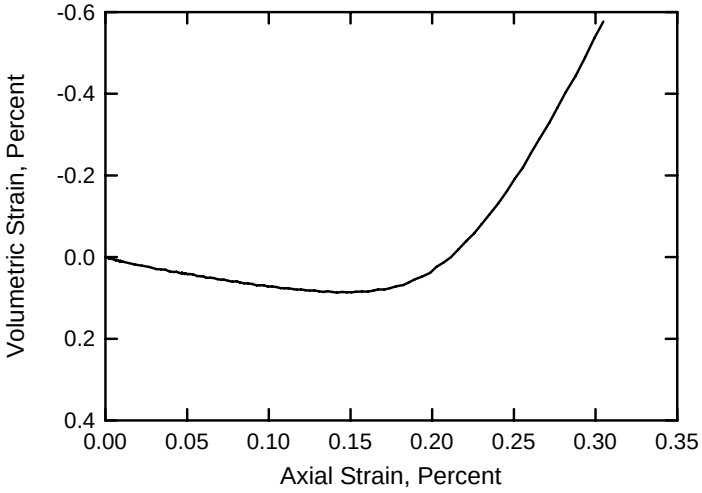

Plate 4

White Masonry Concrete
Test No. 06

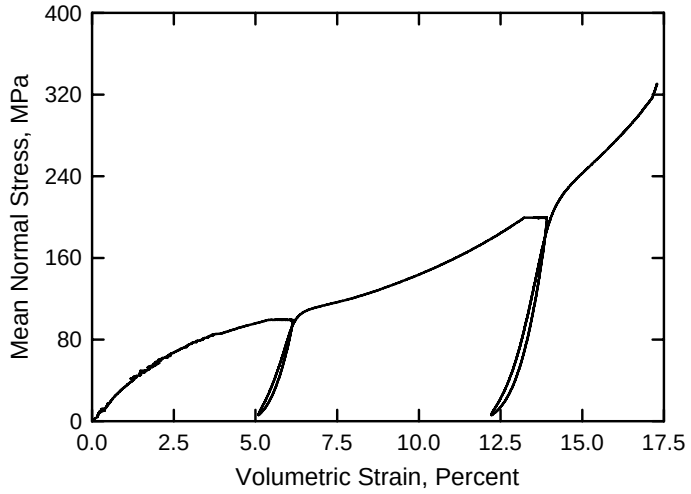

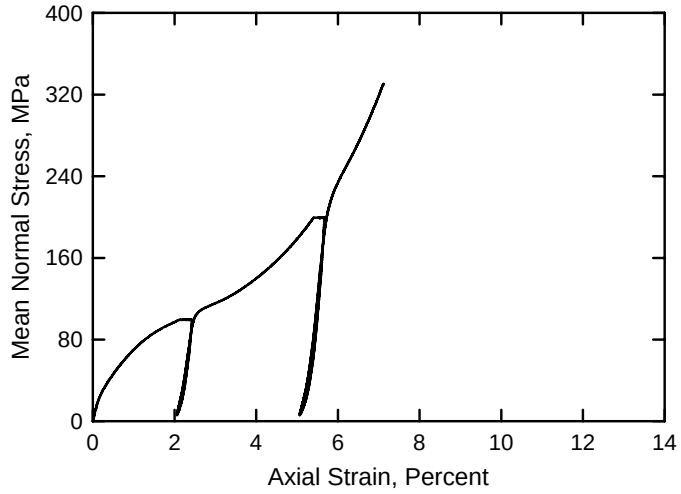

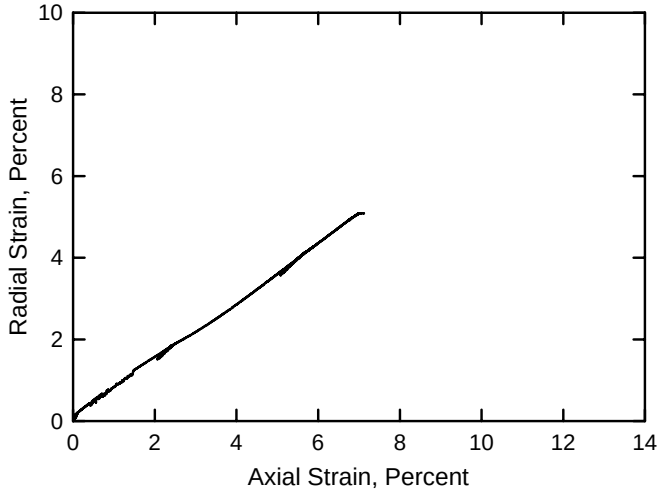

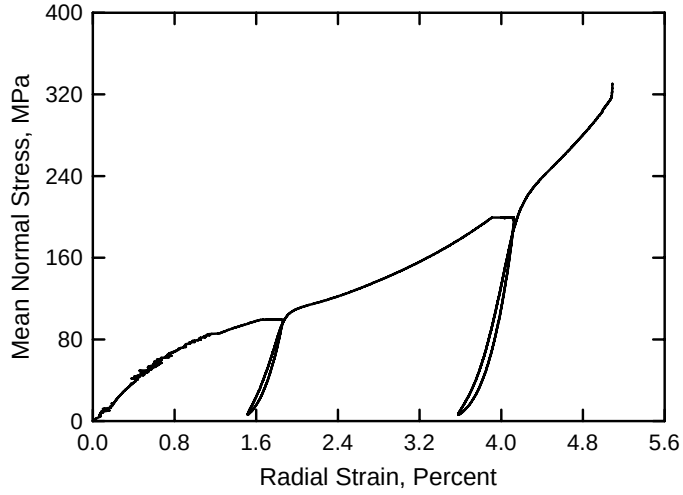

Plate 5

White Masonry Concrete
Test No. 07

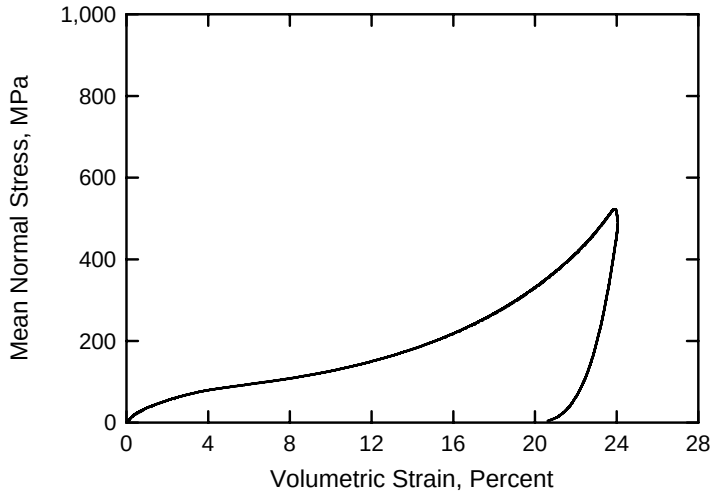

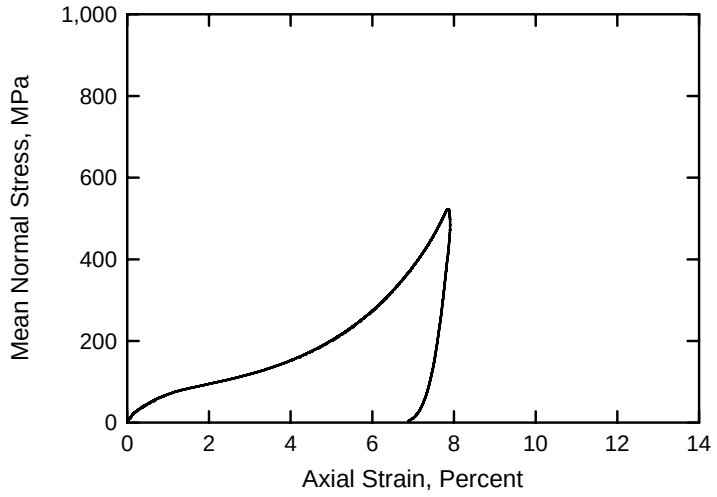

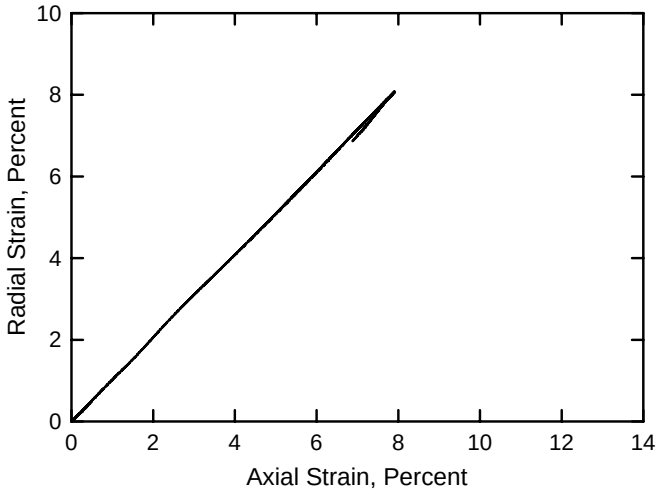

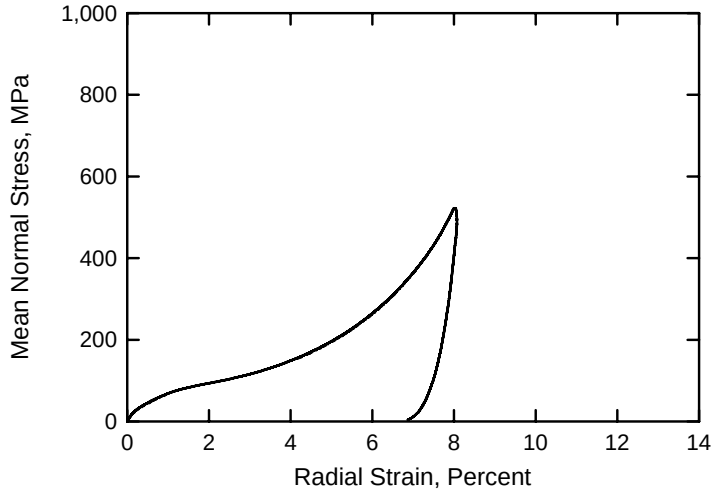

Plate 6

White Masonry Concrete
Test No. 08

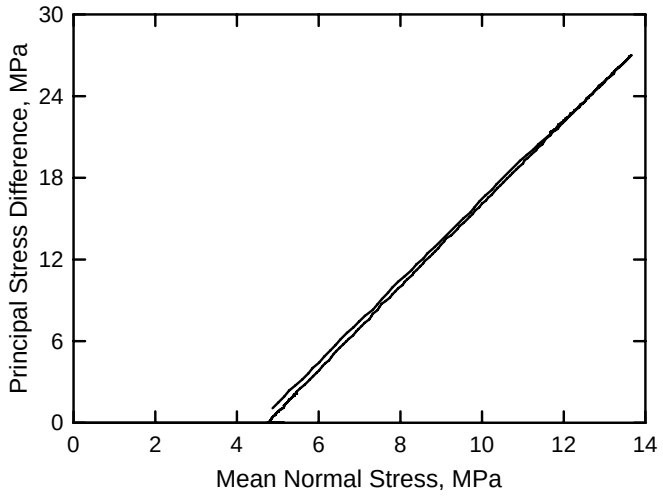

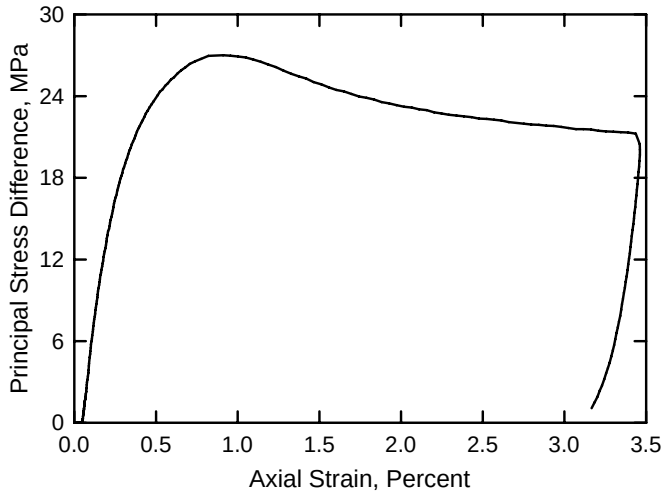

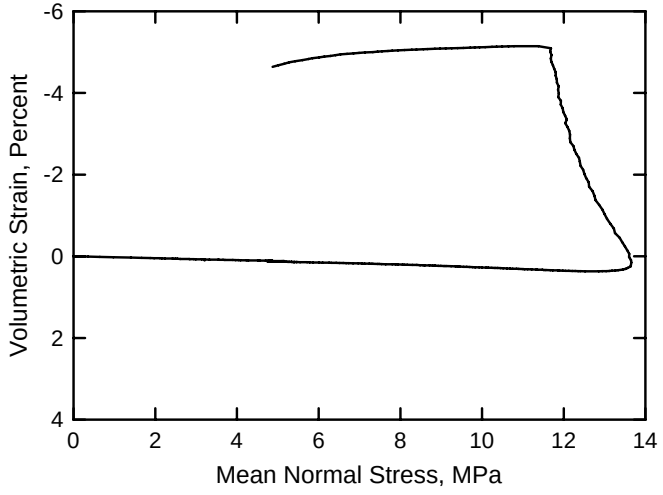

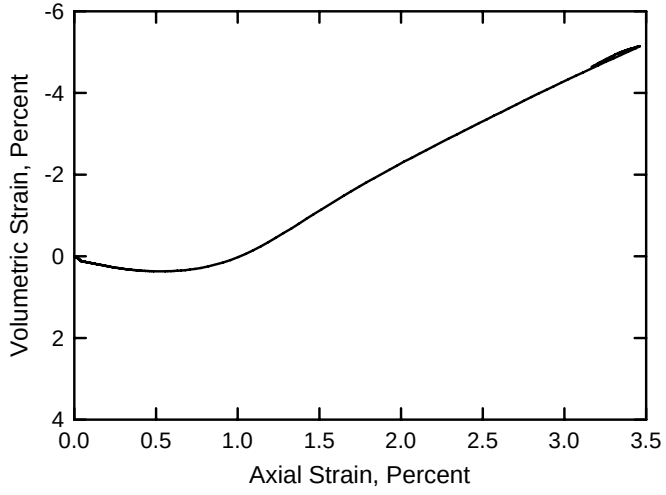

Plate 7

White Masonry Concrete
Test No. 09

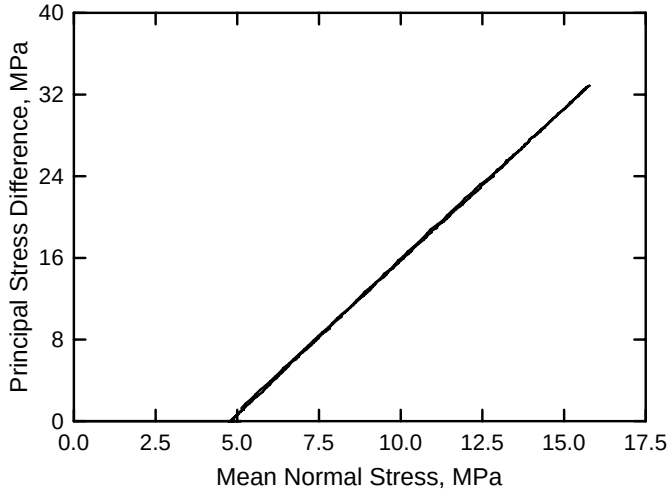

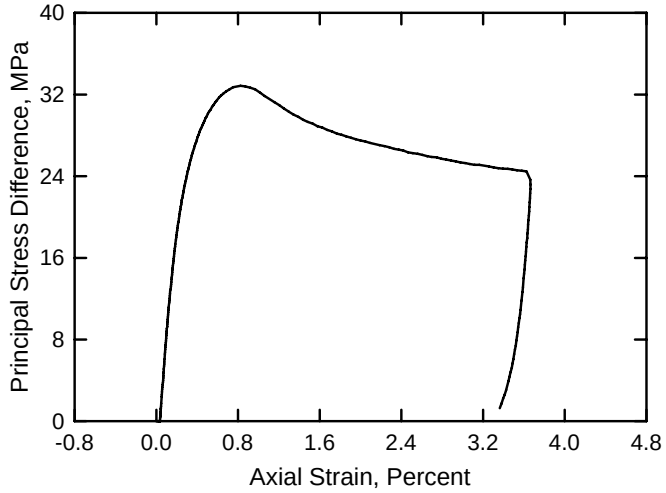

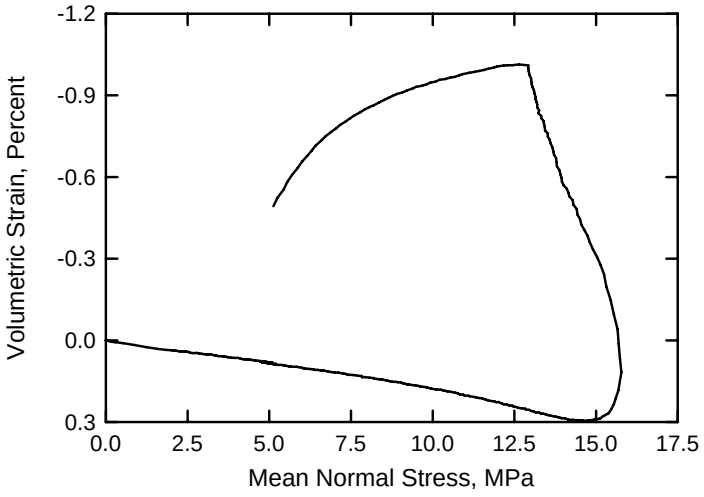

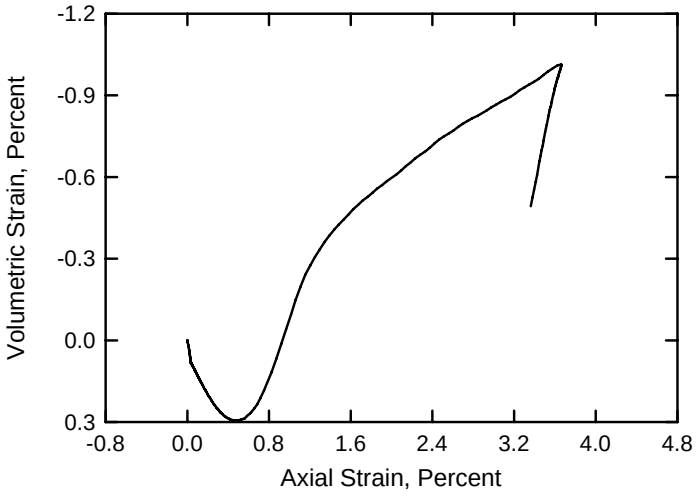

Plate 8

White Masonry Concrete
Test No. 36

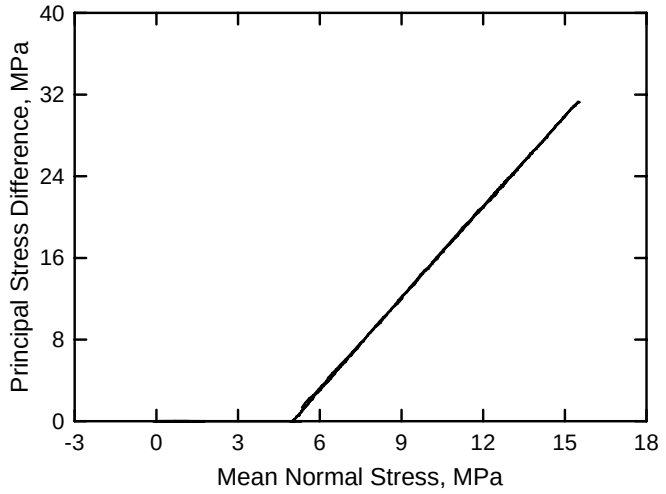

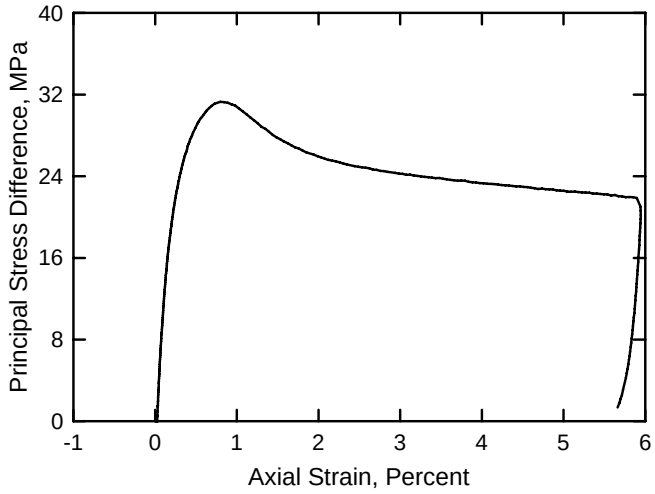

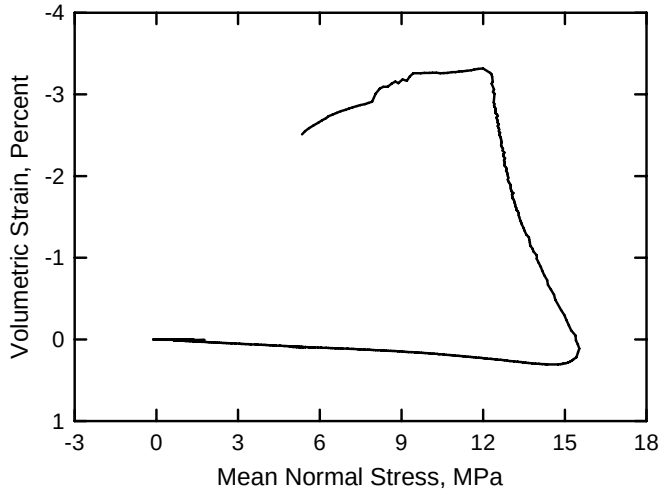

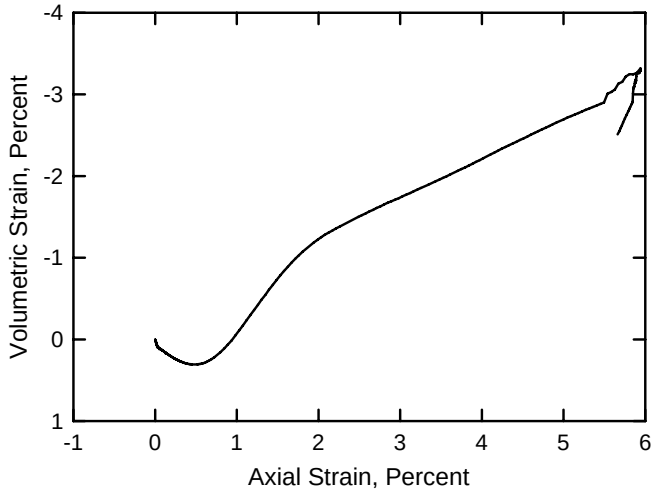

White Masonry Concrete
Test No. 10

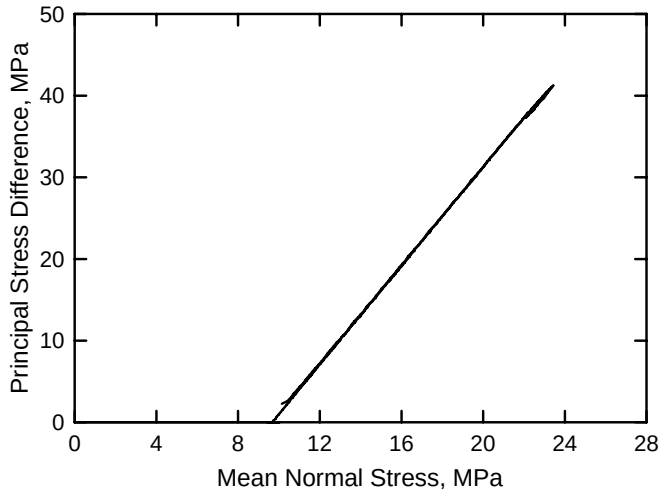

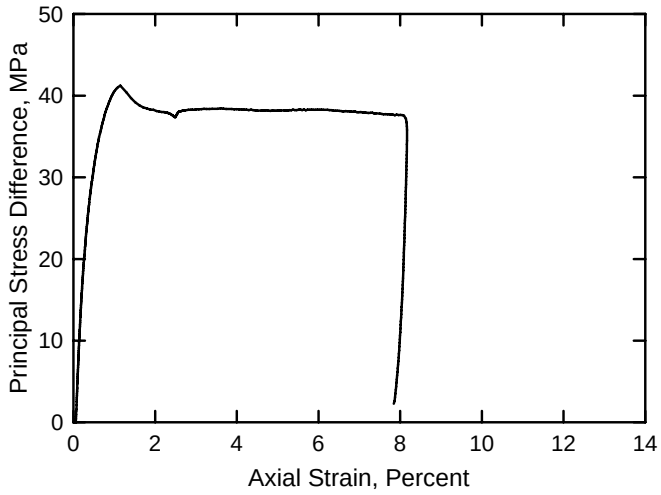

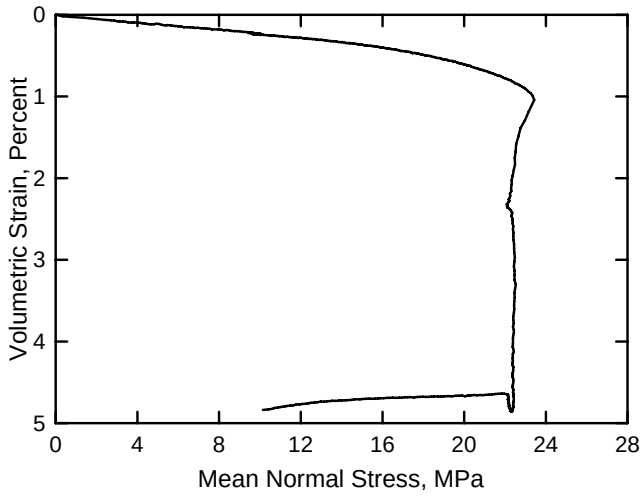

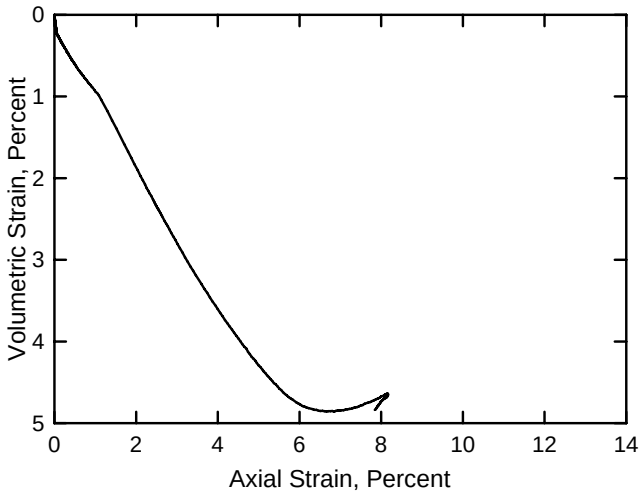

Plate 10

White Masonry Concrete
Test No. 11

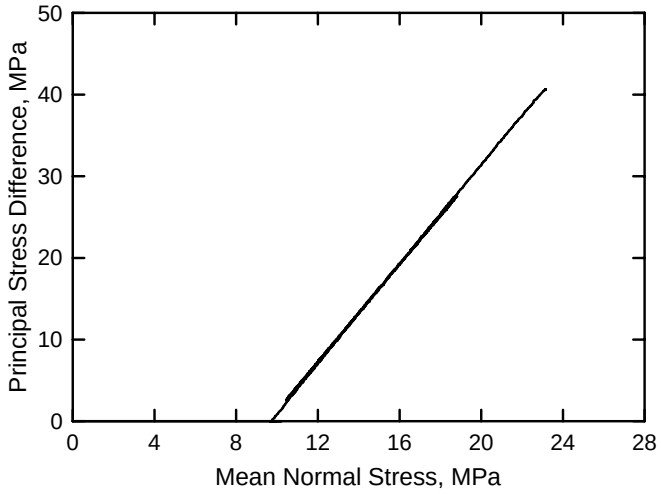

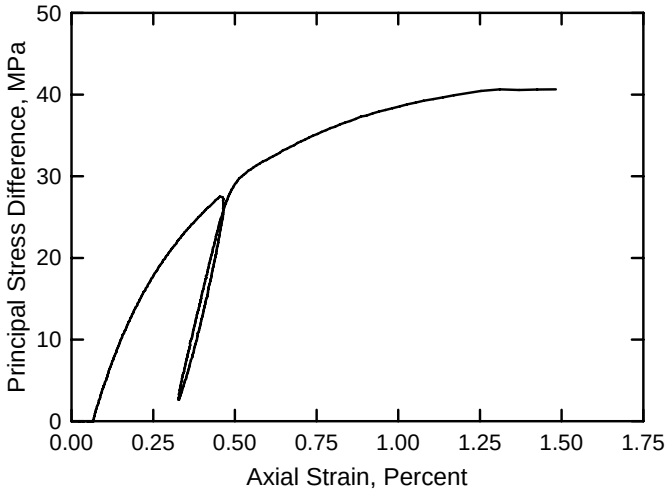

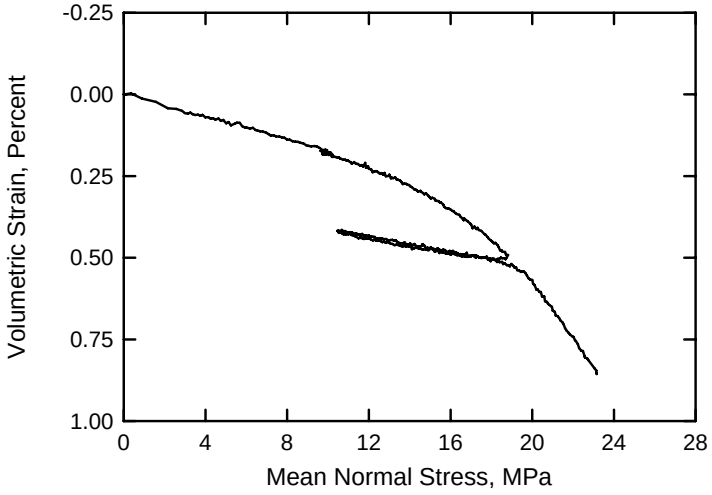

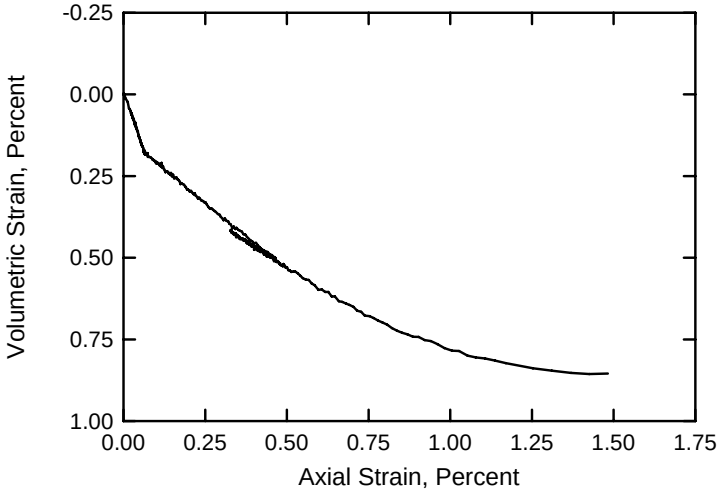

Plate 11

White Masonry Concrete
Test No. 12

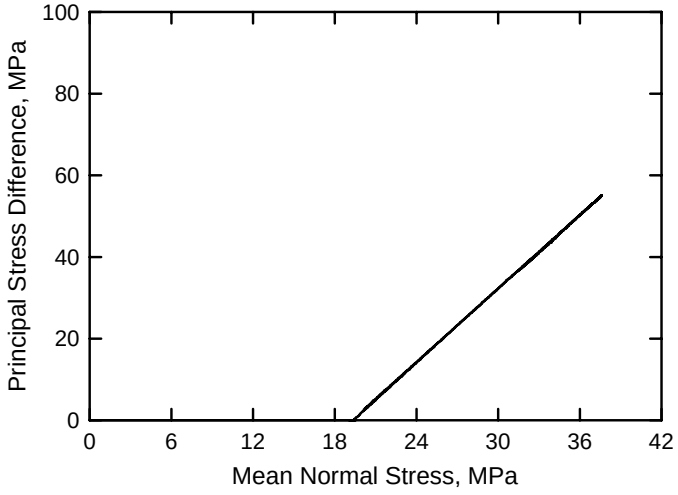

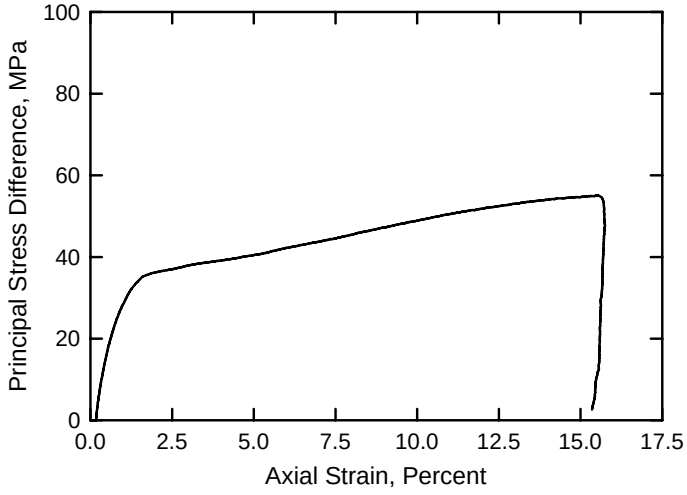

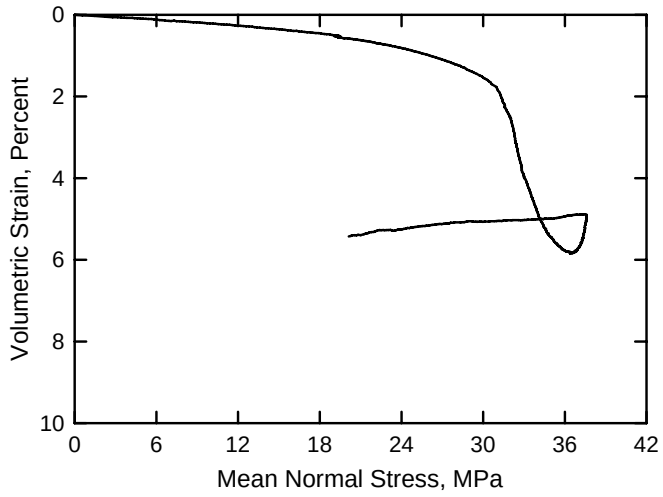

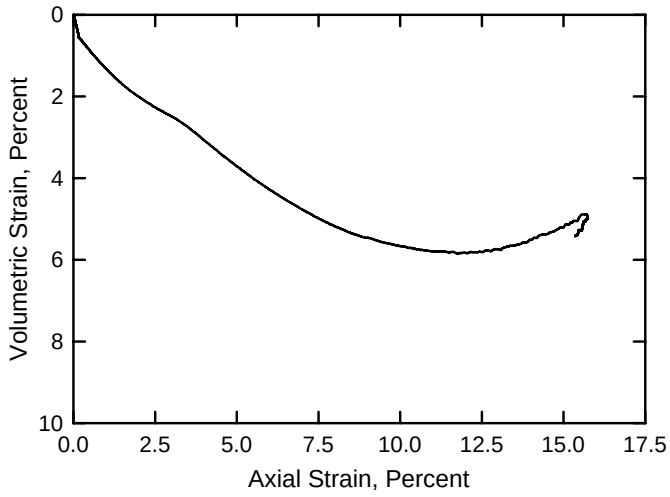

Plate 12

White Masonry Concrete
Test No. 13

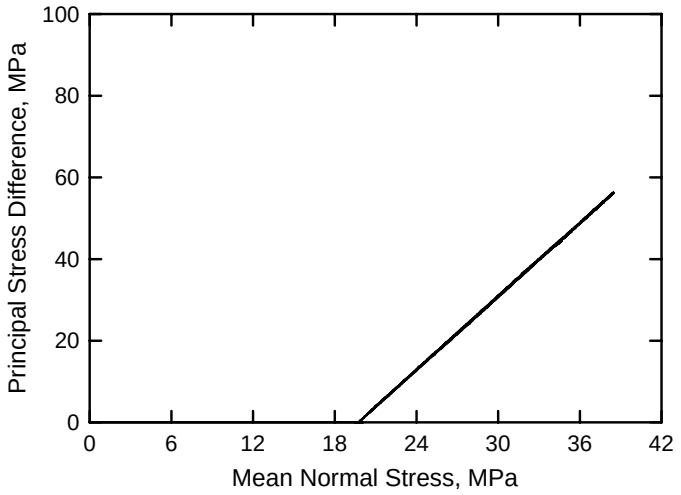

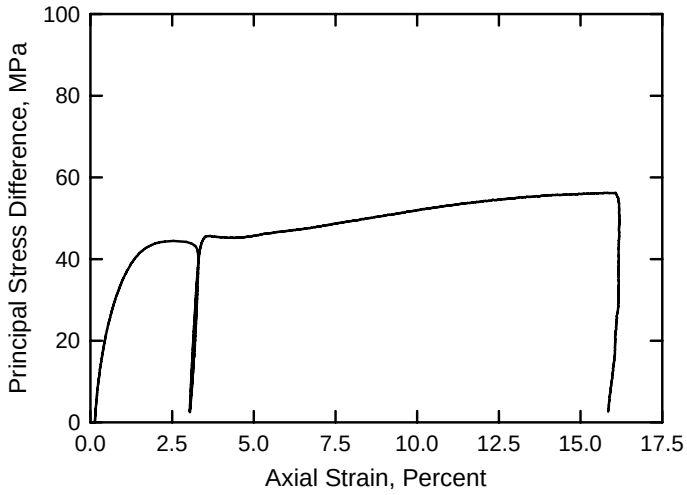

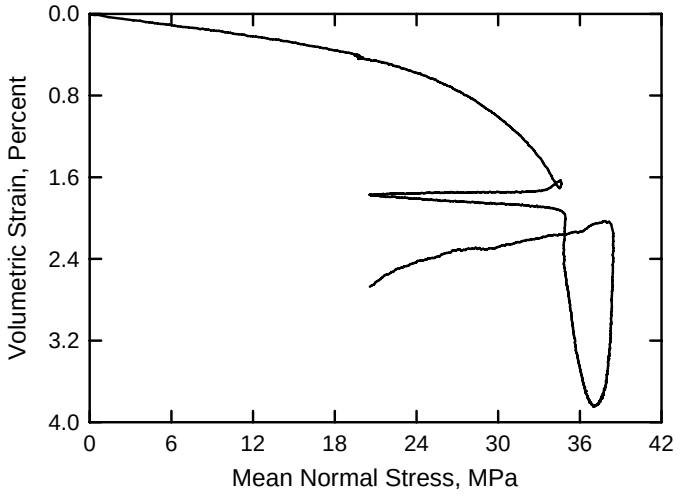

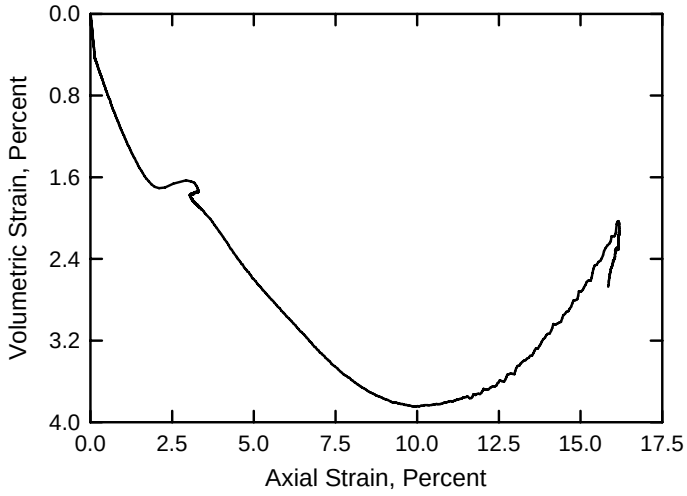

Plate 13

White Masonry Concrete
Test No. 14

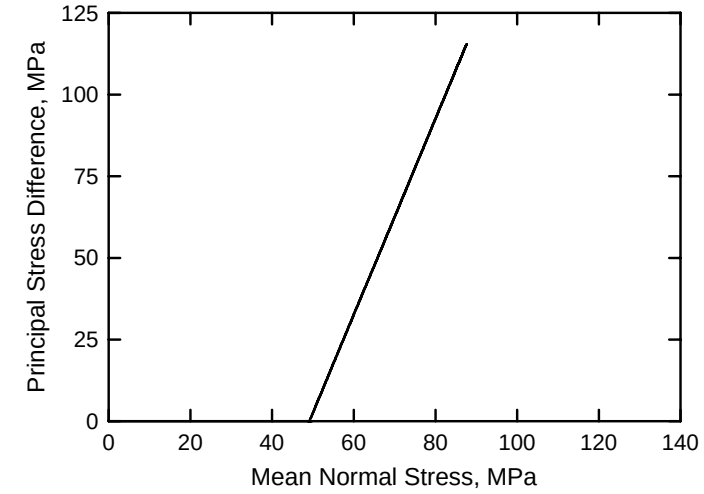

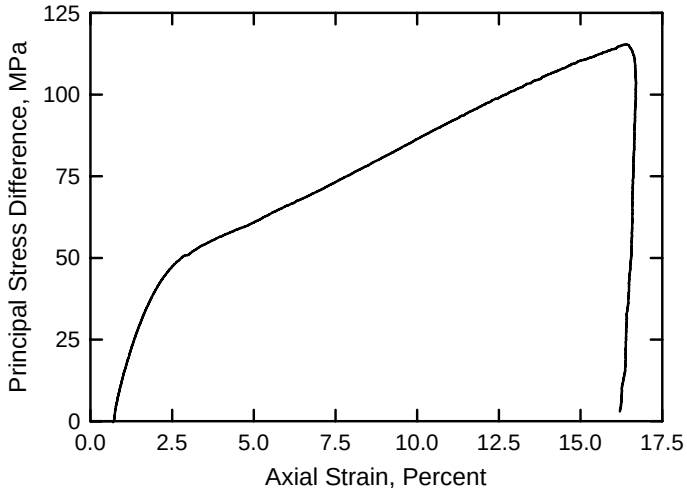

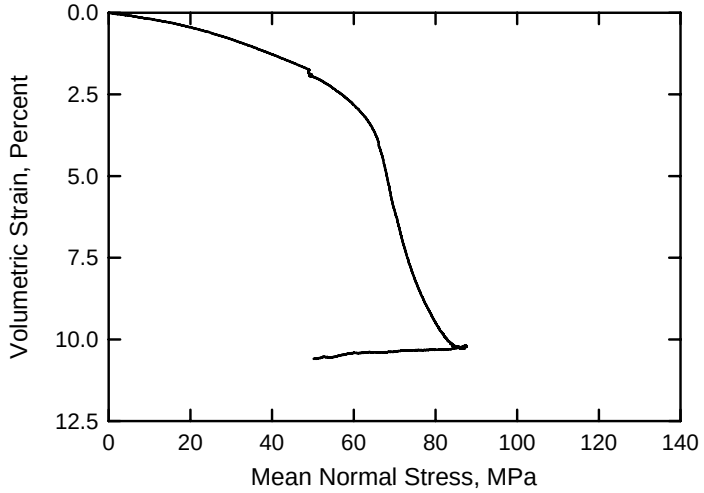

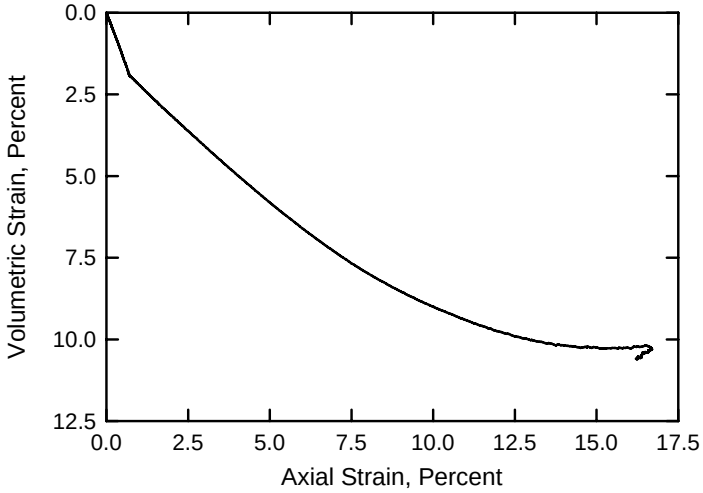

Plate 14

White Masonry Concrete
Test No. 15

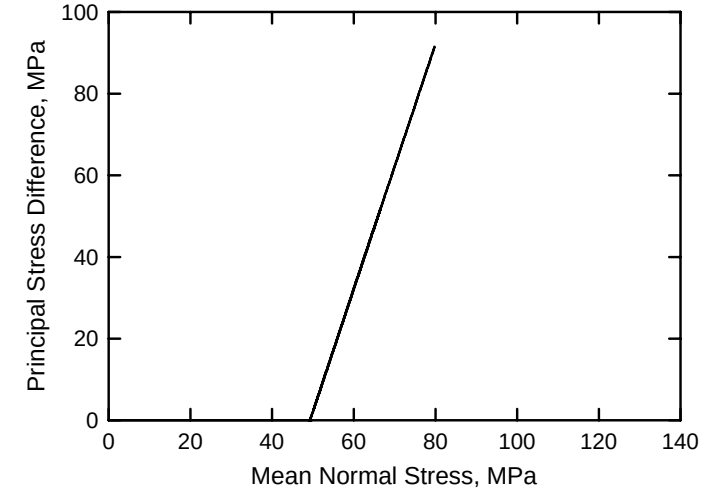

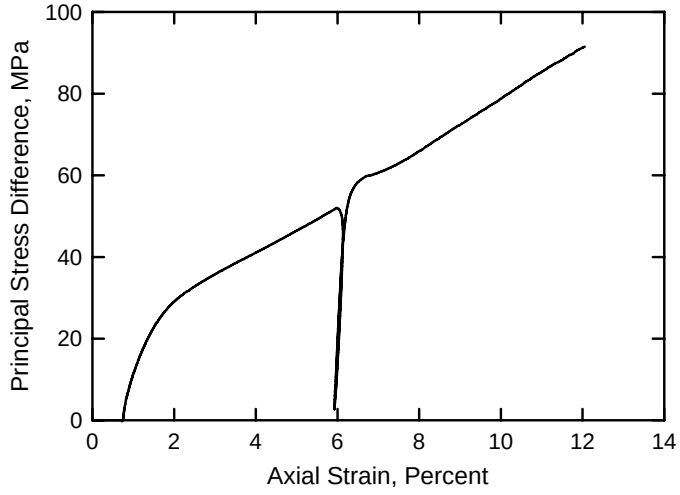

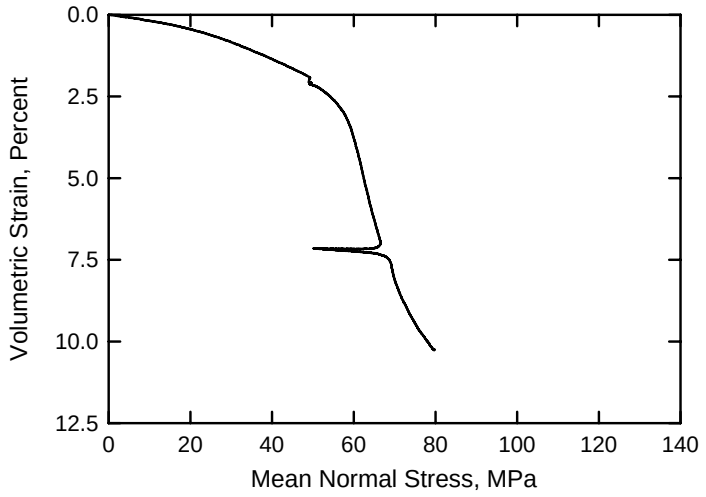

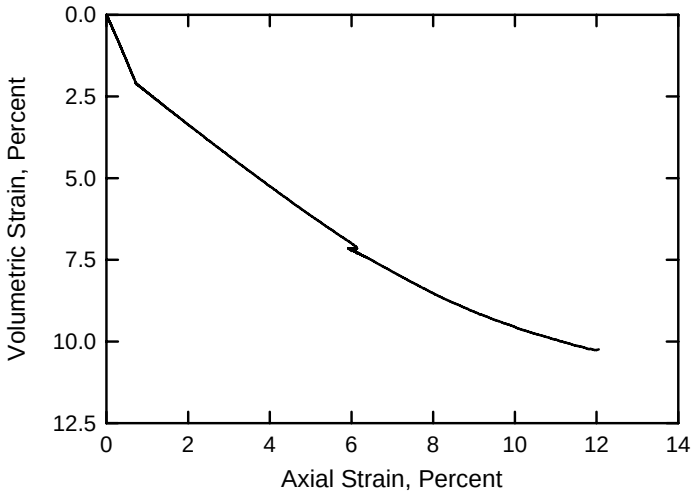

Plate 15

White Masonry Concrete
Test No. 17

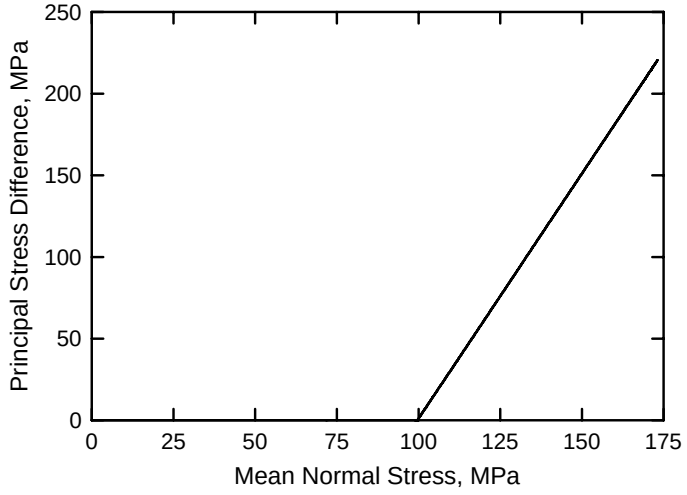

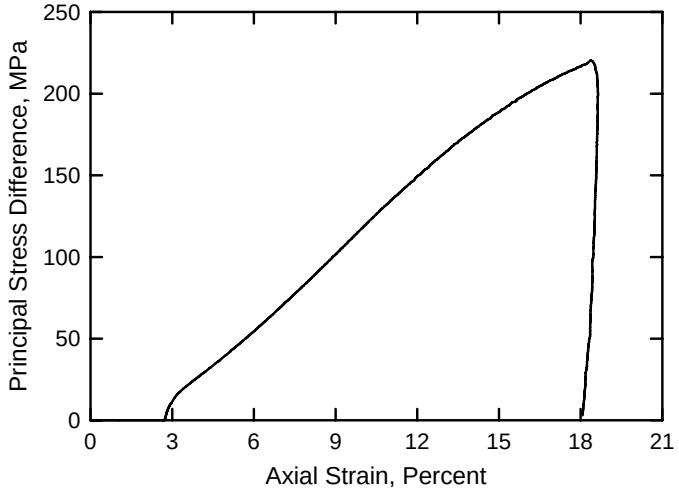

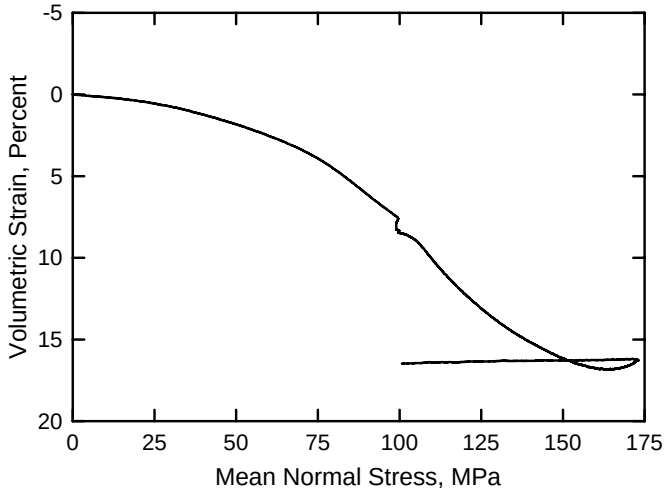

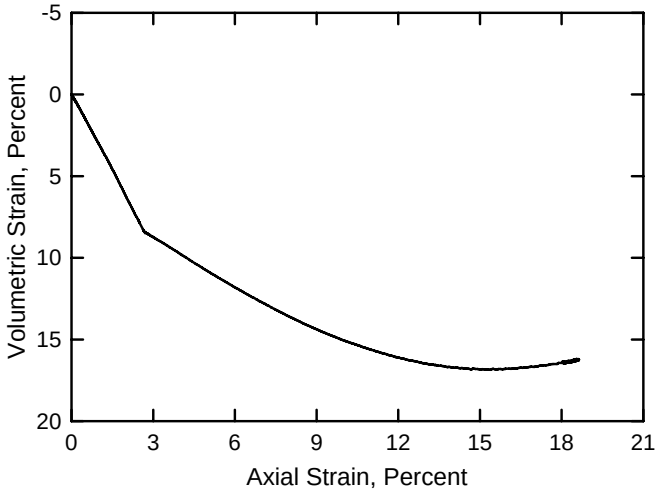

Plate 16

White Masonry Concrete
Test No. 18

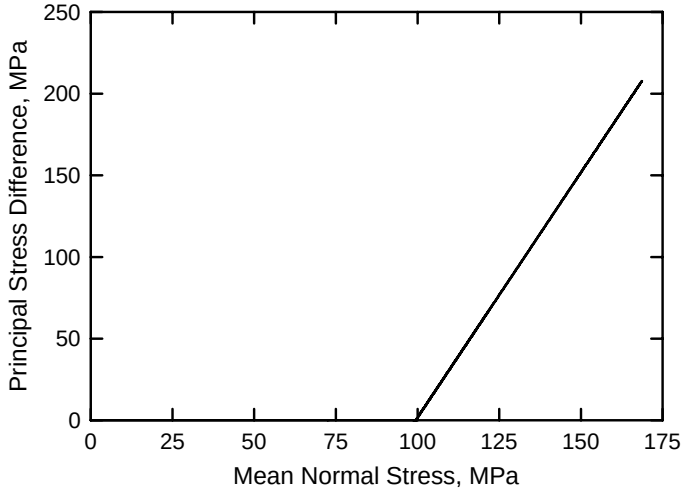

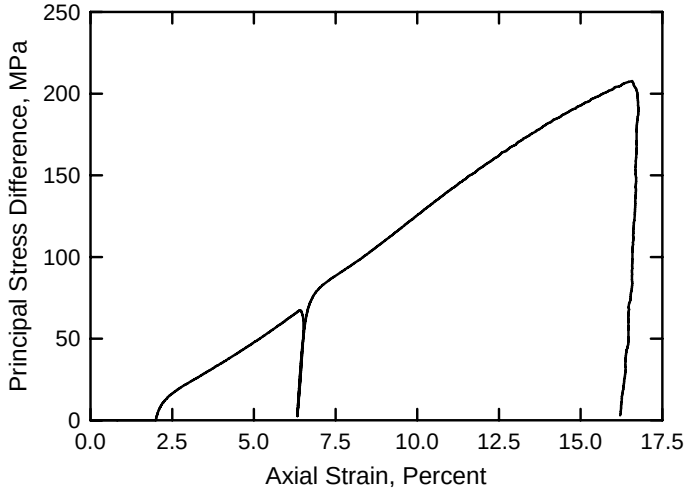

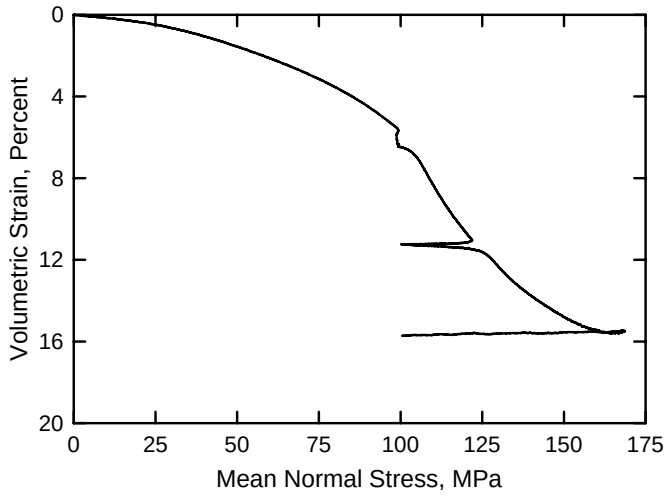

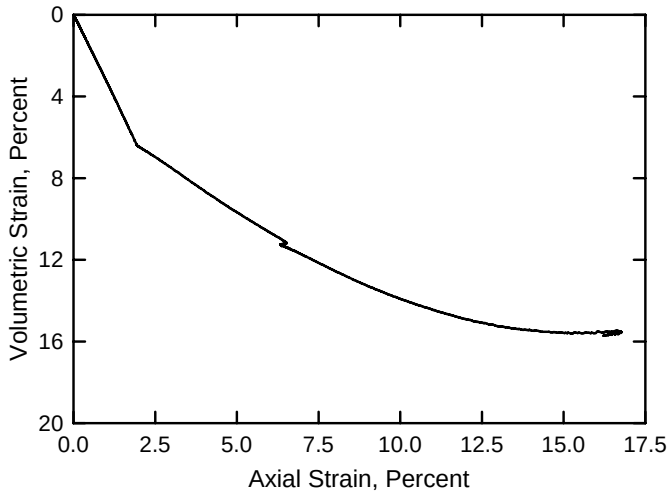

Plate 17

White Masonry Concrete
Test No. 19

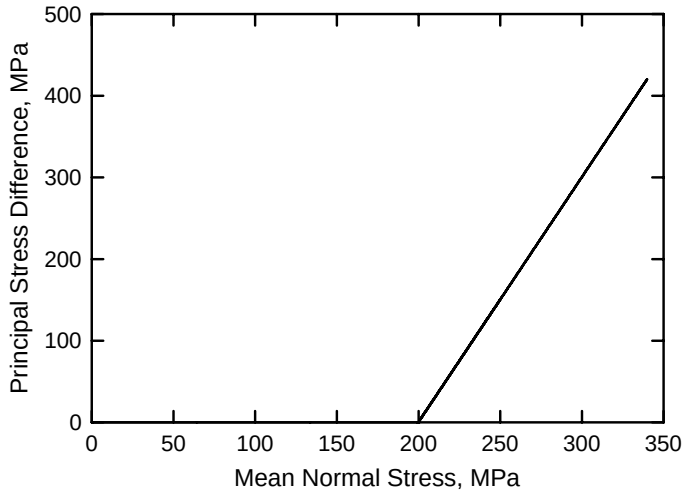

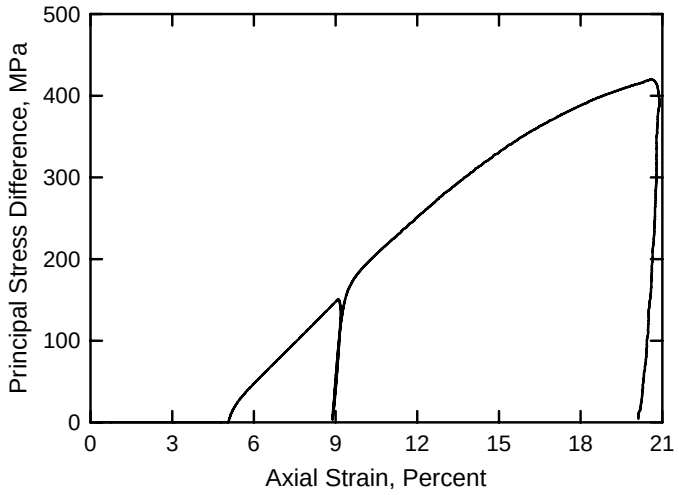

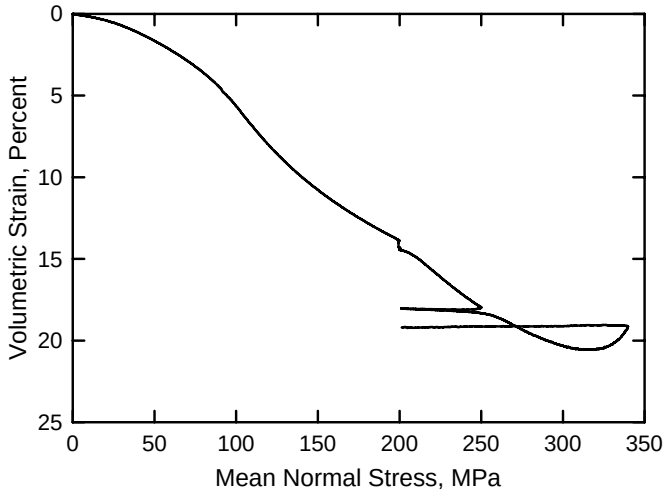

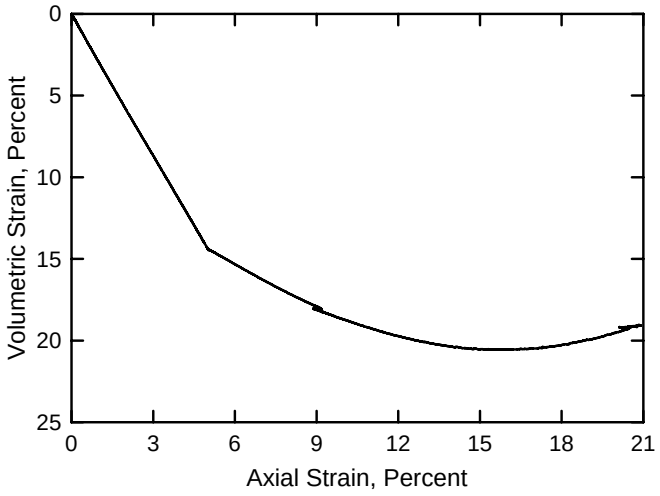

White Masonry Concrete
Test No. 20

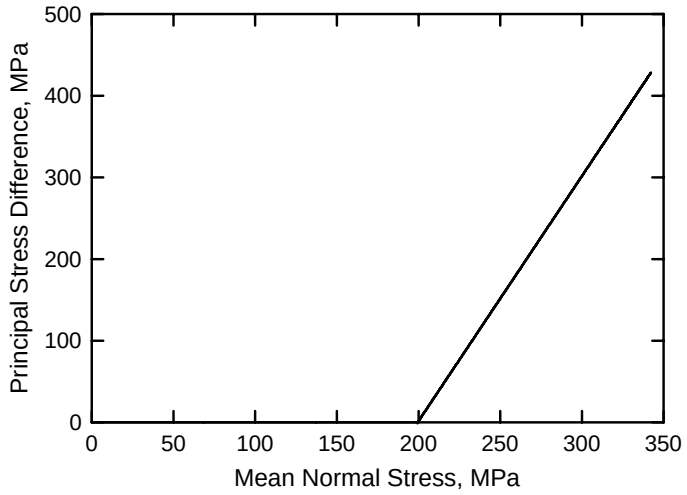

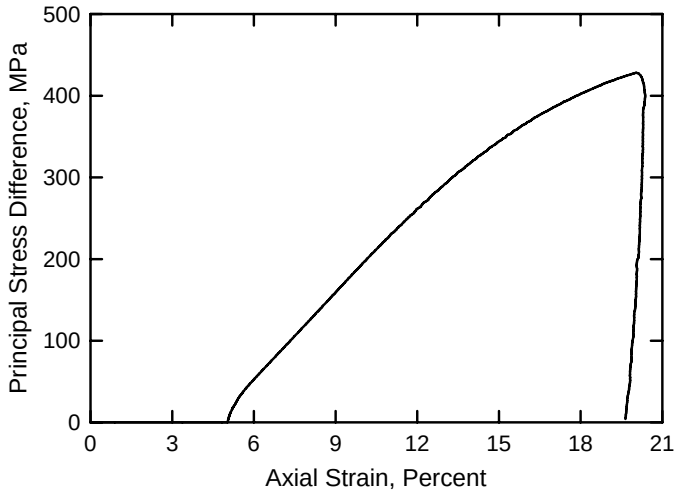

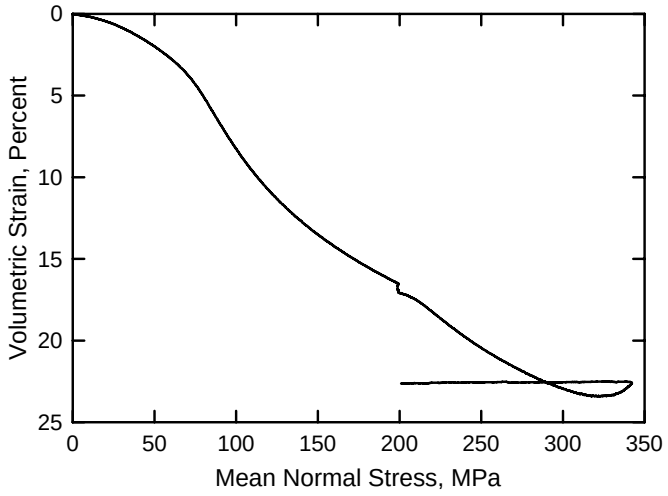

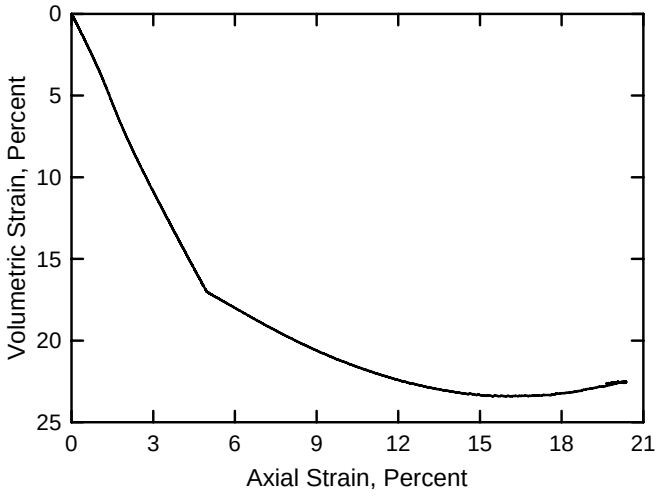

White Masonry Concrete
Test No. 21

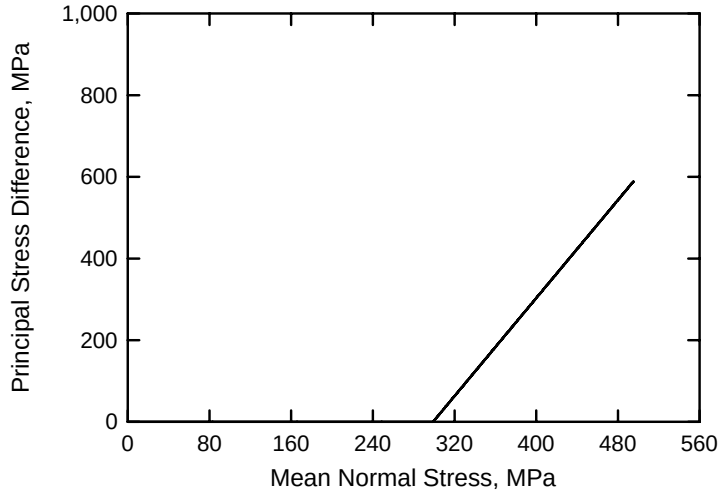

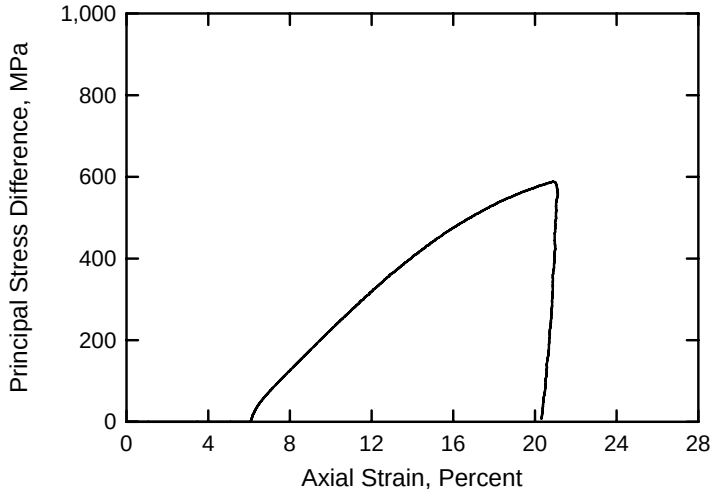

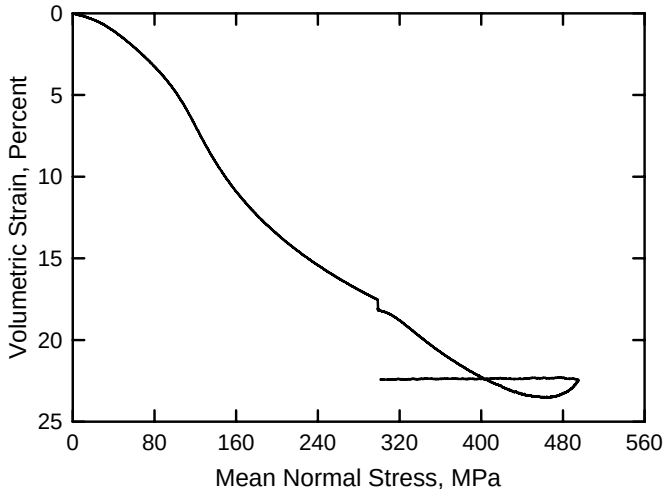

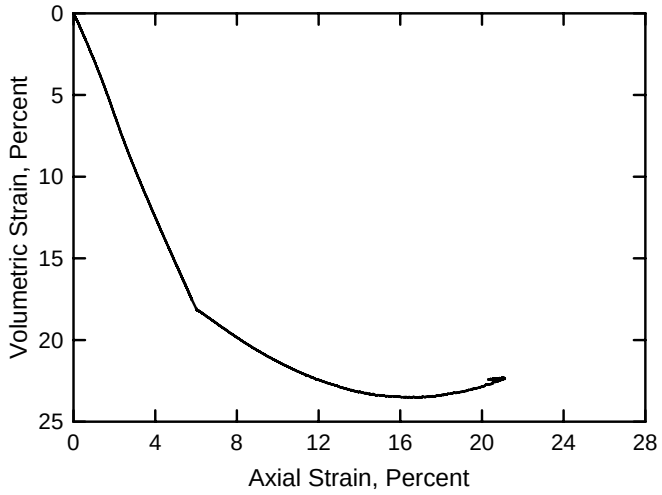

Plate 20

White Masonry Concrete
Test No. 22

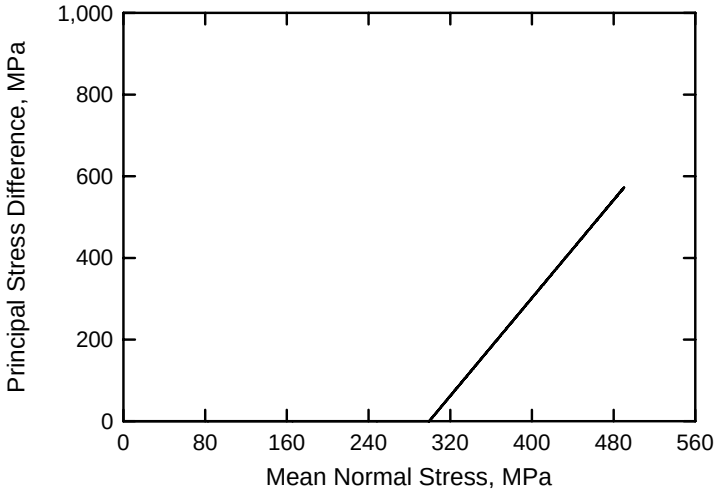

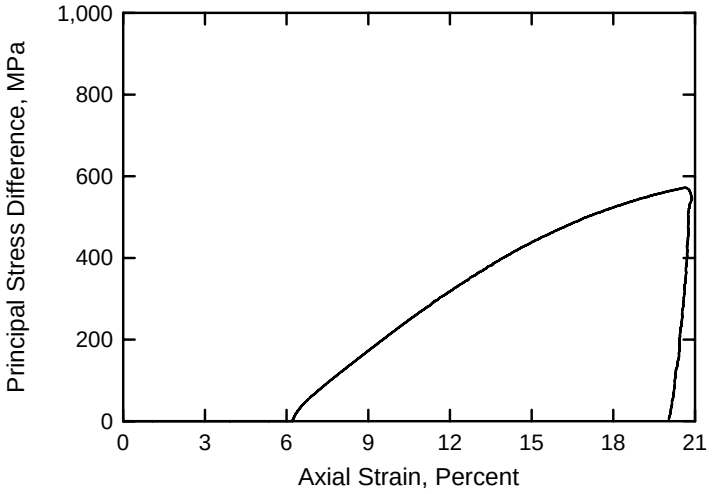

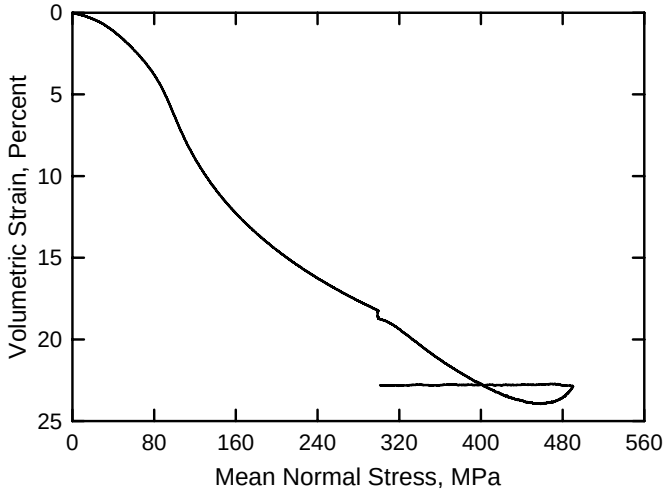

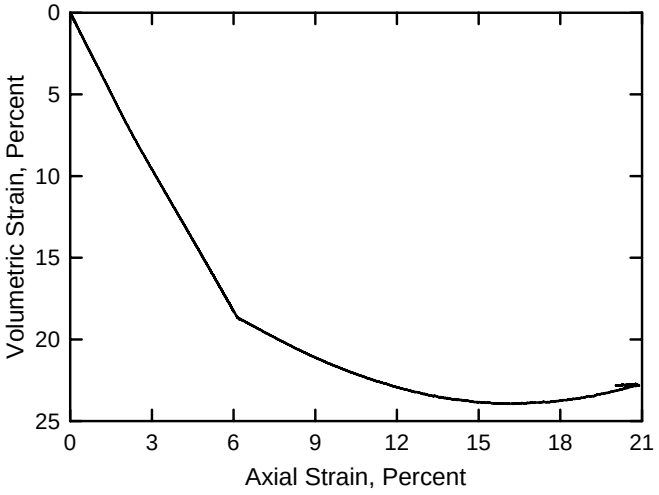

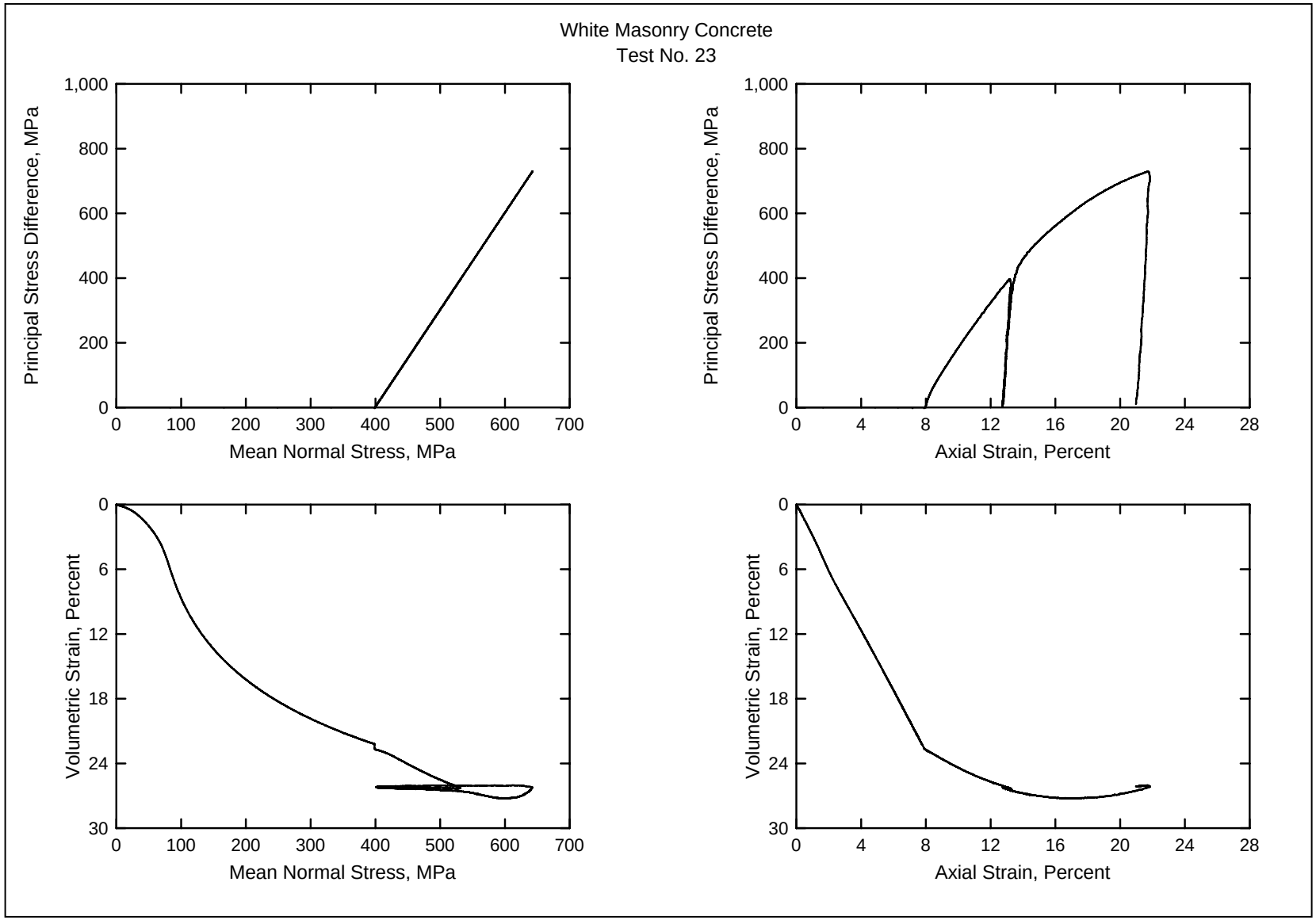
White Masonry Concrete
Test No. 23
Principal Stress Difference, MPa
1,000
800
600
400
200
0
0
100
200
300
400
500
600
700
Mean Normal Stress, MPa
Principal Stress Difference, MPa
1,000
800
600
400
200
0
0
4
8
12
16
20
24
28
Axial Strain, Percent
Volumetric Strain, Percent
0
6
12
18
24
30
0
100
200
300
400
500
600
700
Mean Normal Stress, MPa
Volumetric Strain, Percent
0
6
12
18
24
30
0
4
8
12
16
20
24
28
Axial Strain, Percent

Plate 22

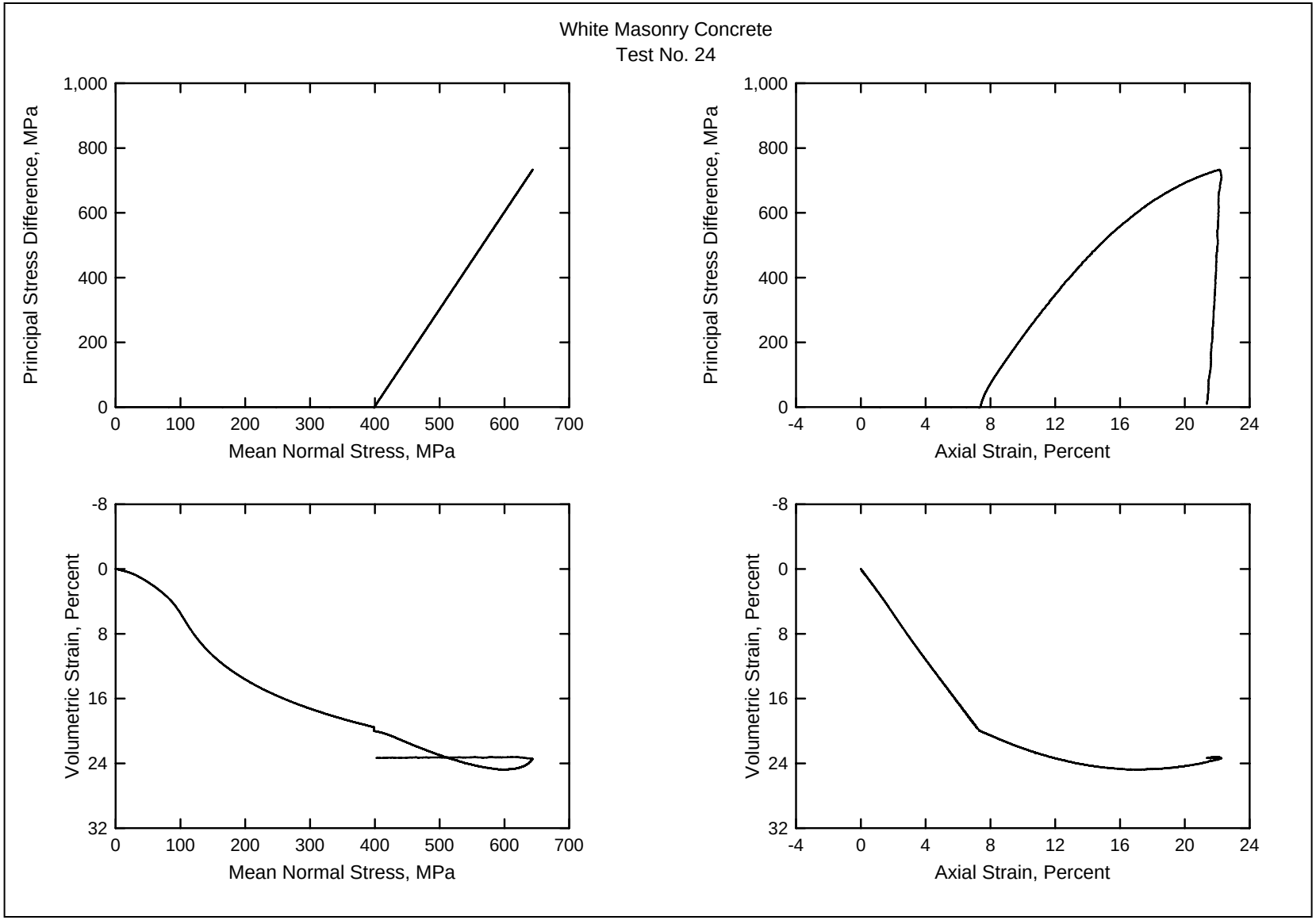
White Masonry Concrete
Test No. 24
Principal Stress Difference, MPa
1,000
800
600
400
200
0
0
100
200
300
400
500
600
700
Mean Normal Stress, MPa
Principal Stress Difference, MPa
1,000
800
600
400
200
0
-4
0
4
8
12
16
20
24
Axial Strain, Percent
Volumetric Strain, Percent
-8
0
8
16
24
32
0
100
200
300
400
500
600
700
Mean Normal Stress, MPa
Volumetric Strain, Percent
-8
0
8
16
24
32
-4
0
4
8
12
16
20
24
Axial Strain, Percent

Plate 23

White Masonry Concrete
Test No. 25

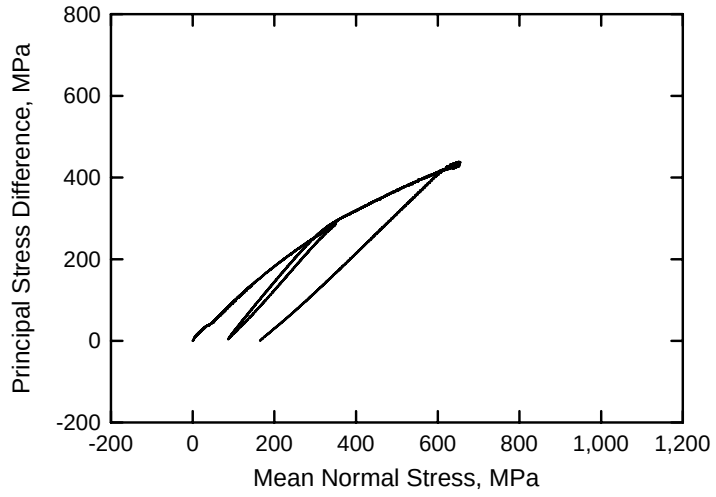

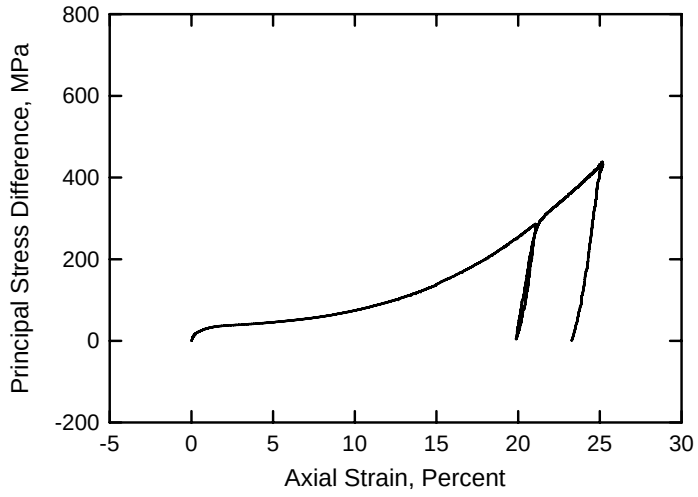

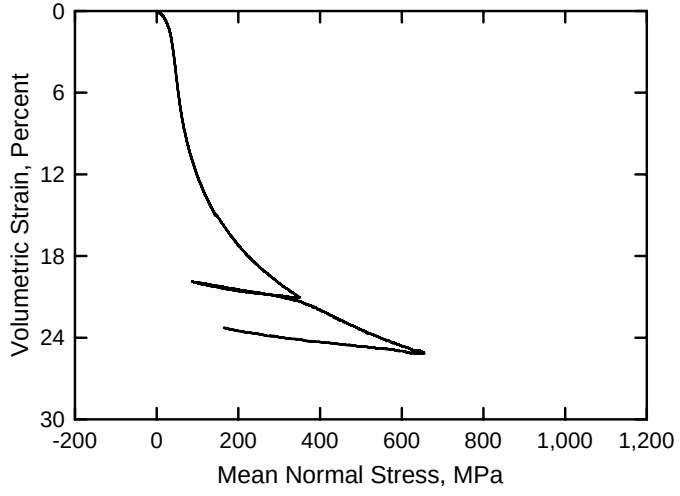

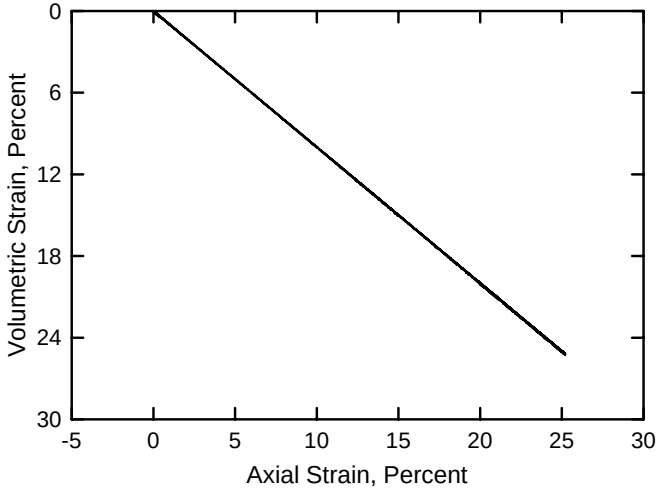

White Masonry Concrete
Test No. 26

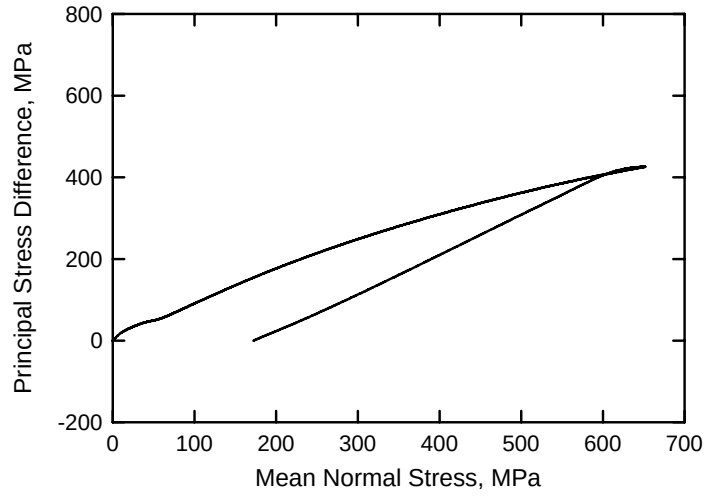

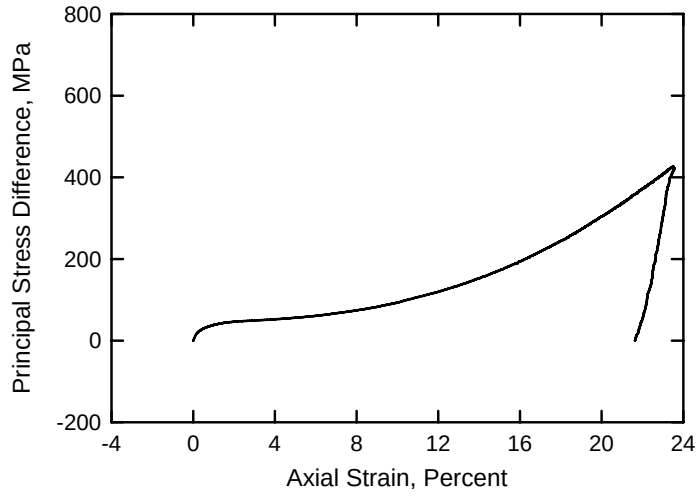

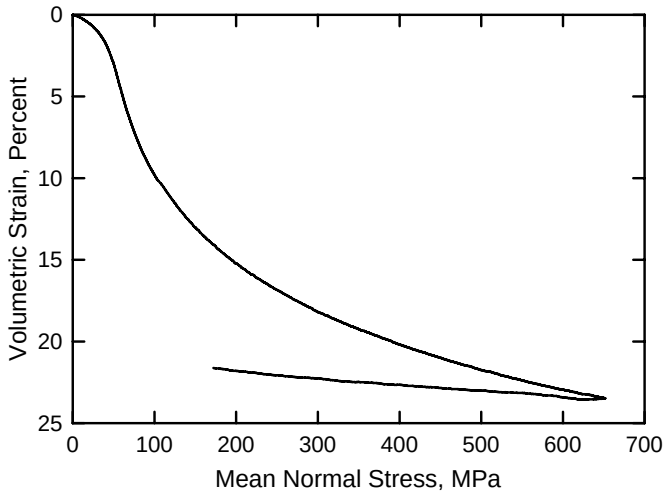

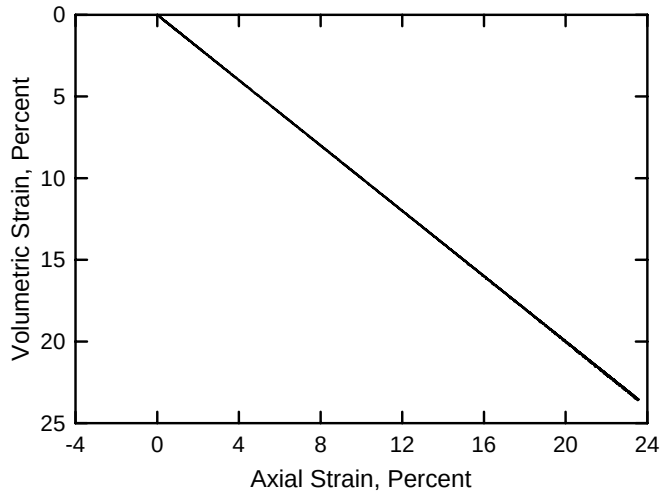

White Masonry Concrete
Test No. 27

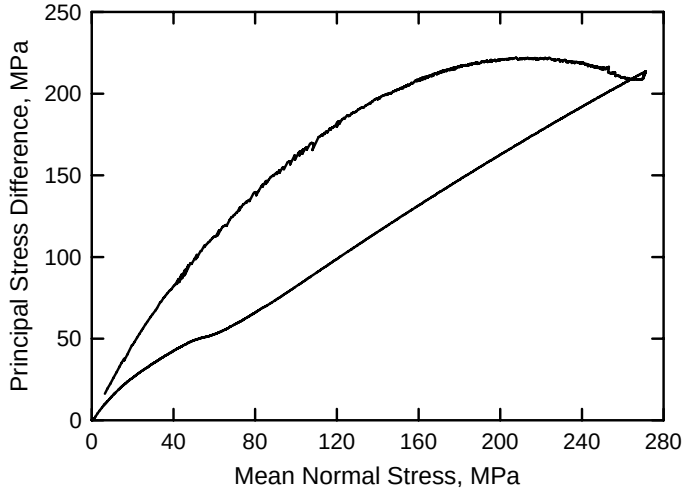

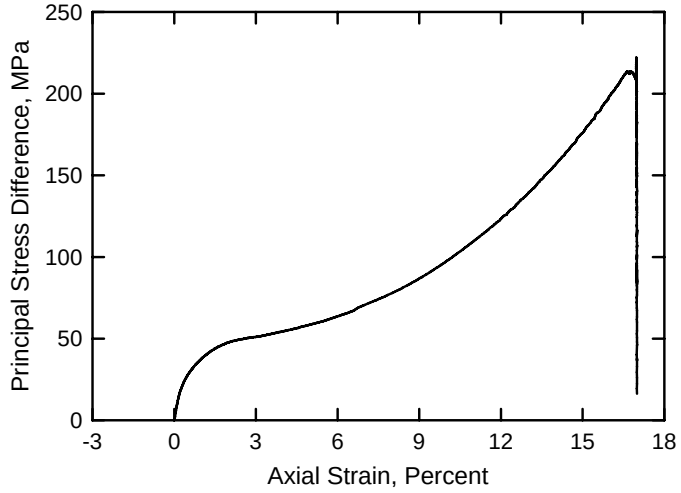

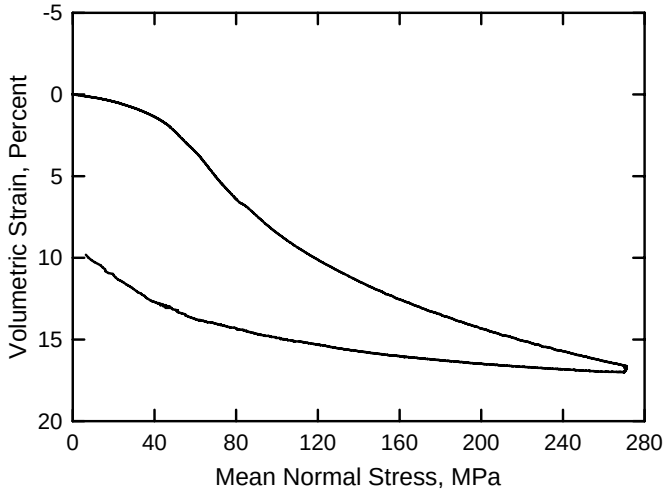

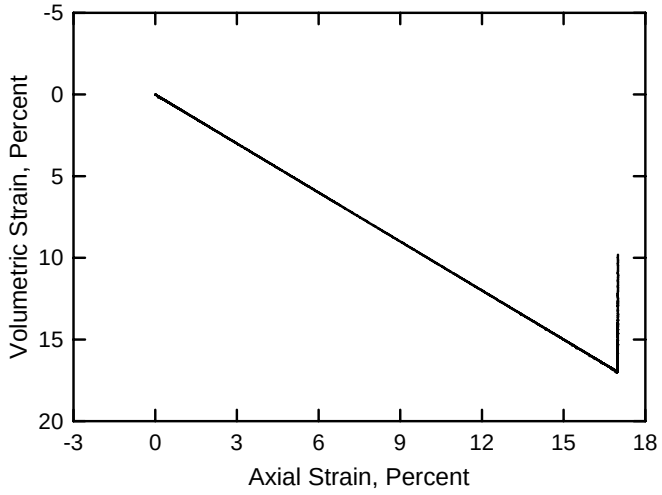

White Masonry Concrete
Test No. 28

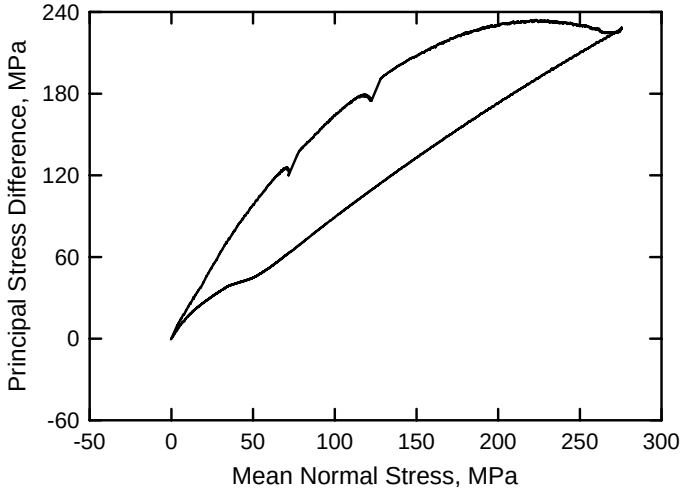

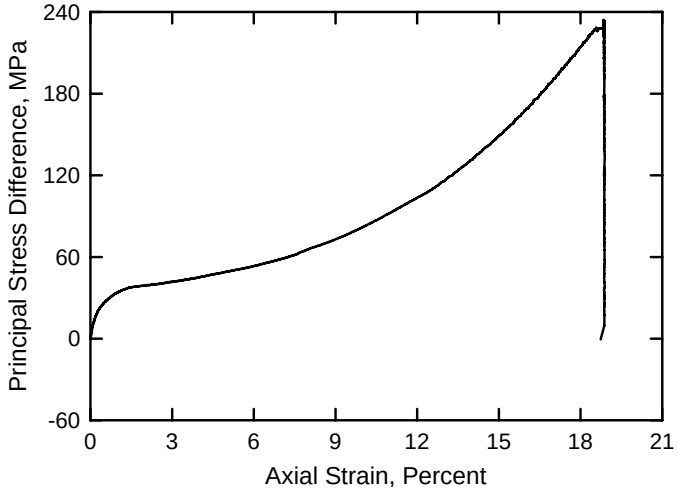

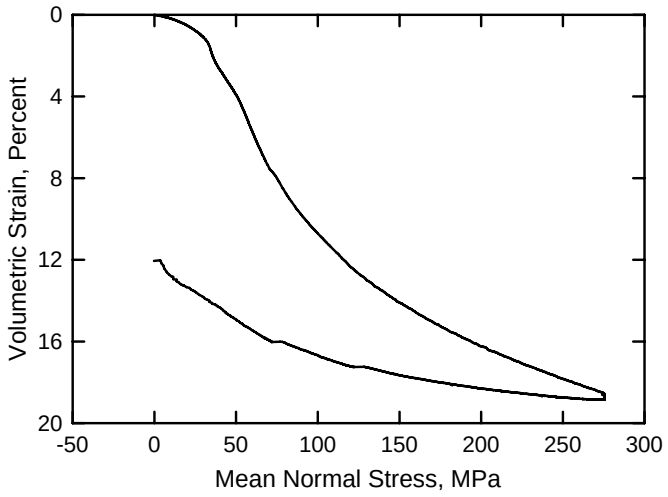

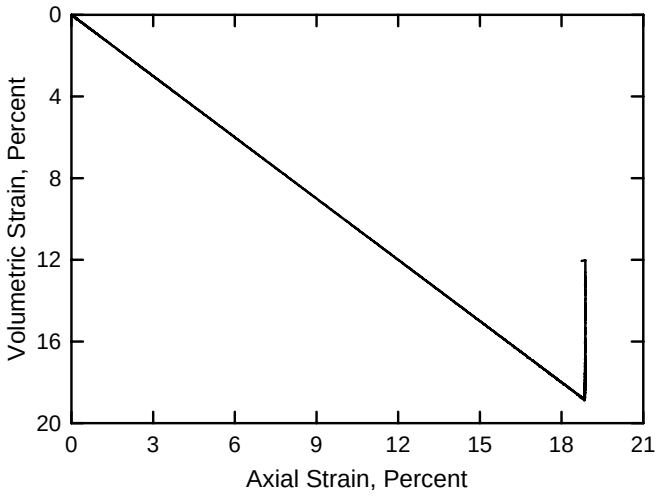

White Masonry Concrete
Test No. 29

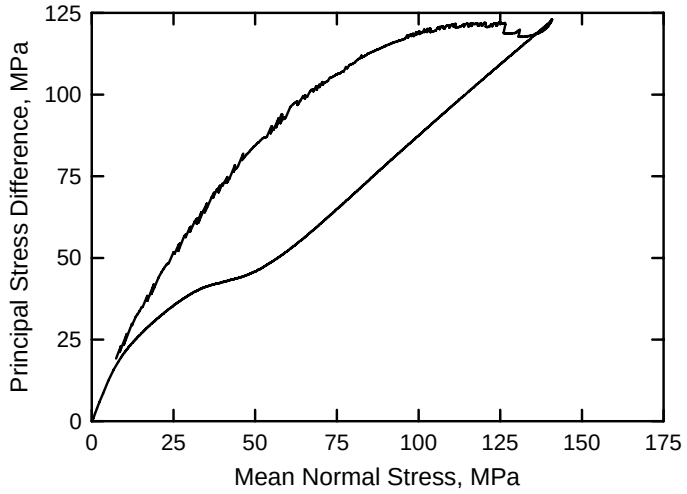

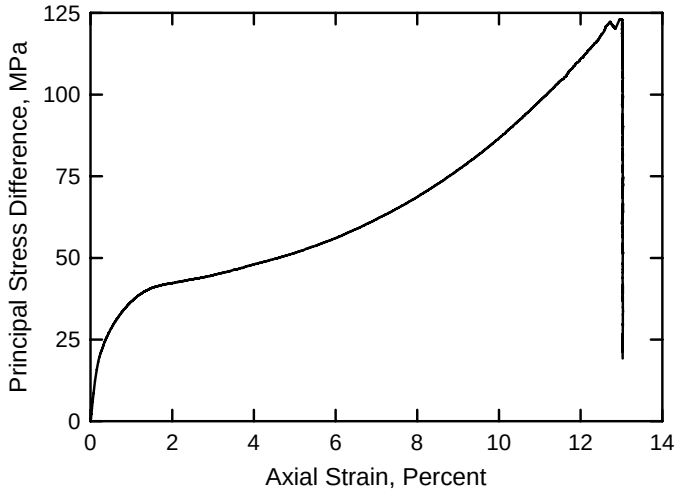

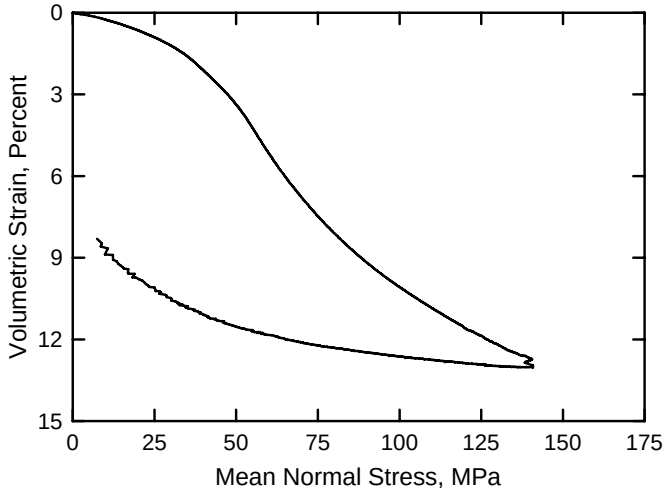

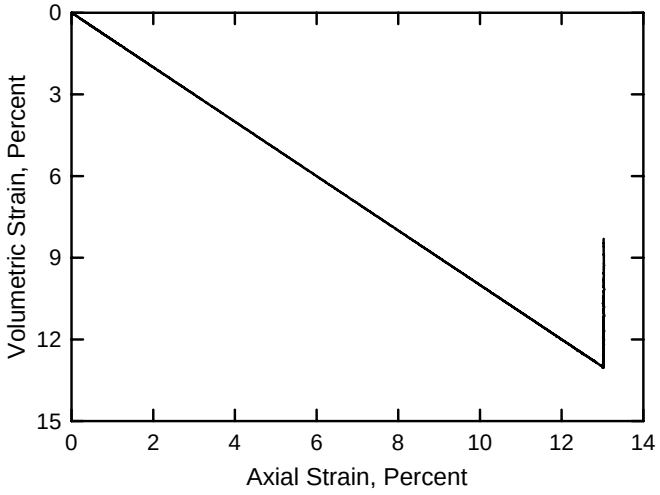

Plate 28

White Masonry Concrete
Test No. 30

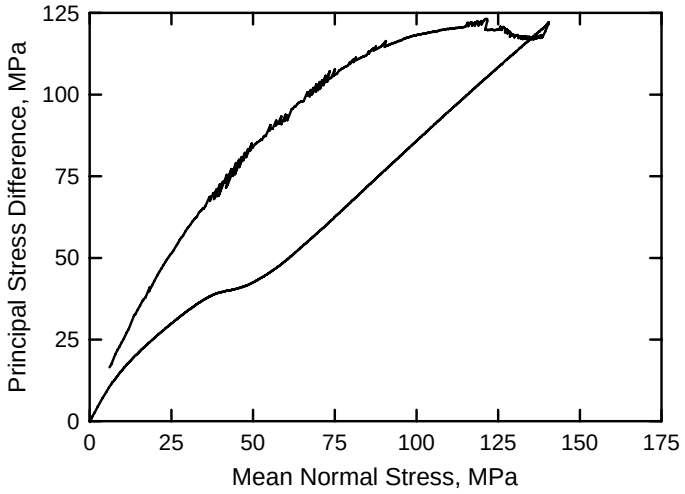

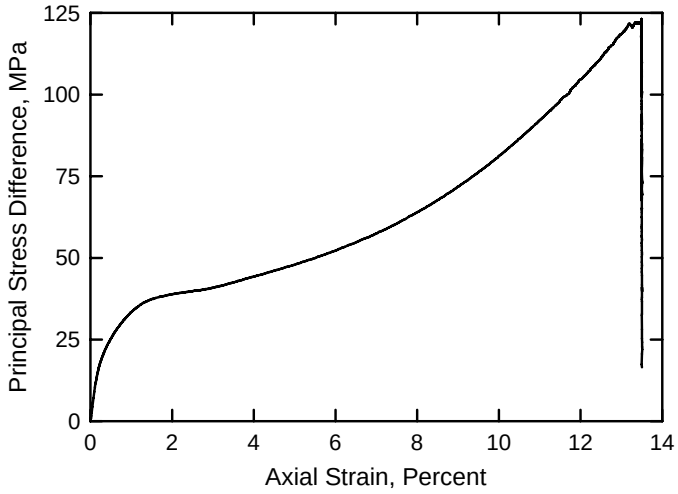

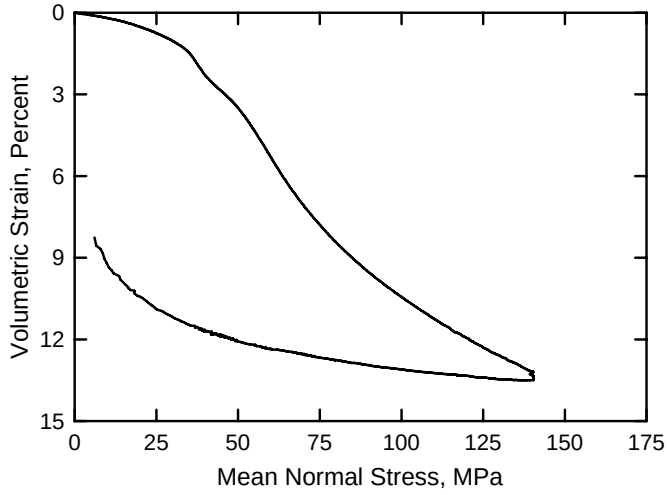

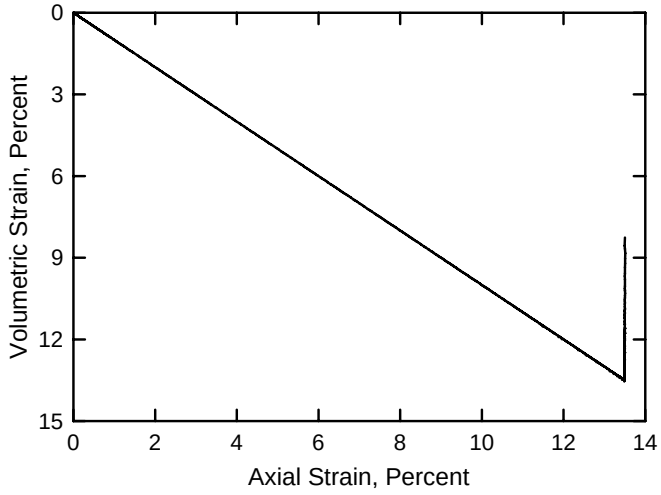

White Masonry Concrete
Test No. 31

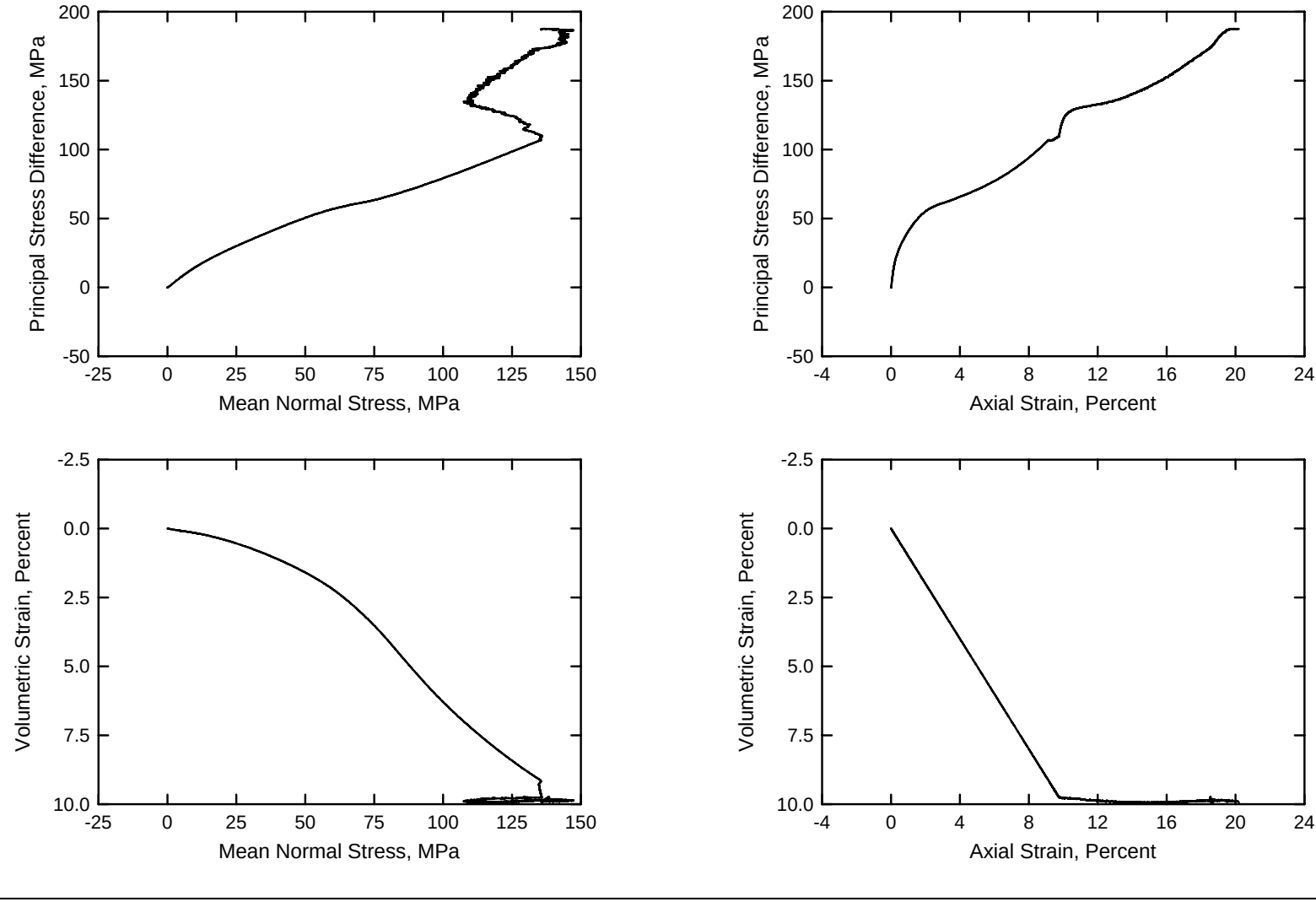

Plate 30

White Masonry Concrete
Test No. 32

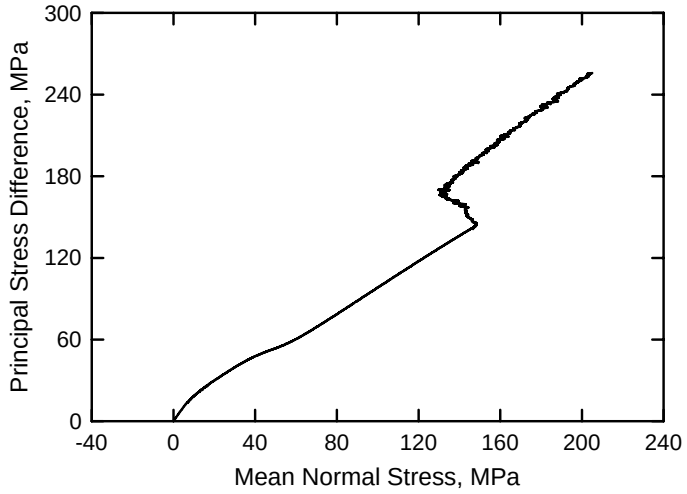

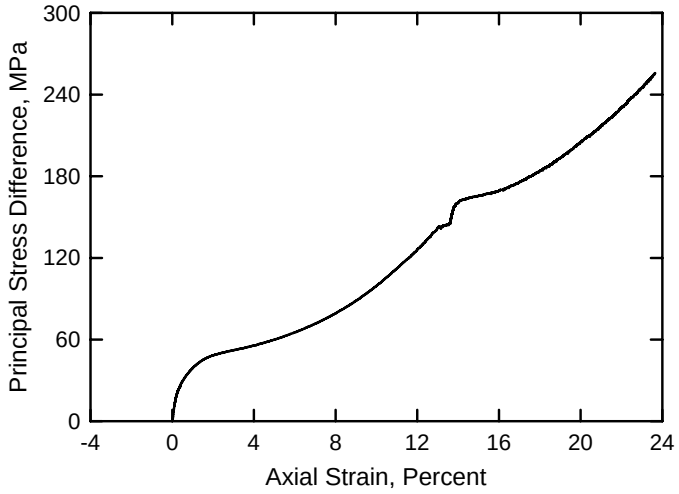

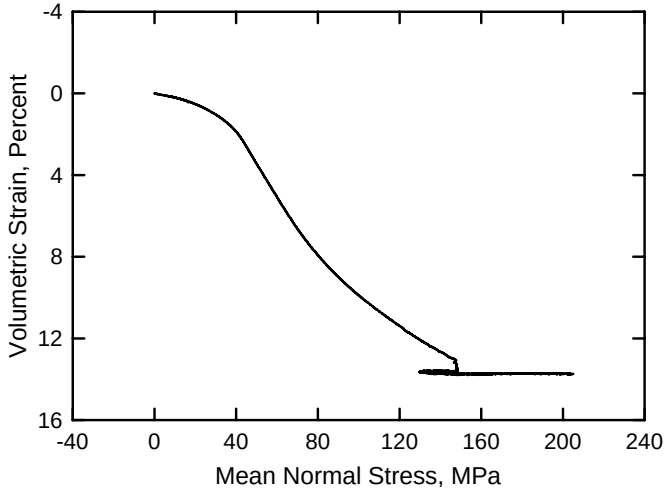

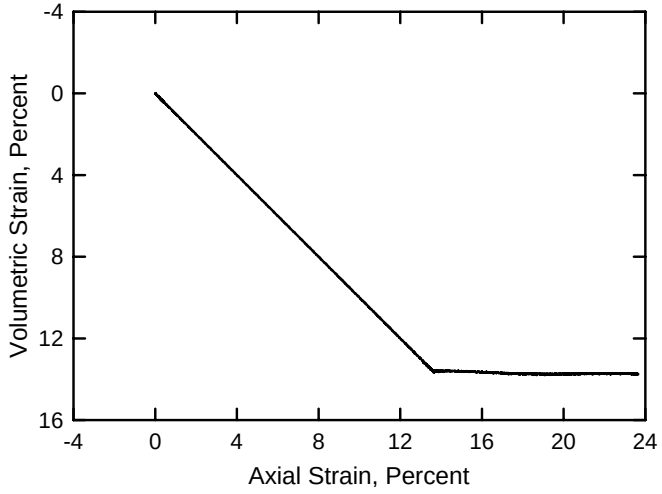

White Masonry Concrete
Test No. 33

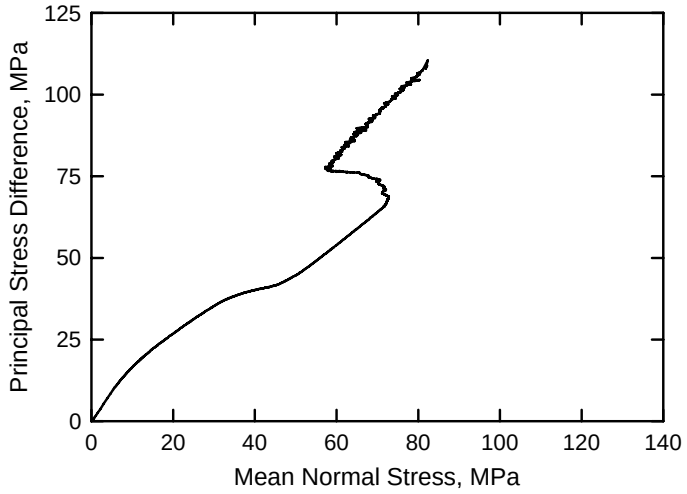

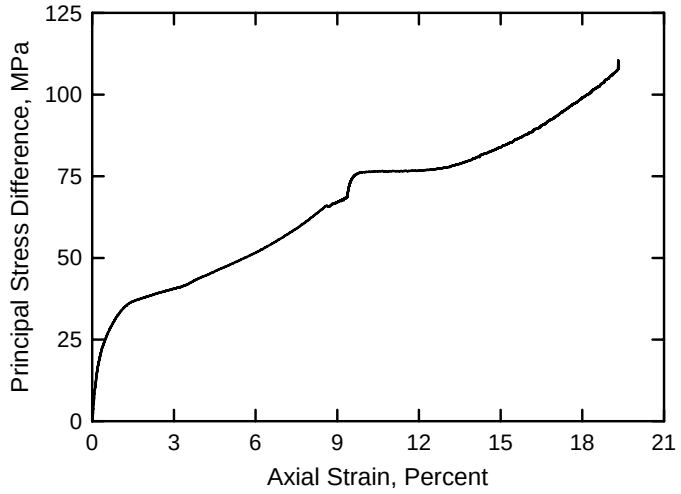

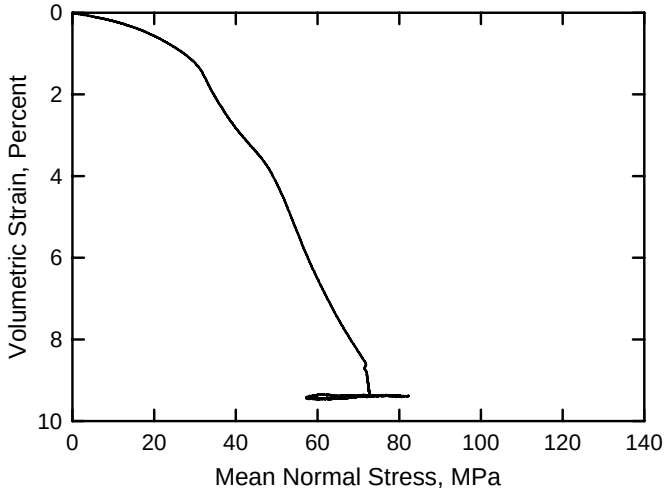

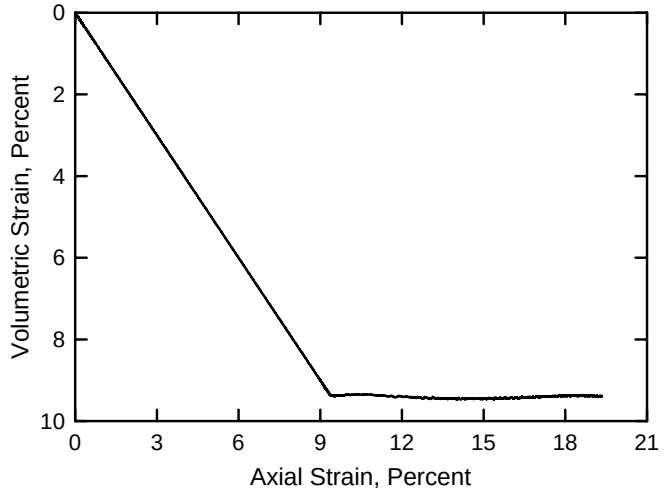

White Masonry Concrete
Test No. 37

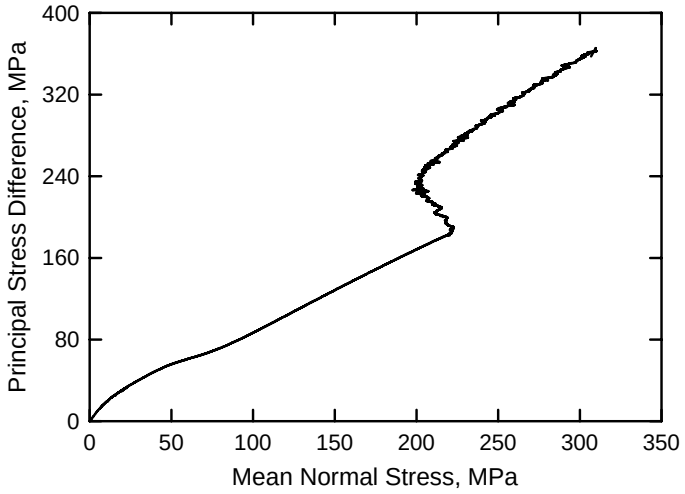

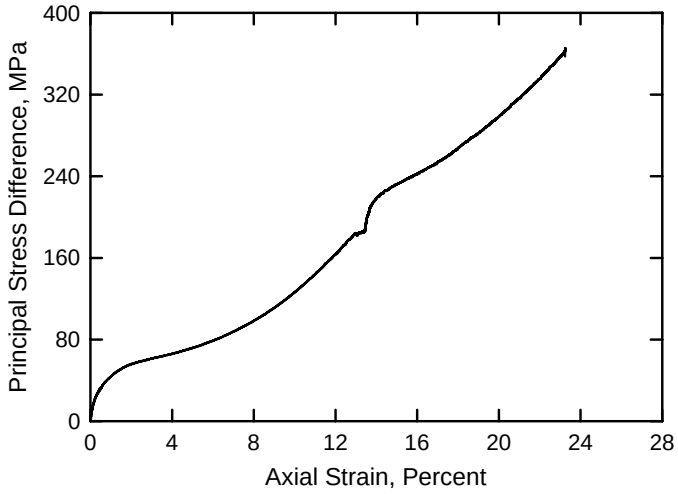

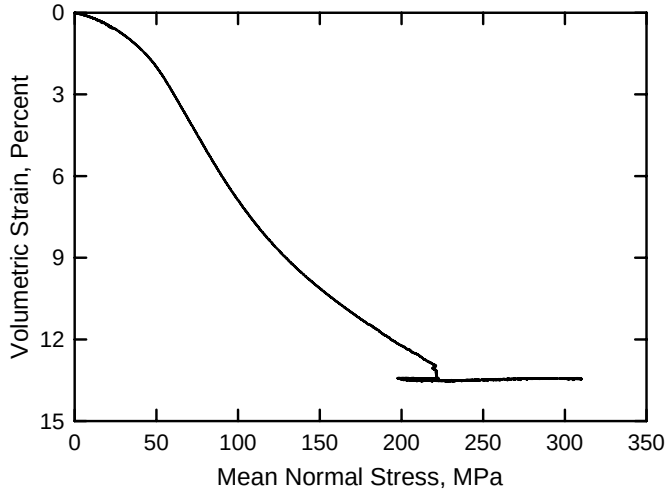

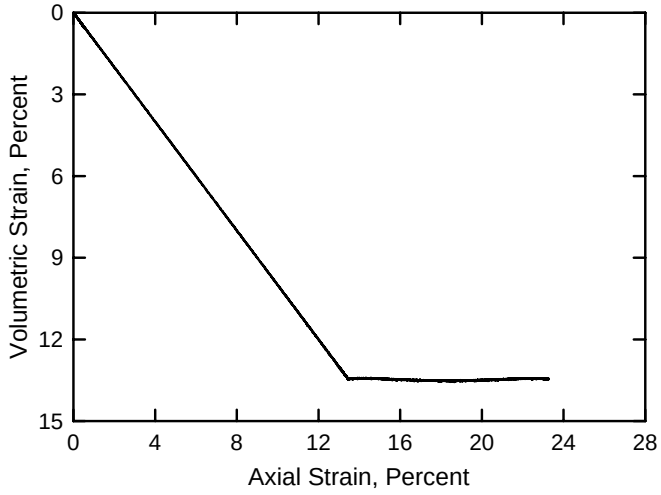

White Masonry Concrete
Test No. 38

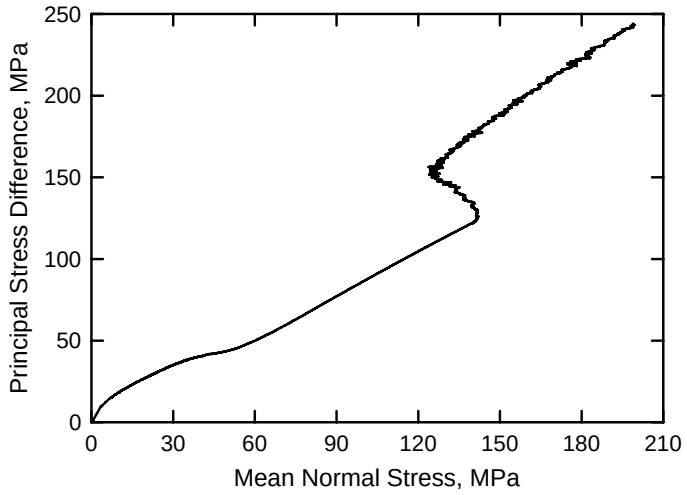

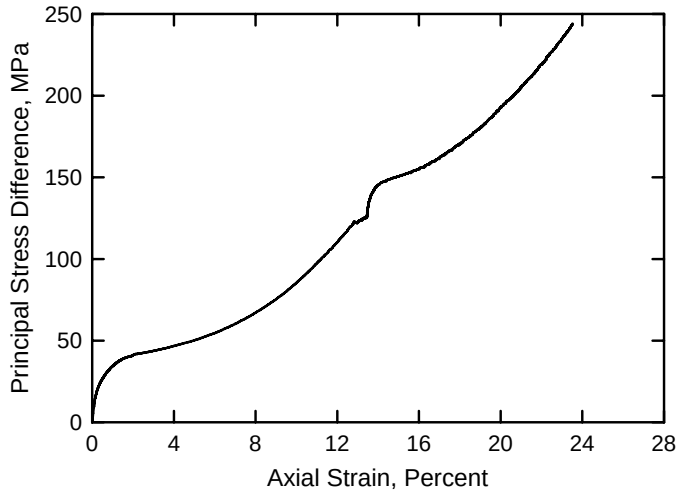

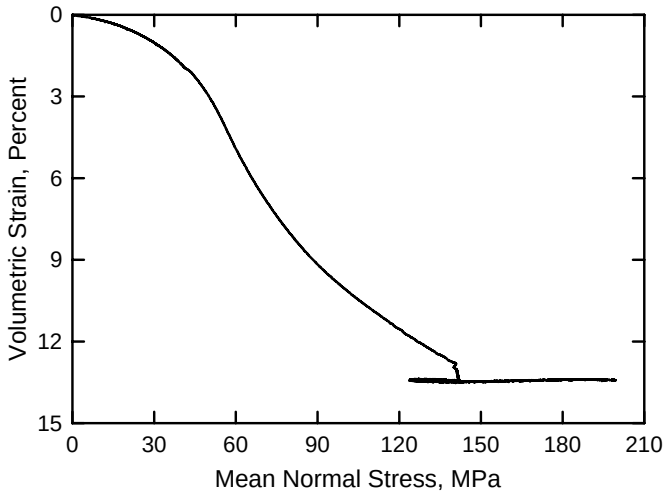

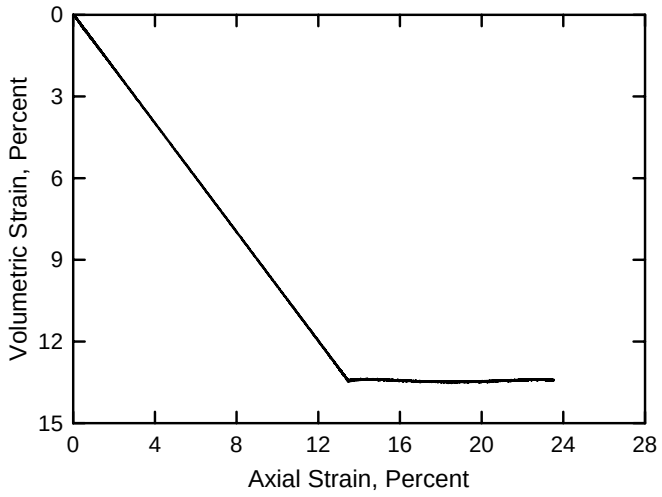

White Masonry Concrete
Test No. 34

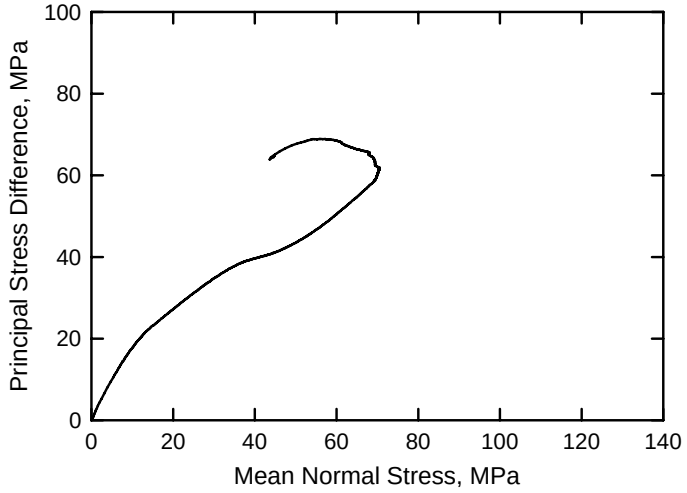

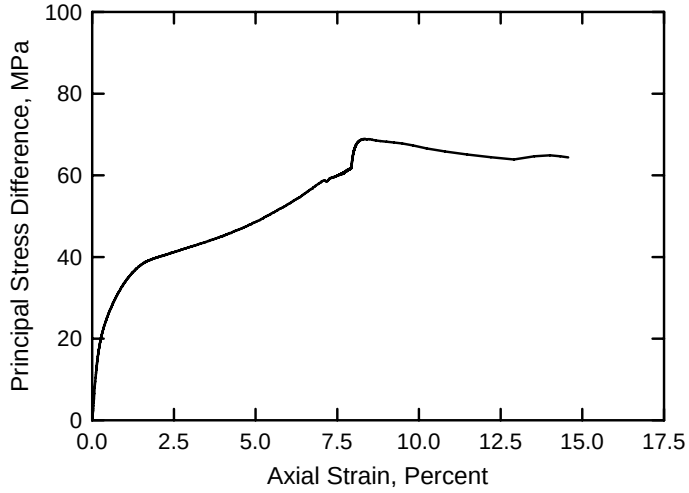

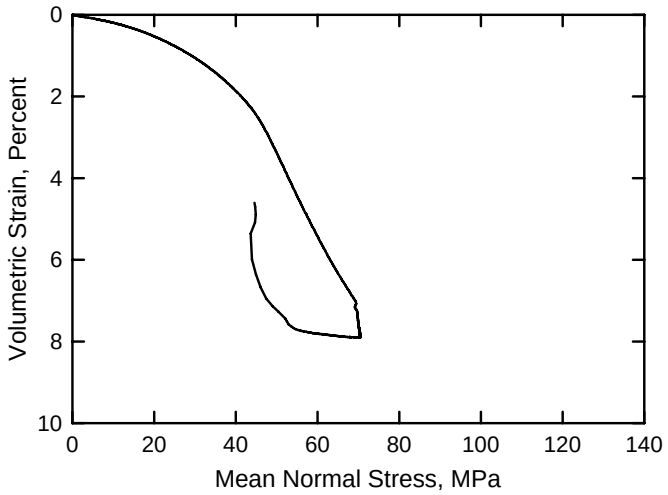

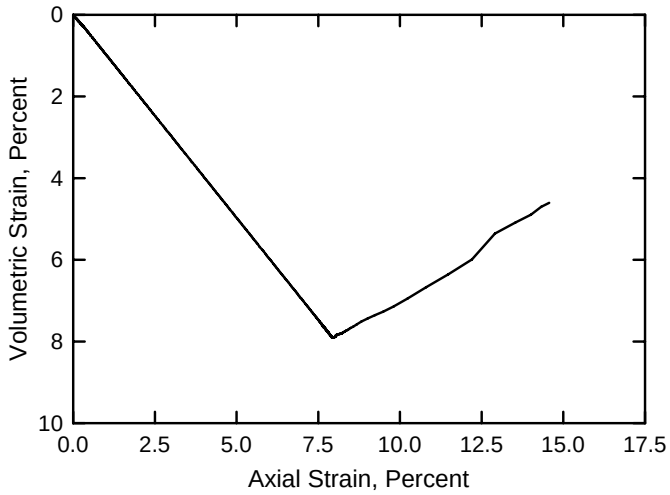

Plate 35

White Masonry Concrete
Test No. 35

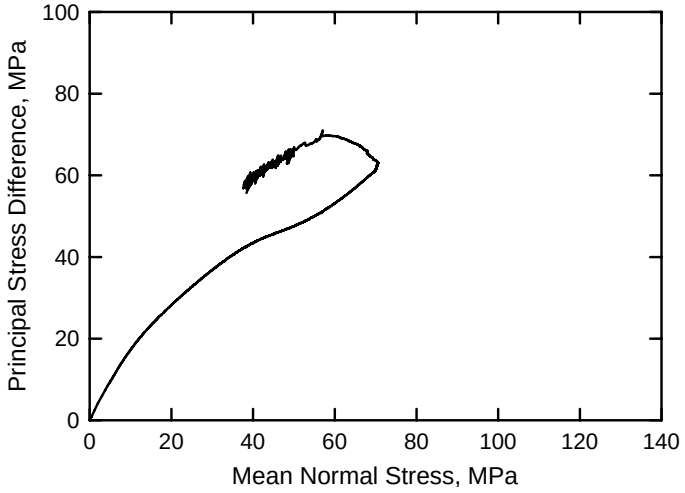

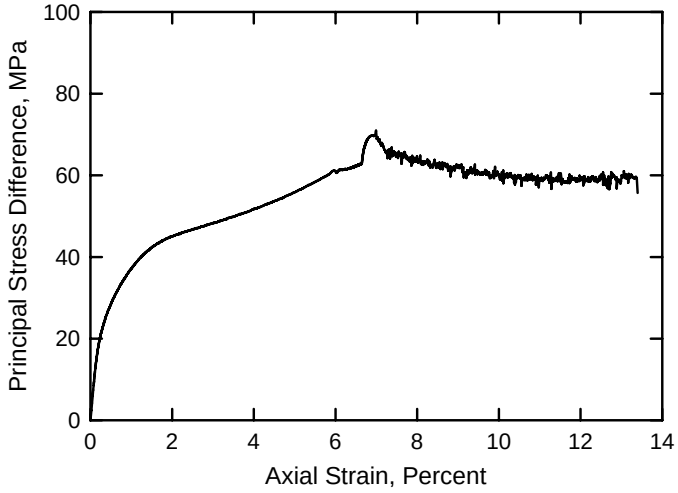

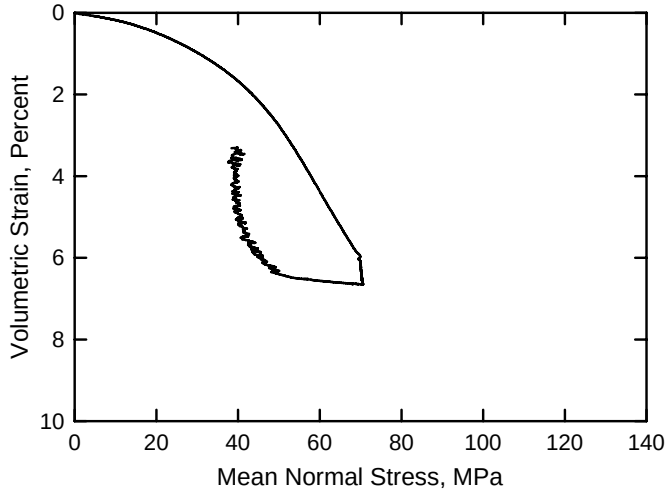

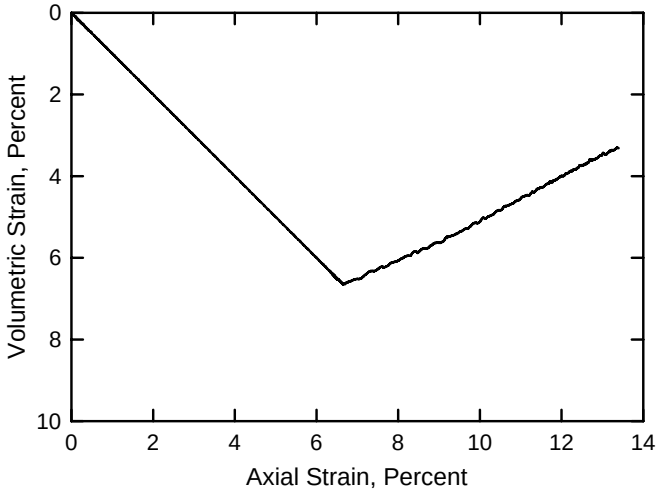

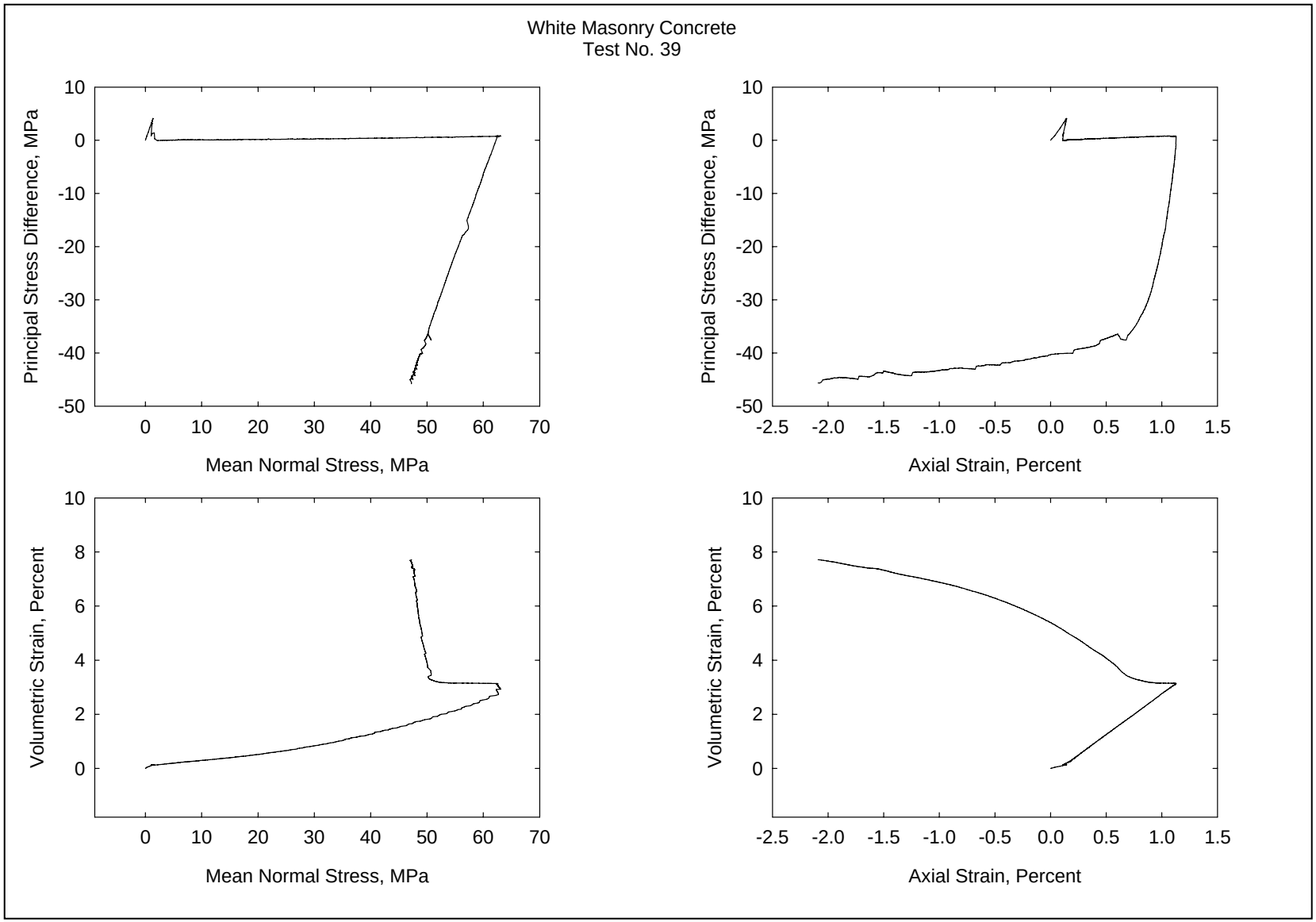
White Masonry Concrete
Test No. 39
Principal Stress Difference, MPa
Mean Normal Stress, MPa
Principal Stress Difference, MPa
Axial Strain, Percent
Volumetric Strain, Percent
Mean Normal Stress, MPa
Volumetric Strain, Percent
Axial Strain, Percent

Plate 37

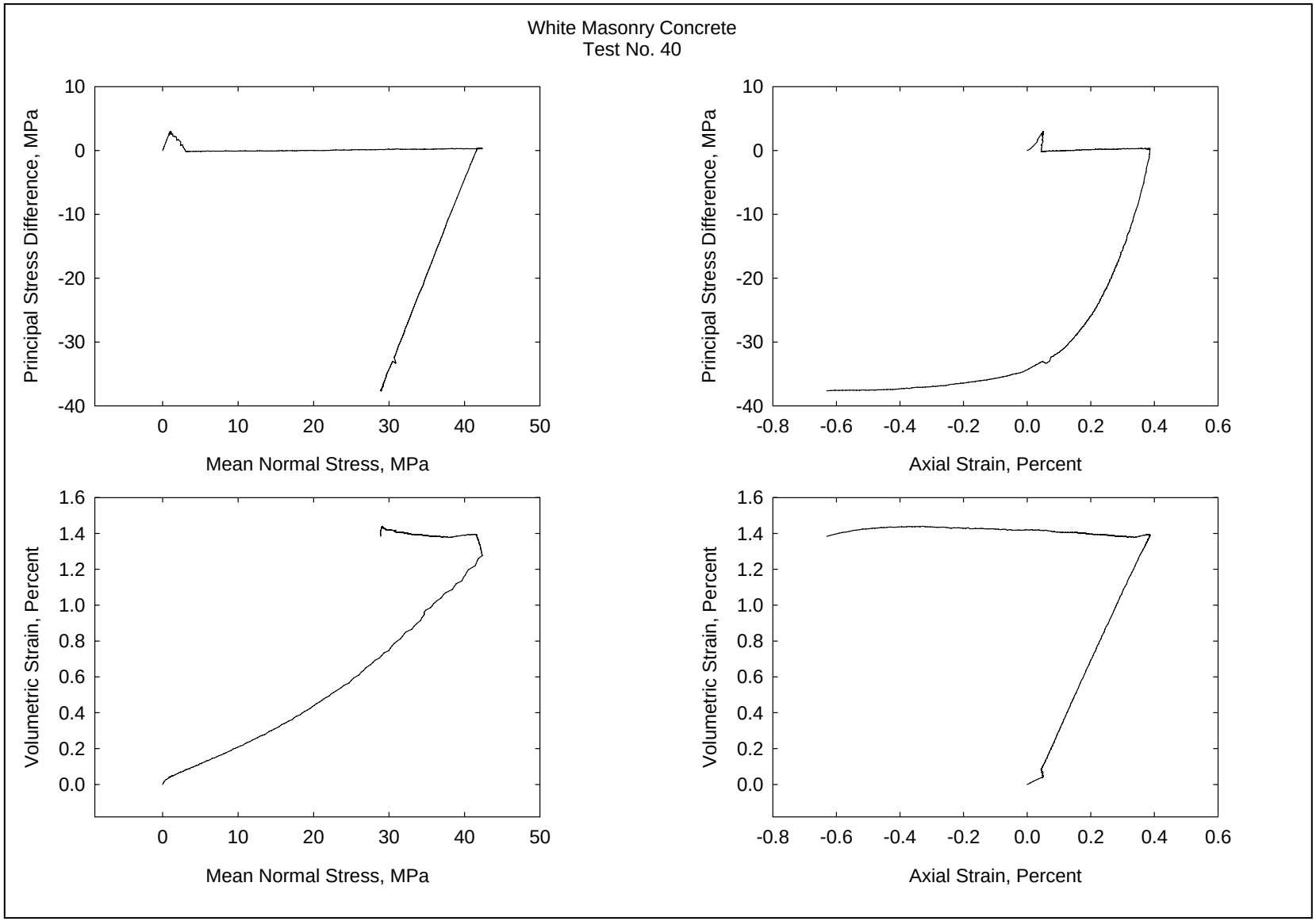
White Masonry Concrete
Test No. 40
Principal Stress Difference, MPa
Mean Normal Stress, MPa
Principal Stress Difference, MPa
Axial Strain, Percent
Volumetric Strain, Percent
Mean Normal Stress, MPa
Volumetric Strain, Percent
Axial Strain, Percent

Plate 38

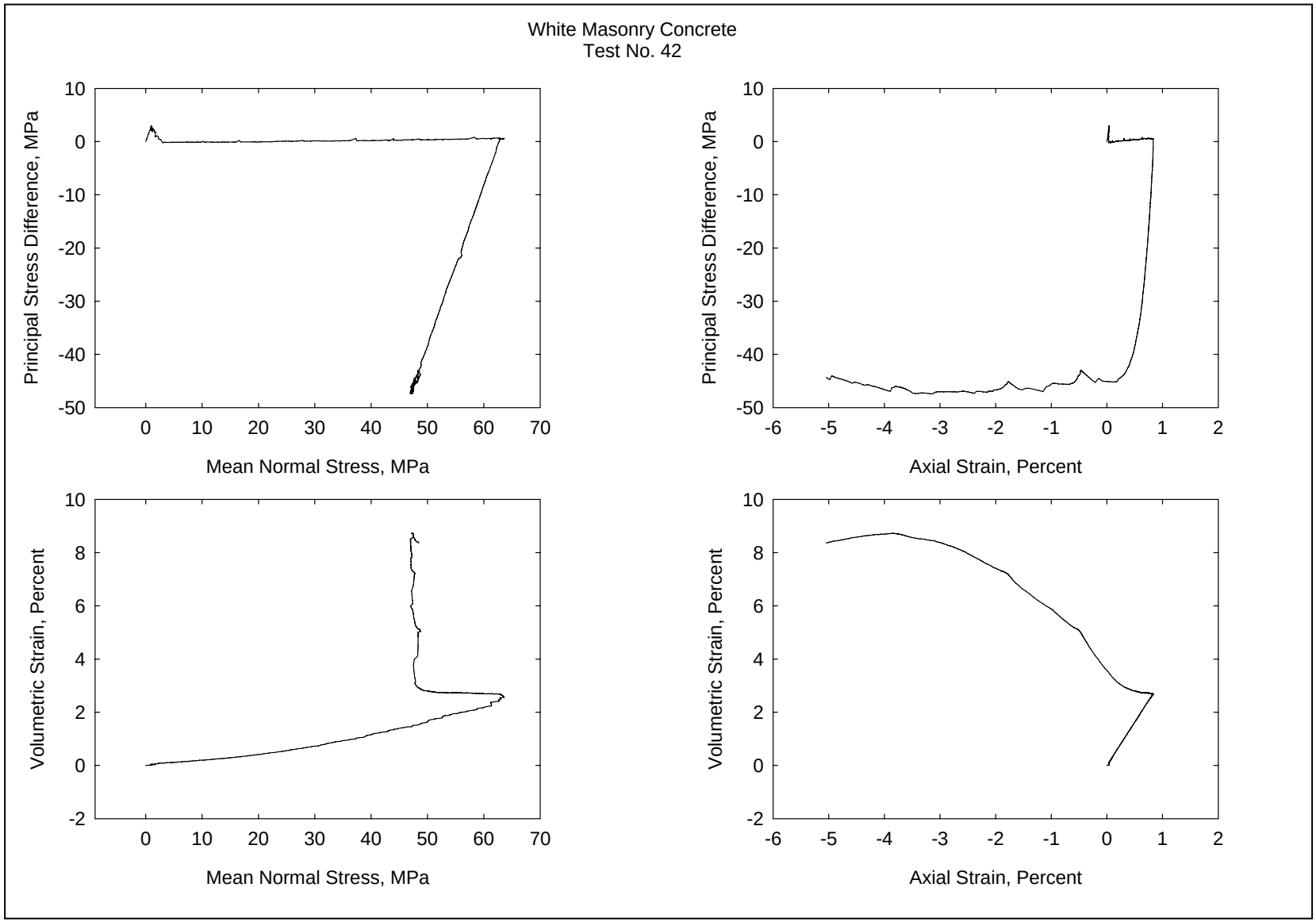
White Masonry Concrete
Test No. 42
Principal Stress Difference, MPa
Mean Normal Stress, MPa
Principal Stress Difference, MPa
Axial Strain, Percent
Volumetric Strain, Percent
Mean Normal Stress, MPa
Volumetric Strain, Percent
Axial Strain, Percent

Plate 39

REPORT DOCUMENTATION PAGE

Form Approved
OMB No. 0704-0188

1. REPORT DATE *(DD-MM-YYYY)*	**2. REPORT TYPE**	**3. DATES COVERED** *(From - To)*
September 2006	Final report	

4. TITLE AND SUBTITLE

Laboratory Characterization of White Masonry Concrete

5a. CONTRACT NUMBER

5b. GRANT NUMBER

5c. PROGRAM ELEMENT NUMBER

6. AUTHOR(S)

Erin M. Williams, Stephen A. Akers, and Paul A. Reed

5d. PROJECT NUMBER

5e. TASK NUMBER

5f. WORK UNIT NUMBER
AT40

7. PERFORMING ORGANIZATION NAME(S) AND ADDRESS(ES)

U.S. Army Engineer Research and Development Center
Geotechnical and Structures Laboratory
3909 Halls Ferry Road
Vicksburg, MS 39180-6199

8. PERFORMING ORGANIZATION REPORT NUMBER

ERDC/GSL TR-06-16

9. SPONSORING / MONITORING AGENCY NAME(S) AND ADDRESS(ES)

Headquarters, U.S. Army Corps of Engineers
Washington, DC 20314-1000

10. SPONSOR/MONITOR'S ACRONYM(S)

11. SPONSOR/MONITOR'S REPORT NUMBER(S)

12. DISTRIBUTION / AVAILABILITY STATEMENT

Approved for public release; distribution is unlimited.

13. SUPPLEMENTARY NOTES

14. ABSTRACT

Personnel of the Geotechnical and Structures Laboratory, U.S. Army Engineer Research and Development Center, conducted a laboratory investigation to characterize the strength and constitutive property behavior of a white masonry concrete (WMC). Forty-four mechanical property tests consisting of two hydrostatic compression tests, four unconfined compression (UC) tests, 17 triaxial compression (TXC) tests, two uniaxial strain tests, four uniaxial strain load/biaxial unload (UX/BX) tests, five uniaxial strain load/constant volume tests, two uniaxial strain load/constant strain ratio tests, five direct pull (DP) tests, and three reduced triaxial extension (RTE) tests were successfully completed. In addition to the mechanical property tests, nondestructive pulse-velocity measurements were performed on each specimen. The TXC tests exhibited a continuous increase in principal stress difference with increasing confining stress. A recommended compression failure surface was developed from the TXC and UC test results. Test data from the RTE and DP tests were used to develop a recommended extension failure surface for WMC. Results from the stress paths of the strain path tests and the recommended compression failure surface exhibited good agreement except for the UX/BX tests.

15. SUBJECT TERMS

Concrete
Compression tests
Extension tests
Material characterization
Material properties

16. SECURITY CLASSIFICATION OF:			**17. LIMITATION OF ABSTRACT**	**18. NUMBER OF PAGES**	**19a. NAME OF RESPONSIBLE PERSON**
a. REPORT	**b. ABSTRACT**	**c. THIS PAGE**			**19b. TELEPHONE NUMBER** *(include area code)*
UNCLASSIFED	UNCLASSIFED	UNCLASSIFED		99	